Mathematical modeling of crossed nanophotonic structures with generalized scattering-matrix method and local Fourier modal analysis

Hwi Kim and Byoungho Lee*

National Creative Research Center for Active Plasmonics Application Systems, Inter-University Semiconductor Research Center and School of Electrical Engineering, Seoul National University, Gwanak-Gu Sillim-Dong, Seoul 151-744, South Korea

**Corresponding author: byoungho@snu.ac.kr*

Received November 7, 2007; accepted January 7, 2008;
posted January 23, 2008 (Doc. ID 89387); published March 20, 2008

We propose a novel electromagnetic analysis scheme for crossed nanophotonic structures. The developed scheme is based on the mathematical modeling with the local Fourier modal analysis and the generalized scattering-matrix method. The mathematical Bloch eigenmodes of two-port block and four-port intersection block structures are analyzed by the local Fourier modal analysis. The interconnections of two-port blocks and four-port intersection block are described by the generalized scattering-matrix method. This scheme provides the linear system theory of general crossed nanophotonic structures. © 2008 Optical Society of America

OCIS codes: 000.3860, 000.6800, 050.1960, 050.1950, 050.0050, 050.1940.

1. INTRODUCTION

The mathematical modeling is a critical issue in nanophotonics. The dynamics of electromagnetic fields on a nanoscale can be described by the vectorial solution of the Maxwell equations. Therefore, mathematical modeling and numerical analysis methods for solving the Maxwell equations have been researched intensively. At present, there are various established methods of obtaining the numerical solutions of the Maxwell equations. In general, the methods can be classified into two types of space-domain and spatial-frequency-domain methods. The space-domain methods represent the Maxwell equations as partial differential equations in space domain and analyze the numerical values of the field distributions at spatial points. On the other hand, the spatial-frequency-domain methods represent the Maxwell equations as algebraic linear equations in the spatial-frequency domain and analyze the Fourier representation of the field distribution. In the point of view of mathematical modeling, the spatial-frequency-domain method can give the more systematic and flexible approach than the space-domain methods. A refined linear system theory of complex electromagnetic structures can be built based on the spatial-frequency-domain method. In the spatial-frequency-domain method, the mathematical Bloch modes represented by the pseudo-Fourier series span the eigensystems of the Maxwell equations. The electromagnetic field distributions in a finite region are expressed by the superposition of the Bloch eigenmodes with specific coupling coefficients determined by the boundary conditions. Within this framework, the Bloch eigenmodes constitute the system basis and the coupling coefficients of the Bloch eigenmodes, which constitute spectral information, are variables to be processed. Recently, this linear system approach became much required in nanophotonics. Large-scale system-level integration of nanophotonic devices [1–6], i.e., nanophotonic network, is considered as an ultimate point of the advances in nanophotonics. The use of conventional methods for analyzing nanophotonic networks is almost impossible without some specific innovations because of the limitation of computing resources. The nanophotonic networks are composed of many and various photonic devices. To study the collective dynamics of such nanophotonic networks, the system theory of the nanophotonic networks must be built. During the past decades, one of the spatial-frequency-domain methods, the Fourier modal method (FMM) [7–11] has been intensively researched and many challenging problems related to the foundation of the FMM have been overcome [12–19]. At present, the FMM is considered one of the most efficient and accurate electromagnetic analysis tools for optics and photonics. With the development of the FMM, the scattering-matrix method (SMM) has been developed as a stable wave propagating algorithm in multilayered structures [20–24]. The scattering matrix (S matrix) of an electromagnetic structure is actually a linear system representation of that structure with the Bloch eigenmodes as the system basis. We can have a view of any linear electromagnetic structure as a linear system having its own S matrix.

We can believe that a systematic linear system theory of complex network structures can be built with the SMM and the FMM. The establishment of the linear system theory of the electromagnetic structure on a nanoscale can be considered as a main target of the mathematical modeling in present nanophotonics. However, for achieving the objective, the conventional FMM and SMM must be refined and extended. In this paper, as a prerequisite step for constructing a general linear system theory of general nanophotonic networks, we propose a mathemati-

cal modeling of crossed nanophotonic structures with the development of the local Fourier modal analysis (LFMA) and the generalized SMM (GSMM).

This paper is organized as follows. In Section 2, the four-port crossed nanophotonic structures are defined. In Section 3, the LFMA of two-port blocks is described. In Section 4, the LFMA of four-port blocks is described. In Section 5, the GSMM is formulated for constructing four-port crossed photonic structures. In Section 6, concluding remarks and perspectives of the proposed theory are given.

2. FOUR-PORT CROSSED NANOPHOTONICS STRUCTURES

In the near future of nanophotonics, global structures such as networks and circuits will become a main issue based on previous and present active research on local structures such as individual devices and elements. In Fig. 1, the collective system of such nanophotonic devices, more generally photonic blocks, is presented. Let us call this kind of system a nanophotonic network. The functional photonic blocks are represented by geometric figures: circle, rectangles, and so on. The interaction of the blocks is denoted by bidirectional arrows between photonic blocks such as two-port blocks, four-port cross blocks, two-port light sources, and general blocks having more ports.

At present, such a network or global phenomena cannot be correctly, or at least reasonably, analyzed without impractical huge computing resources. Although the optical fields act in accordance with the definite Maxwell equations, the information needed to represent the optical field is too huge for us to directly analyze. Therefore, the development of rigorous and efficient mathematical modeling of nanophotonic networks is an urgent and important theme at present.

For this, we can take a technical approach to deal with such global structures with an intuitive assumption. First, in practical nanophotonic networks, optical fields are usually localized on engineered structures or devices such as waveguides and resonators. Thus we can obtain a reasonable solution of the Maxwell equations around these local areas where the optical field energy is not negligible. Then, we should have a systematic mathematical model to describe the relationship and interactions between each locally analyzed region.

This concept is the motivation for the development of the linear system theory of nanophotonic networks. In this paper, as a prerequisite step for constructing a general linear system theory, the electromagnetic analysis on the basic element, four-port crossed nanophotonic structure, is investigated.

Figure 2 shows a schematic of a four-port cross block. As an analysis example, a two-dimensional photonic crystal cross-waveguide structure [2] shown in Fig. 2(a) is chosen. This cross-waveguide structure is composed of five subparts: ports 1–4 and the intersection cross block. The complete characterizations of the four-port cross block and the two-port block are represented by the 4×4 and the 2×2 S matrix, respectively.

For convenience, let the S matrices of two-port blocks placed along the transverse direction and those placed along the longitudinal direction be distinguished by

$$\mathbf{S}=\begin{pmatrix}\vec{T} & \vec{R}\\ \overleftarrow{R} & \overleftarrow{T}\end{pmatrix}, \tag{1a}$$

$$\mathbf{S}=\begin{pmatrix}T_{\uparrow} & R_{\downarrow}\\ R_{\uparrow} & T_{\downarrow}\end{pmatrix}. \tag{1b}$$

The 4×4 S matrix of a four-port cross-block is defined by

$$\mathbf{S}=\begin{pmatrix}\mathbf{S}_{11} & \mathbf{S}_{21} & \mathbf{S}_{31} & \mathbf{S}_{41}\\ \mathbf{S}_{12} & \mathbf{S}_{22} & \mathbf{S}_{32} & \mathbf{S}_{42}\\ \mathbf{S}_{13} & \mathbf{S}_{23} & \mathbf{S}_{33} & \mathbf{S}_{43}\\ \mathbf{S}_{14} & \mathbf{S}_{24} & \mathbf{S}_{34} & \mathbf{S}_{44}\end{pmatrix}. \tag{2}$$

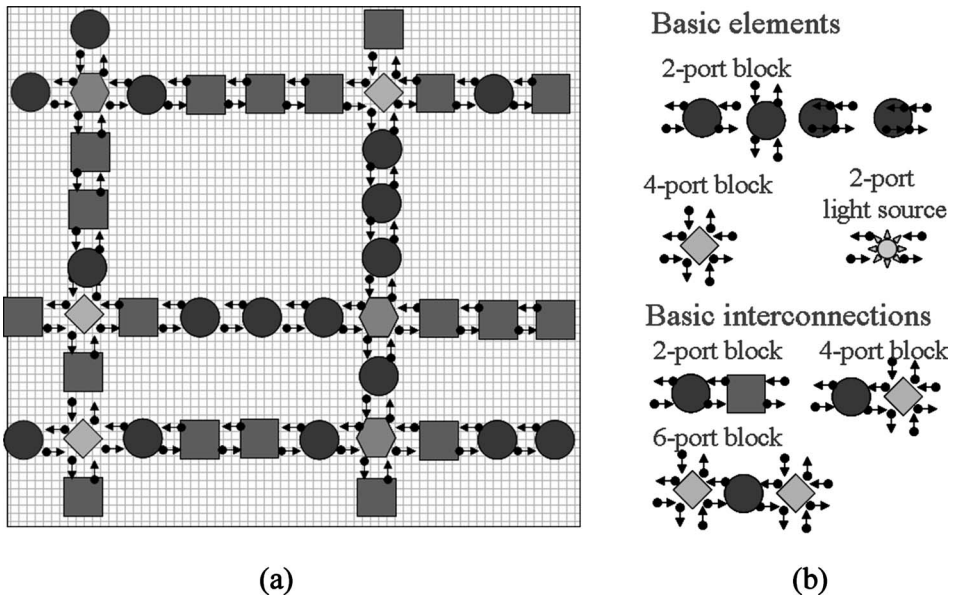

Fig. 1. (a) Schematic of nanophotonic network, (b) basic elements and interconnections.

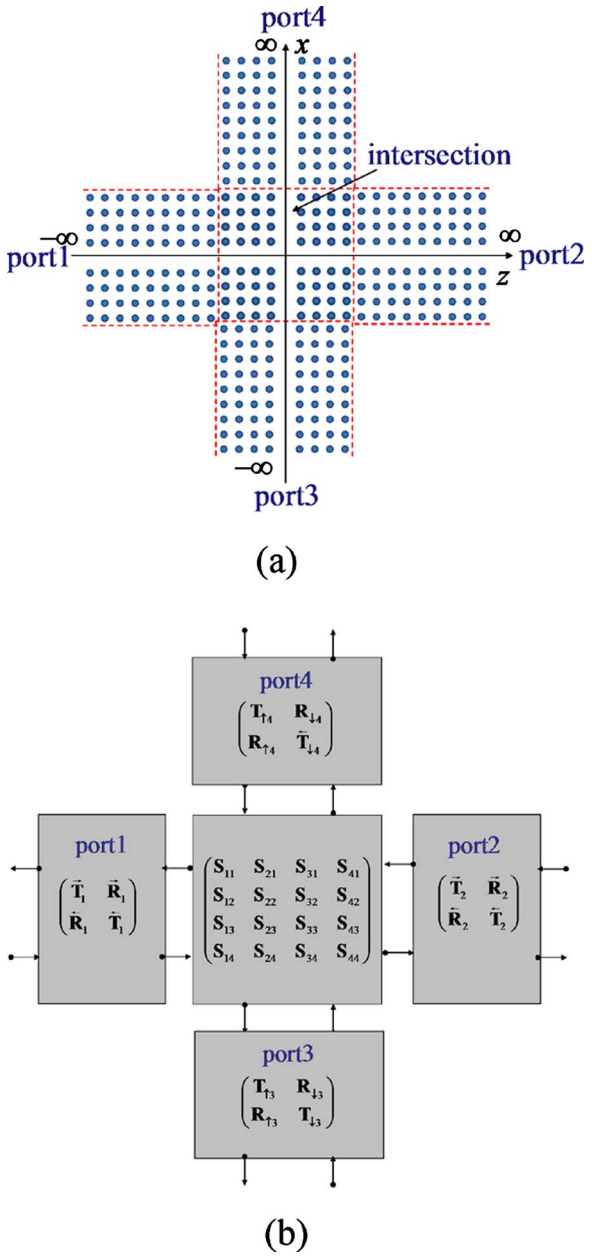

Fig. 2. (Color online) (a) Photonic crystal cross waveguide structure, (b) S-matrix diagram of the photonic crystal cross waveguide structure.

In two-dimensional geometry, four vertex points (x_+,z_-), (x_+,z_+), (x_-,z_-), and (x_-,z_+) define the four boundaries where the cross block contacts ports 1–4. Figure 2(b) shows the S-matrix diagram of photonic crystal cross-waveguide structure.

For building the mathematical modeling of the described nanophotonic structures, the following basic elements should be prepared.

(i) S matrices, Bloch eigenmodes represented by pseudo-Fourier series, coupling coefficient operators of two-port blocks placed along the transverse direction and the longitudinal direction.

(ii) S matrices, Bloch eigenmodes represented by pseudo-Fourier series, coupling coefficient operators of four-port blocks.

(iii) Generalized recursion formulas for interconnecting the S matrices of composing blocks and updating internal coupling coefficients operators of each block.

The analysis will be processed step-by-step. After completing the analysis of the 4×4 S matrix of the four-port intersection block, ports 1–4 will be connected to the intersection block consecutively. At each stage, the S matrices of the combined blocks will be updated. The detail of this interconnection will be manifested in Section 5.

The proposed modeling scheme is made up of two key subtheories, LFMA and GSMM. The main task of the LFMA is to analyze the Bloch eigenmodes as the form of the pseudo-Fourier representation and to manifest the S matrix and the coupling coefficient matrix operator of the block. Conventional FMM is only applied to a one-dimensionally layered structure, i.e., a two-port block structure. The application of the conventional SMM is restricted to two-port block structures with the combination with the FMM. This property has been considered an inherent limitation of the FMMs. However, the proposed LFMA overcomes this limitation and can successfully analyze the four-port cross blocks with four boundaries. Furthermore, the interconnections of two- and two-port blocks, four- and two-port blocks, and four- and four-port blocks are systematically described by the proposed GSMM.

In the LFMA, the local Fourier representation of internal Bloch eigenmodes is identified as the mathematical basis of internal electromagnetic field distributions and the coupling coefficients of each eigenmode are determined to satisfy the transverse field continuation conditions at the given four boundaries. The relationships between coupling coefficients of Bloch eigenmodes within each block in the interconnected structures are described by the GSMM. The proposed analysis of four-port crossed nanophotonic structures provides a basic framework for the general analysis of complex large-scale integrated nanophotonic networks.

3. LOCAL FOURIER MODAL ANALYSIS OF TWO-PORT BLOCKS

In this section, the LFMA of two-port blocks is described. The S matrix and coupling coefficient matrix operator of two-port blocks are analyzed by the LFMA.

The Bloch eigenmodes of the Maxwell equations take the form of the pseudo-Fourier series

$$\underline{\tilde{E}}_k = \exp(j(k_{x,0}x + k_{y,0}y + k_{z,0}z))\underline{E}_k(x,y,z), \tag{3a}$$

$$\underline{\tilde{H}}_k = \exp(j(k_{x,0}x + k_{y,0}y + k_{z,0}z))\underline{H}_k(x,y,z), \tag{3b}$$

where the mode envelops $\underline{E}_k(x,y,z)$ and $\underline{H}_k(x,y,z)$ are periodic functions with respect to x, y, and z and $\underline{k}$ indicates the wave vector $(k_{x,0},k_{y,0},k_{z,0})$. Let us consider a Q-layer multilayer block $M^{(1,Q)}$ with the longitudinal size of Λ_z as shown in Fig. 3(a). The S-matrix $\mathbf{S}^{(1,Q)}$ and coupling coefficient matrix operators $\tilde{\mathbf{C}}_a$ and $\tilde{\mathbf{C}}_b$ give a complete characterization of the electromagnetic properties of the block [see Fig. 3(b)].

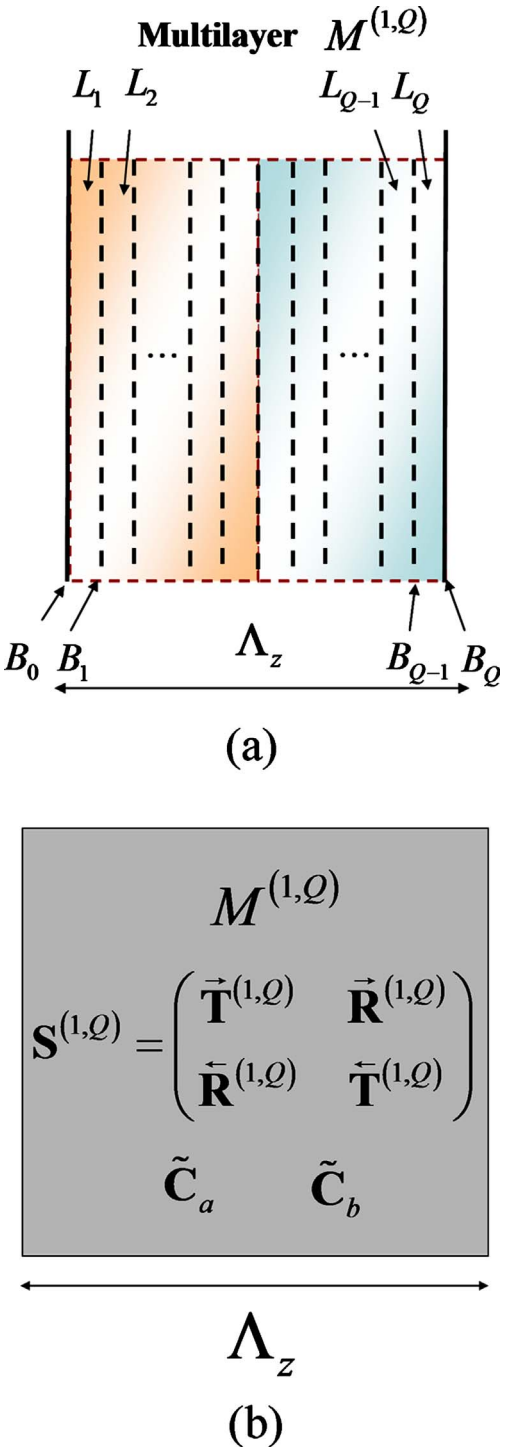

Fig. 3. (Color online) (a) Multilayer structure and (b) S-matrix and coupling coefficient matrix operator.

In addition, we can extract the Bloch eigenmodes by solving the Bloch-mode eigenvalue equation [25] formulated by the rigorous coupled-wave analysis (RCWA) method and the extended scattering-matrix method (ESMM) [11,20]. In Fig. 4(a), the concept of the Bloch-mode computation with the ESMM is illustrated. The field profile of a Bloch eigenmode at the right boundary takes the form of the field profile at the left boundary multiplied by the eigenvalue $\beta=\exp(jk_{z,0})$ as indicated in Fig. 3(b).

Let the Fourier spectra of the right- and left-direction propagating portions of a Bloch eigenmode at the left boundary denoted by $\vec{w}$ and $\overleftarrow{w}$, respectively. Then $\vec{w}$ and $\overleftarrow{w}$ should satisfy the Bloch mode condition

$$\begin{bmatrix} \beta\vec{w} \\ \overleftarrow{w} \end{bmatrix} = \begin{pmatrix} \vec{\mathbf{T}}^{(1,Q)} & \vec{\mathbf{R}}^{(1,Q)} \\ \overleftarrow{\mathbf{R}}^{(1,Q)} & \overleftarrow{\mathbf{T}}^{(1,Q)} \end{pmatrix} \begin{bmatrix} \vec{w} \\ \beta\overleftarrow{w} \end{bmatrix}, \tag{4a}$$

where $\vec{\mathbf{T}}^{(1,Q)}$, $\vec{\mathbf{R}}^{(1,Q)}$, $\overleftarrow{\mathbf{R}}^{(1,Q)}$, and $\overleftarrow{\mathbf{T}}^{(1,Q)}$ are the S-matrix components of the multilayer $M^{(1,Q)}$. Equation (4a) can be manipulated to the eigenvalue equation with β as the eigenvalue:

$$\begin{pmatrix} \vec{\mathbf{T}}^{(1,Q)} & \mathbf{0} \\ \overleftarrow{\mathbf{R}}^{(1,Q)} & -\mathbf{I} \end{pmatrix} \begin{bmatrix} \vec{w} \\ \overleftarrow{w} \end{bmatrix} = \beta \begin{pmatrix} \mathbf{I} & -\vec{\mathbf{R}}^{(1,Q)} \\ \mathbf{0} & -\overleftarrow{\mathbf{T}}^{(1,Q)} \end{pmatrix} \begin{bmatrix} \vec{w} \\ \overleftarrow{w} \end{bmatrix}. \tag{4b}$$

Let the gth eigenvalue and eigenvector of Eq. (4b) be denoted by β_g and $(\vec{w}_g, \overleftarrow{w}_g)$. Then the internal coupling coefficient of the gth Bloch eigenmode is determined by, from Eqs. (11e) and (11f) of [20],

$$\mathbf{C}_g = \tilde{\mathbf{C}}_a \vec{w}_g + \beta_g \tilde{\mathbf{C}}_b \overleftarrow{w}_g. \tag{5}$$

In practical implementation, for confirming the numerical stability in solving Eq. (4b), a two-step eigenvalue analysis should be adopted. Let the eigenvalues of the positive and negative eigenmodes be denoted by $\beta^+ = \exp(jk_{z,0}^+)$ and $\beta^- = \exp(jk_{z,0}^-)$, respectively. The absolute value of the eigenvalue of negative eigenmode β^- can be so large to exceed the precision limitation of practical computers. As illustrated in Fig. 4, the eigenvalue equa-

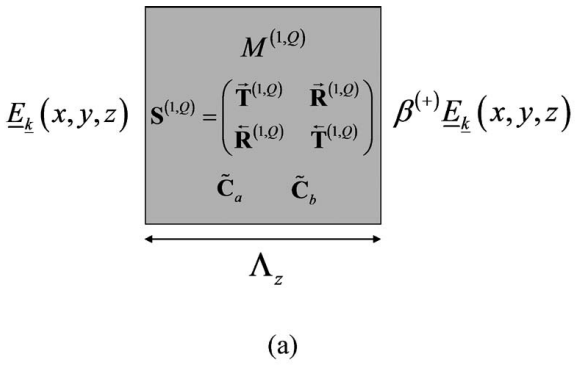

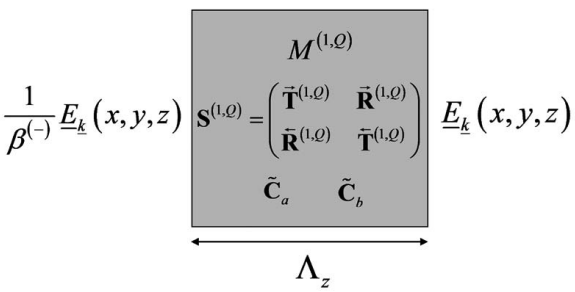

Fig. 4. Schematics of eigenvalue equations of (a) positive and (b) negative Bloch eigenmodes.

tions for obtaining positive and negative eigenmodes are taken, respectively, as

$$\begin{pmatrix} \vec{\mathbf{T}}^{(1,Q)} & \mathbf{0} \\ \vec{\mathbf{R}}^{(1,Q)} & -\mathbf{I} \end{pmatrix} \begin{bmatrix} \vec{w} \\ \vec{w} \end{bmatrix} = \beta^{+} \begin{pmatrix} \mathbf{I} & -\vec{\mathbf{R}}^{(1,Q)} \\ \mathbf{0} & -\vec{\mathbf{T}}^{(1,Q)} \end{pmatrix} \begin{bmatrix} \vec{w} \\ \vec{w} \end{bmatrix}, \quad (6a)$$

$$\frac{1}{\beta^{-}} \begin{pmatrix} \vec{\mathbf{T}}^{(1,Q)} & \mathbf{0} \\ \vec{\mathbf{R}}^{(1,Q)} & -\mathbf{I} \end{pmatrix} \begin{bmatrix} \vec{w} \\ \vec{w} \end{bmatrix} = \begin{pmatrix} \mathbf{I} & -\vec{\mathbf{R}}^{(1,Q)} \\ \mathbf{0} & -\vec{\mathbf{T}}^{(1,Q)} \end{pmatrix} \begin{bmatrix} \vec{w} \\ \vec{w} \end{bmatrix}. \quad (6b)$$

Now, the obtained Bloch eigenmode holds the conventional form of the RCWA, i.e., separate two-dimensional pseudo-Fourier representation at each staircase layer with its own coupling coefficients given as

$$\underline{E}^{(1,Q)}_{(q),g} = \sum_{m=-M}^{M} \sum_{n=-N}^{N} [\underline{x} E^{(1,Q)}_{(q),x,mng}(z) + \underline{y} E^{(1,Q)}_{(q),y,mng}(z) + \underline{z} E^{(1,Q)}_{(q),z,mng}(z)] \exp[j(k_{x,m}x + k_{y,n}y)], \quad (7a)$$

$$\underline{H}^{(1,Q)}_{(q),g} = \sum_{m=-M}^{M} \sum_{n=-N}^{N} [\underline{x} H^{(1,Q)}_{(q),x,mng}(z) + \underline{y} H^{(1,Q)}_{(q),y,mng}(z) + \underline{z} H^{(1,Q)}_{(q),z,mng}(z)] \exp[j(k_{x,m}x + k_{y,n}y)], \quad (7b)$$

where q is the layer index for $1 \le q \le Q$ and $\underline{x}$, $\underline{y}$, and $\underline{z}$ indicate unit directional vectors. It is noted that the Fourier coefficients of the electric field and the magnetic field in Eqs. (7a) and (7b) are functions of the z variable. Let d_q denote the thickness of the qth layer and $l_{n,n+m}$ be defined by $l_{n,n+m} = d_n + d_{n+1} + \cdots d_{n+m}$. Using the simple discrete Fourier transform (DFT), we can find the equivalent Fourier expansion of these z-variable dependent Fourier coefficients as

$$\begin{aligned} &\exp(-jk^{(g)}_{z,0}) E^{(1,Q)}_{(1),x,mng}(z) && \text{for } 0 \le z \le l_{1,1} \\ &\exp(-jk^{(g)}_{z,0}) E^{(1,Q)}_{(2),x,mng}(z) && \text{for } l_{1,1} \le z \le l_{1,2} \\ &\quad \vdots \\ &\exp(-jk^{(g)}_{z,0}) E^{(1,Q)}_{(Q),x,mng}(z) && \text{for } l_{1,Q-1} \le z \le l_{1,Q} \\ &\approx \sum_{p=-H}^{H} E^{(g)}_{x,m,n,p} \exp(jG_{z,p}z), \end{aligned} \quad (8)$$

where $G_{z,p}$ is the z-direction reciprocal vector defined by $G_{z,p} = (2\pi/\Lambda_z)p$. By the same manner, we can find the equivalent Fourier expansion of other Fourier coefficients. Therefore, the gth Bloch eigenmode takes the pseudo-Fourier representation as

$$\underline{E}_{(g)}(x,y,z) = \sum_{m=-M}^{M} \sum_{n=-N}^{N} \sum_{p=-H}^{H} (E^{(g)}_{x,m,n,p}\underline{x} + E^{(g)}_{y,m,n,p}\underline{y} + E^{(g)}_{z,m,n,p}\underline{z}) \exp(j(k_{x,m}x + k_{y,n}y + k^{(g)}_{z,p}z)), \quad (9a)$$

$$\underline{H}_{(g)}(x,y,z) = \sum_{m=-M}^{M} \sum_{n=-N}^{N} \sum_{p=-H}^{H} (H^{(g)}_{x,m,n,p}\underline{x} + H^{(g)}_{y,m,n,p}\underline{y} + H^{(g)}_{z,m,n,p}\underline{z}) \exp(j(k_{x,m}x + k_{y,n}y + k^{(g)}_{z,p}z)), \quad (9b)$$

where $k^{(g)}_{z,p}$ is defined by $k^{(g)}_{z,p} = k^{(g)}_{z,0} + 2\pi p/\Lambda_z$. This pseudo-Fourier representation is a basis for unfolding the LFMA of the four-port intersection block in Section 4, which is a key feature of the proposed LFMA mostly distinguished from the conventional expressions, Eqs. (7a) and (7b), of the conventional FMM. After obtaining the eigenvalues and eigenvectors of the main eigenvalue equation (4b), the obtained eigenmodes must be classified into two categories, positive (forward) and negative (backward) modes, with respect to eigenvalues holding one of the forms, $jk^{(g)}_{z,0} = a^{(g)} + jb^{(g)}$, $jk^{(g)}_{z,0} = a^{(g)} - jb^{(g)}$, $jk^{(g)}_{z,0} = -a^{(g)} + jb^{(g)}$, and $jk^{(g)}_{z,0} = -a^{(g)} - jb^{(g)}$ where $a^{(g)} > 0$ and $b^{(g)} > 0$. The eigenmodes with eigenvalues of $jk^{(g)}_{z,0} = a^{(g)} + jb^{(g)}$ or $jk^{(g)}_{z,0} = a^{(g)} - jb^{(g)}$ are referred to as negative mode and the notation $k^{(g)-}_{z,0}$ with the minus superscript is used to indicate the negative mode. The eigenmodes with eigenvalues of $jk^{(g)}_{z,0} = -a^{(g)} + jb^{(g)}$ and $jk^{(g)}_{z,0} = -a^{(g)} - jb^{(g)}$ are referred to as positive mode and the notation $k^{(g)+}_{z,0}$ with the plus superscript is used to indicate the positive mode. In particular, the eigenmodes with pure real eigenvalues of $jk^{(g)}_{z,0} = jb^{(g)}$ and $jk^{(g)}_{z,0} = -jb^{(g)}$ with $a^{(g)} = 0$ are classified to the positive mode. The numbers of the positive and negative modes are denoted by M^{+} and M^{-}, respectively. The sum of M^{+} and M^{-} is $M^{+} + M^{-} = 4(2M+1)(2N+1)$. With these conventions, the gth positive $(\underline{E}^{+}_{(g)}, \underline{H}^{+}_{(g)})$ and negative $(\underline{E}^{-}_{(g)}, \underline{H}^{-}_{(g)})$ eigenmodes are represented as, respectively,

$$\underline{E}^{\pm}_{(g)}(x,y,z) = \sum_{m=-M}^{M} \sum_{n=-N}^{N} \sum_{p=-M}^{M} (E^{(g)\pm}_{x,m,n,p}\underline{x} + E^{(g)\pm}_{y,m,n,p}\underline{y} + E^{(g)\pm}_{z,m,n,p}\underline{z}) \exp(j(k_{x,m}x + k_{y,n}y + k^{(g)\pm}_{z,p}z)), \quad (10a)$$

$$\underline{H}^{\pm}_{(g)}(x,y,z) = \sum_{m=-M}^{M} \sum_{n=-N}^{N} \sum_{p=-M}^{M} (H^{(g)\pm}_{x,m,n,p}\underline{x} + H^{(g)\pm}_{y,m,n,p}\underline{y} + H^{(g)\pm}_{z,m,n,p}\underline{z}) \exp(j(k_{x,m}x + k_{y,n}y + k^{(g)\pm}_{z,p}z)). \quad (10b)$$

The pseudo-Fourier representation of the Bloch eigenmodes is the essential factor in the modeling and analysis of four-port crossed nanophotonic structures that will be described in Section 4. Hereafter, the Bloch eigenmodes represented by the pseudo-Fourier series are adopted as the mathematical basis of the electromagnetic field distributions.

As an example of the described LFMA, the Bloch eigenmode analysis of a two-dimensional photonic crystal waveguide structure [26–29] is presented in Fig. 5. Figure 5(a) shows a two-dimensional photonic crystal waveguide. The period of the circular rod of the photonic crystal is denoted by a. The diameters of the rod, wavelength, and refractive index of the rod are set to $0.4a$, $2.44a$, and 3.4,

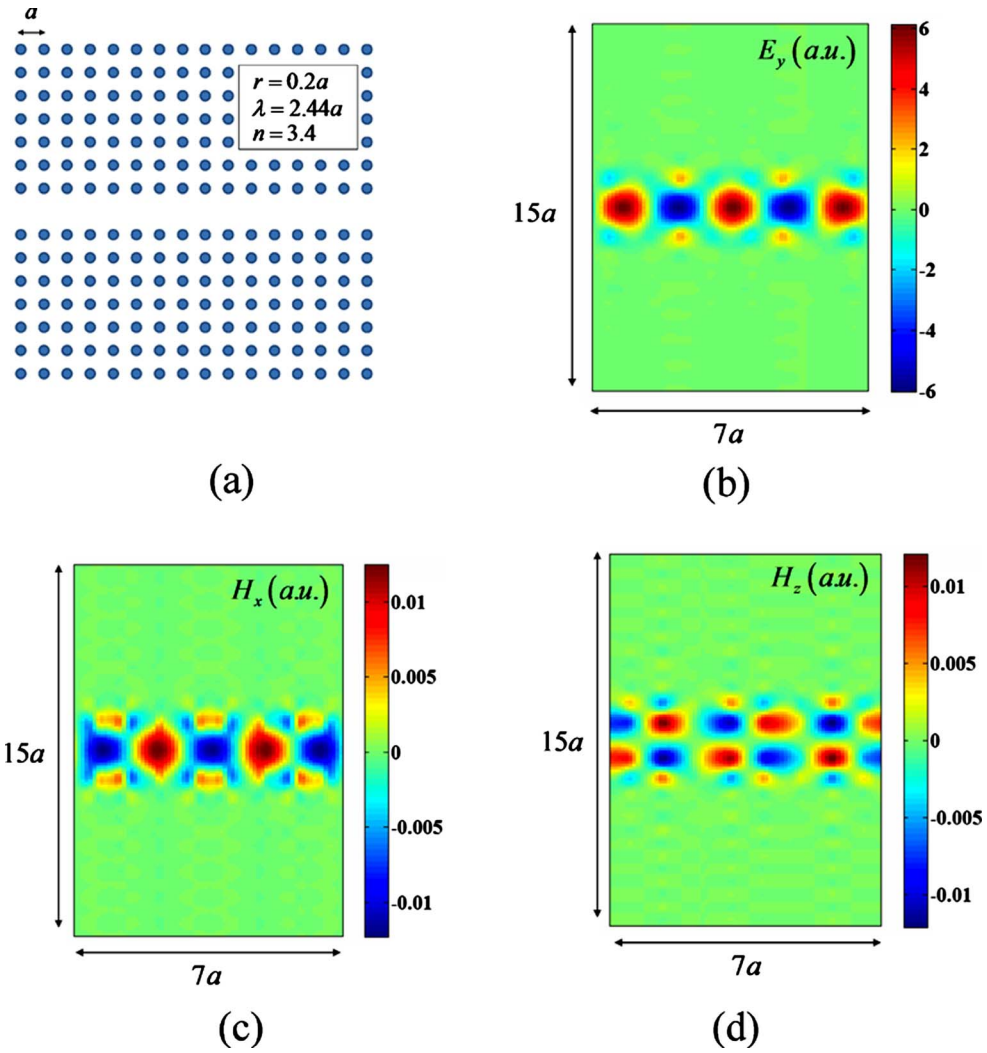

Fig. 5. (Color online) (a) Two-dimensional photonic crystal waveguide and the guided Bloch eigenmode: (b) y-polarization electric field distribution, (c) x-polarization magnetic field distribution, (d) z-polarization magnetic field distribution.

respectively. This waveguide structure is actually a single-mode waveguide. This point can be confirmed by analyzing the obtained eigenvalues. In Figs. 5(b)–5(d), the y-polarization electric field, x-polarization magnetic field, and z-polarization magnetic field distributions of the fundamental mode are presented, respectively.

For convenience, let the two-port blocks be placed along the transverse direction and those placed along the longitudinal direction be distinguished by the prefixes α and β, respectively. Figure 6 illustrates three kinds of α blocks: two-port α block with finite size, two-port half-infinite α block with right boundary, and two-port half-infinite α block with left boundary. On the other hand, Fig. 7 illustrates three kinds of β blocks: two-port β block with finite size, two-port half-infinite β block with upper boundary, and two-port half-infinite β block with lower boundary.

In the representation of the field distributions in α blocks, the subscript α is also used. The reciprocal vectors of α modes are denoted by $(k_{\alpha,x,m}, k_{\alpha,y,n}, k^{(g)}_{\alpha,z,p})$ and defined by

$$(k_{\alpha,x,m}, k_{\alpha,y,n}, k^{(g)}_{\alpha,z,p}) = \left(k_{x,0} + \frac{2\pi}{T_x}m, k_{y,0} + \frac{2\pi}{T_y}n, k^{(g)}_{\alpha,z} + \frac{2\pi}{T_z}p\right). \tag{11}$$

Then let us represent the Bloch eigenmodes of two-port α blocks as

$$\underline{E}^{\pm}_{\alpha,(g)}(x,y,z) = \sum_{m=-M}^{M}\sum_{n=-N}^{N}\sum_{p=-M}^{M} \times (E^{(g)\pm}_{\alpha,x,m,n,p}\underline{x} + E^{(g)\pm}_{\alpha,y,m,n,p}\underline{y} + E^{(g)\pm}_{\alpha,z,m,n,p}\underline{z}) \times \exp(j(k_{\alpha,x,m}x + k_{\alpha,y,n}y + k^{(g)\pm}_{\alpha,z,p}(z - z_{\mp}))), \tag{12a}$$

$$\underline{H}^{\pm}_{\alpha,(g)}(x,y,z) = \sum_{m=-M}^{M}\sum_{n=-N}^{N}\sum_{p=-M}^{M} \times (H^{(g)\pm}_{\alpha,x,m,n,p}\underline{x} + H^{(g)\pm}_{\alpha,y,m,n,p}\underline{y} + H^{(g)\pm}_{\alpha,z,m,n,p}\underline{z}) \times \exp(j(k_{\alpha,x,m}x + k_{\alpha,y,n}y + k^{(g)\pm}_{\alpha,z,p}(z - z_{\mp}))) \tag{12b}$$

In the representation of the field distributions in β blocks, the subscript β is used. The reciprocal vectors of β modes are denoted by $(k^{(g)}_{\beta,x,m}, k_{\beta,y,n}, k_{\beta,z,p})$ and defined by

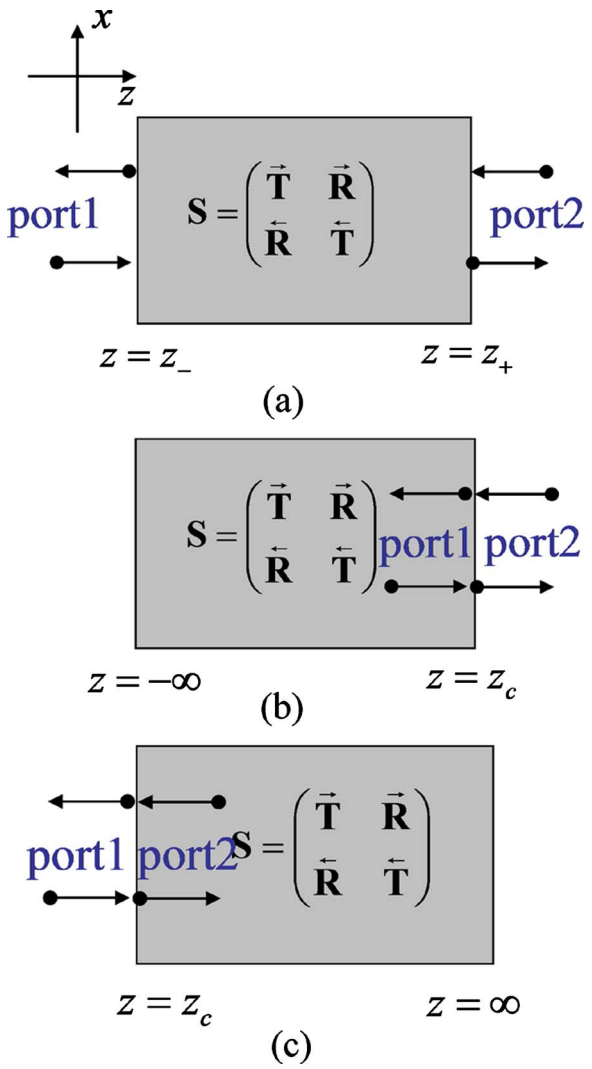

Fig. 6. (Color online) (a) Two-port α block with finite size, (b) two-port half-infinite α block with right boundary, (c) two-port half-infinite α block with left boundary.

$$(k^{(g)}_{\beta,x,m},k_{\beta,y,n},k_{\beta,z,p})=\left(k^{(g)}_{\beta,x,0}+\frac{2\pi}{T_x}m,k_{y,0}+\frac{2\pi}{T_y}n,k_{z,0}+\frac{2\pi}{T_z}p\right). \tag{13}$$

The Bloch eigenmodes of two-port β blocks are represented by the pseudo-Fourier series with the subscript β as

$$\underline{E}^{\pm}_{\beta,(g)}(x,y,z)=\sum_{m=-M}^{M}\sum_{n=-N}^{N}\sum_{p=-M}^{M}\times(E^{(g)\pm}_{\beta,x,m,n,p}\underline{x}+E^{(g)\pm}_{\beta,y,m,n,p}\underline{y}+E^{(g)\pm}_{\beta,z,m,n,p}\underline{z})\times\exp(j(k^{(g)\pm}_{\beta,x,m}(x-x_{\mp})+k_{\beta,y,n}y+k_{\beta,z,p}z)), \tag{14a}$$

$$\underline{H}^{\pm}_{\beta,(g)}(x,y,z)=\sum_{m=-M}^{M}\sum_{n=-N}^{N}\sum_{p=-M}^{M}\times(H^{(g)\pm}_{\beta,x,m,n,p}\underline{x}+H^{(g)\pm}_{\beta,y,m,n,p}\underline{y}+H^{(g)\pm}_{\beta,z,m,n,p}\underline{z})\times\exp(j(k^{(g)\pm}_{\beta,x,m}(x-x_{\mp})+k_{\beta,y,n}y+k_{\beta,z,p}z)). \tag{14b}$$

Let us note the meanings of the local coordinate of the β block, (x',y',z') shown in Fig. 7(a). In practical computation, β blocks are analyzed on the local coordinate (x',y',z') for convenience. When converting the information obtained in the local coordinate (x',y',z') to those in the default coordinate (x,y,z) a careful consideration of the following relations is required:

$$\varepsilon'(x',y',z')=\varepsilon(z',y',-x'), \tag{15a}$$

$$\mu'(x',y',z')=\mu(z',y',-x'), \tag{15b}$$

$$(E_{x,m,n,p},E_{y,m,n,p},E_{z,m,n,p})=(E_{z',p,n,-m},E_{y',p,n,-m},-E_{x',p,n,-m}), \tag{15c}$$

$$(H_{x,m,n,p},H_{y,m,n,p},H_{z,m,n,p})=(H_{z',p,n,-m},H_{y',p,n,-m},-H_{x',p,n,-m}). \tag{15d}$$

Next, the S matrices of two-port blocks are derived. In Fig. 8, the bidirectional characterization of a two-port α block with the left boundary at $z=z_-$ and right-boundary at $z=z_+$ is schematically presented. The S-matrix components are obtained by the following bidirectional charac-

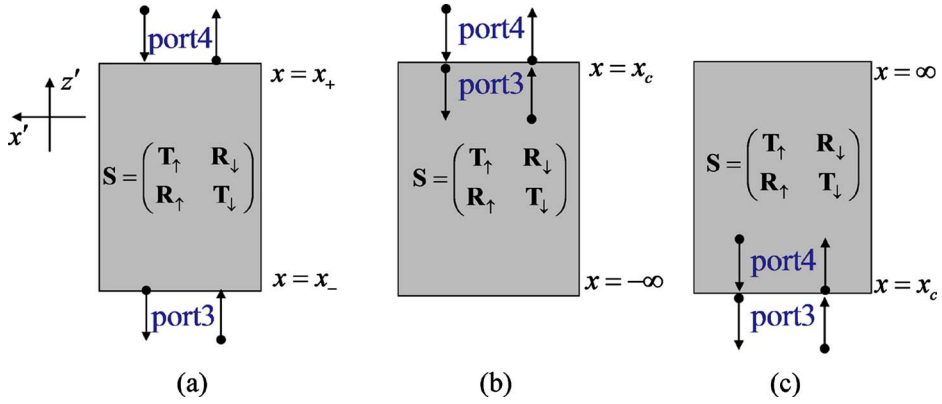

Fig. 7. (Color online) (a) Two-port β block with finite size, (b) two-port half-infinite β block with upper boundary, (c) two-port half-infinite β block with lower boundary.

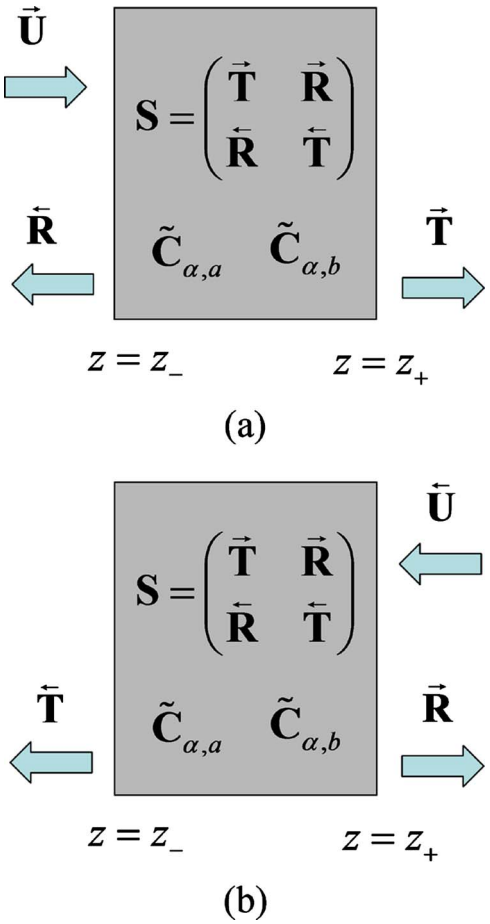

Fig. 8. (Color online) (a) Left-to-right and (b) right-to-left directional characterizations. The left and right boundaries are set at $z=z_-$ and z_+, respectively.

terization procedure. Let us consider the left-to-right directional characterization of the multilayer for obtaining the layer S matrix of this structure, $\mathbf{S}$. The excitation field of the left boundary, $\underline{\vec{U}}$, the reflection field $\underline{\overleftarrow{R}}$, and the transmission field $\underline{\vec{T}}$ are given, respectively, by

$$\underline{\vec{U}}=\sum_{m=-M}^{M}\sum_{n=-N}^{N}(\vec{u}_{x,m,n}\underline{x}+\vec{u}_{y,m,n}\underline{y}+\vec{u}_{z,m,n}\underline{z})\times\exp(j(k_{x,m}x+k_{y,n}y+k_{z,m,n}(z-z_-))),\quad(16a)$$

$$\underline{\overleftarrow{R}}=\sum_{m=-M}^{M}\sum_{n=-N}^{N}(\overleftarrow{r}_{x,m,n}\underline{x}+\overleftarrow{r}_{y,m,n}\underline{y}+\overleftarrow{r}_{z,m,n}\underline{z})\times\exp(j(k_{x,m}x+k_{y,n}y-k_{z,m,n}(z-z_-))),\quad(16b)$$

$$\underline{\vec{T}}=\sum_{m=-M}^{M}\sum_{n=-N}^{N}(\vec{t}_{x,m,n}\underline{x}+\vec{t}_{y,m,n}\underline{y}+\vec{t}_{z,m,n}\underline{z})\times\exp(j(k_{x,m}x+k_{y,n}y+k_{z,m,n}(z-z_+))).\quad(16c)$$

By the same manner, the right-to-left characterization is performed. In the case of the right-to-left characterization; the excitation field of the right boundary, $\underline{\overleftarrow{U}}$; the reflection field $\underline{\vec{R}}$; and the transmission field $\underline{\overleftarrow{T}}$ are given, respectively, by

$$\underline{\overleftarrow{U}}=\sum_{m=-M}^{M}\sum_{n=-N}^{N}(\overleftarrow{u}_{x,m,n}\underline{x}+\overleftarrow{u}_{y,m,n}\underline{y}+\overleftarrow{u}_{z,m,n}\underline{z})\times\exp(j(k_{x,m}x+k_{y,n}y-k_{z,m,n}(z-z_+))),\quad(17a)$$

$$\underline{\vec{R}}=\sum_{m=-M}^{M}\sum_{n=-N}^{N}(\vec{r}_{x,m,n}\underline{x}+\vec{r}_{y,m,n}\underline{y}+\vec{r}_{z,m,n}\underline{z})\times\exp(j(k_{x,m}x+k_{y,n}y+k_{z,m,n}(z-z_+))),\quad(17b)$$

$$\underline{\overleftarrow{T}}=\sum_{m=-M}^{M}\sum_{n=-N}^{N}(\overleftarrow{t}_{x,m,n}\underline{x}+\overleftarrow{t}_{y,m,n}\underline{y}+\overleftarrow{t}_{z,m,n}\underline{z})\times\exp(j(k_{x,m}x+k_{y,n}y-k_{z,m,n}(z-z_+))).\quad(17c)$$

Then the transverse field continuation boundary conditions of the left-to-right characterization and the right-to-left characterization of the two-port α blocks read, respectively, as

$$\begin{pmatrix}\mathbf{W}_{\alpha,h} & \mathbf{W}_{\alpha,h}\\ \mathbf{V}_{\alpha,h} & -\mathbf{V}_{\alpha,h}\end{pmatrix}\begin{pmatrix}\vec{\mathbf{U}}\\ \overleftarrow{\mathbf{R}}\end{pmatrix}=\begin{pmatrix}\mathbf{W}_{\alpha,+}(0) & \mathbf{W}_{\alpha,-}(z_--z_+)\\ \mathbf{V}_{\alpha,+}(0) & \mathbf{V}_{\alpha,-}(z_--z_+)\end{pmatrix}\times\begin{pmatrix}\mathbf{C}^+_{\alpha,a}\\ \mathbf{C}^-_{\alpha,a}\end{pmatrix}\quad\text{at } z=z_-,\quad(18a)$$

$$\begin{pmatrix}\mathbf{W}_{\alpha,h} & \mathbf{W}_{\alpha,h}\\ \mathbf{V}_{\alpha,h} & -\mathbf{V}_{\alpha,h}\end{pmatrix}\begin{pmatrix}\vec{\mathbf{T}}\\ \mathbf{0}\end{pmatrix}=\begin{pmatrix}\mathbf{W}_{\alpha,+}(z_+-z_-) & \mathbf{W}_{\alpha,-}(0)\\ \mathbf{V}_{\alpha,+}(z_+-z_-) & \mathbf{V}_{\alpha,-}(0)\end{pmatrix}\times\begin{pmatrix}\mathbf{C}^+_{\alpha,a}\\ \mathbf{C}^-_{\alpha,a}\end{pmatrix}\quad\text{at } z=z_+,\quad(18b)$$

$$\begin{pmatrix}\mathbf{W}_{\alpha,h} & \mathbf{W}_{\alpha,h}\\ \mathbf{V}_{\alpha,h} & -\mathbf{V}_{\alpha,h}\end{pmatrix}\begin{pmatrix}\mathbf{0}\\ \overleftarrow{\mathbf{T}}\end{pmatrix}=\begin{pmatrix}\mathbf{W}_{\alpha,+}(0) & \mathbf{W}_{\alpha,-}(z_--z_+)\\ \mathbf{V}_{\alpha,+}(0) & \mathbf{V}_{\alpha,-}(z_--z_+)\end{pmatrix}\times\begin{pmatrix}\mathbf{C}^+_{\alpha,b}\\ \mathbf{C}^-_{\alpha,b}\end{pmatrix}\quad\text{at } z=z_-,\quad(18c)$$

$$\begin{pmatrix}\mathbf{W}_{\alpha,h} & \mathbf{W}_{\alpha,h}\\ \mathbf{V}_{\alpha,h} & -\mathbf{V}_{\alpha,h}\end{pmatrix}\begin{pmatrix}\overleftarrow{\mathbf{R}}\\ \overleftarrow{\mathbf{U}}\end{pmatrix}=\begin{pmatrix}\mathbf{W}_{\alpha,+}(z_+-z_-) & \mathbf{W}_{\alpha,-}(0)\\ \mathbf{V}_{\alpha,+}(z_+-z_-) & \mathbf{V}_{\alpha,-}(0)\end{pmatrix}\times\begin{pmatrix}\mathbf{C}^+_{\alpha,b}\\ \mathbf{C}^-_{\alpha,b}\end{pmatrix}\quad\text{at } z=z_+,\quad(18d)$$

where $\mathbf{W}_{\alpha,h}$ and $\mathbf{V}_{\alpha,h}$ are $[2(2M+1)(2N+1)]\times[2(2M+1)\times(2N+1)]$ matrices given, respectively, by

$$\mathbf{W}_{\alpha,h}=\begin{pmatrix}I & 0\\ 0 & I\end{pmatrix},\quad(19a)$$

$$\mathbf{V}_{\alpha,h}=\begin{pmatrix}\frac{1}{\omega\mu_0}\frac{k_{\alpha,x,m}k_{\alpha,y,n}}{k_{\alpha,z,m,n}} & \frac{1}{\omega\mu_0}\frac{(k^2_{\alpha,z,m,n}+k^2_{\alpha,x,m})}{k_{\alpha,z,m,n}}\\ -\frac{1}{\omega\mu_0}\frac{(k^2_{\alpha,y,n}+k^2_{\alpha,z,m,n})}{k_{\alpha,z,m,n}} & -\frac{1}{\omega\mu_0}\frac{k_{\alpha,y,n}k_{\alpha,x,m}}{k_{\alpha,z,m,n}}\end{pmatrix}.\quad(19b)$$

$\mathbf{W}_{\alpha,+}(z)$ and $\mathbf{V}_{\alpha,+}(z)$ are $[2(2M+1)(2N+1)]\times M^{+}$ matrices indicating the part of the positive modes given, respectively, by

$$\mathbf{W}_{\alpha,+}(z)=\begin{pmatrix}\sum_{p=-H}^{H}\tilde{E}^{(1)+}_{\alpha,y,m,n,p}e^{jk^{(1)+}_{\alpha,z,p}z} & \cdots & \sum_{p=-H}^{H}\tilde{E}^{(M^{+})+}_{\alpha,y,m,n,p}e^{jk^{(M^{+})+}_{\alpha,z,p}z}\\ \sum_{p=-H}^{H}\tilde{E}^{(1)+}_{\alpha,x,m,n,p}e^{jk^{(1)+}_{\alpha,z,p}z} & \cdots & \sum_{p=-H}^{H}\tilde{E}^{(M^{+})+}_{\alpha,x,m,n,p}e^{jk^{(M^{+})+}_{\alpha,z,p}z}\end{pmatrix}, \tag{19c}$$

$$\mathbf{V}_{\alpha,+}(z)=\begin{pmatrix}\sum_{p=-H}^{H}\tilde{H}^{(1)+}_{\alpha,y,m,n,p}e^{jk^{(1)+}_{\alpha,z,p}z} & \cdots & \sum_{p=-H}^{H}\tilde{H}^{(M^{+})+}_{\alpha,y,m,n,p}e^{jk^{(M^{+})+}_{\alpha,z,p}z}\\ \sum_{p=-H}^{H}\tilde{H}^{(1)+}_{\alpha,x,m,n,p}e^{jk^{(1)+}_{\alpha,z,p}z} & \cdots & \sum_{p=-H}^{H}\tilde{H}^{(M^{+})+}_{\alpha,x,m,n,p}e^{jk^{(M^{+})+}_{\alpha,z,p}z}\end{pmatrix}. \tag{19d}$$

$\mathbf{W}_{\alpha,-}(z)$ and $\mathbf{V}_{\alpha,-}(z)$ are $[2(2M+1)(2N+1)]\times M^{-}$ matrices indicating the part of the negative modes, given, respectively, by

$$\mathbf{W}_{\alpha,-}(z)=\begin{pmatrix}\sum_{p=-H}^{H}\tilde{E}^{(1)-}_{\alpha,y,m,n,p}e^{jk^{(1)-}_{\alpha,z,p}z} & \cdots & \sum_{p=-H}^{H}\tilde{E}^{(M-)-}_{\alpha,y,m,n,p}e^{jk^{(M-)-}_{\alpha,z,p}z}\\ \sum_{p=-H}^{H}\tilde{E}^{(1)-}_{\alpha,x,m,n,p}e^{jk^{(1)-}_{\alpha,z,p}z} & \cdots & \sum_{p=-H}^{H}\tilde{E}^{(M^{-})-}_{\alpha,x,m,n,p}e^{jk^{(M^{-})-}_{\alpha,z,p}z}\end{pmatrix}, \tag{19e}$$

$$\mathbf{V}_{\alpha,-}(z)=\begin{pmatrix}\sum_{p=-H}^{H}\tilde{H}^{(1)-}_{\alpha,y,m,n,p}e^{jk^{(1)-}_{\alpha,z,p}z} & \cdots & \sum_{p=-H}^{H}\tilde{H}^{(M^{-})-}_{\alpha,y,m,n,p}e^{jk^{(M^{-})-}_{\alpha,z,p}z}\\ \sum_{p=-H}^{H}\tilde{H}^{(1)-}_{\alpha,x,m,n,p}e^{jk^{(1)-}_{\alpha,z,p}z} & \cdots & \sum_{p=-H}^{H}\tilde{H}^{(M^{-})-}_{\alpha,x,m,n,p}e^{jk^{(M^{-})-}_{\alpha,z,p}z}\end{pmatrix}. \tag{19f}$$

$\vec{\mathbf{U}}$ and $\overleftarrow{\mathbf{U}}$ are the input operator, $[2(2M+1)(2N+1)]\times[2(2M+1)(2N+1)]$ identity matrices. $\overleftarrow{\mathbf{R}}$,$\vec{\mathbf{R}}$, and $\vec{\mathbf{T}}$,$\overleftarrow{\mathbf{T}}$ are the reflection and transmission coefficient matrix operators, respectively.

The coupling coefficient operators S-matrix components, $\mathbf{C}^{+}_{\alpha,a}$, $\mathbf{C}^{-}_{\alpha,a}$, $\mathbf{C}^{+}_{\alpha,b}$, and $\mathbf{C}^{-}_{\alpha,b}$ are obtained by, from Eqs. (18a)–(18d),

$$\begin{bmatrix}\mathbf{C}^{+}_{\alpha,a}\\ \mathbf{C}^{-}_{\alpha,a}\end{bmatrix}=\begin{pmatrix}\mathbf{W}^{-1}_{\alpha,h}\mathbf{W}_{\alpha,+}(0)+\mathbf{V}^{-1}_{\alpha,h}\mathbf{V}_{\alpha,+}(0)\\ \mathbf{W}^{-1}_{\alpha,h}\mathbf{W}_{\alpha,+}(z_{+}-z_{-})-\mathbf{V}^{-1}_{\alpha,h}\mathbf{V}_{\alpha,+}(z_{+}-z_{-})\end{pmatrix}\begin{pmatrix}\mathbf{W}^{-1}_{\alpha,h}\mathbf{W}_{\alpha,-}(z_{-}-z_{+})+\mathbf{V}^{-1}_{\alpha,h}\mathbf{V}_{\alpha,-}(z_{-}-z_{+})\\ \mathbf{W}^{-1}_{\alpha,h}\mathbf{W}_{\alpha,-}(0)-\mathbf{V}^{-1}_{\alpha,h}\mathbf{V}_{\alpha,-}(0)\end{pmatrix}^{-1}\begin{bmatrix}2\vec{\mathbf{U}}\\ \mathbf{0}\end{bmatrix}, \tag{20a}$$

$$\begin{bmatrix}\mathbf{C}^{+}_{\alpha,b}\\ \mathbf{C}^{-}_{\alpha,b}\end{bmatrix}=\begin{pmatrix}\mathbf{W}^{-1}_{\alpha,h}\mathbf{W}_{\alpha,+}(0)+\mathbf{V}^{-1}_{\alpha,h}\mathbf{V}_{\alpha,+}(0)\\ \mathbf{W}^{-1}_{\alpha,h}\mathbf{W}_{\alpha,+}(z_{+}-z_{-})-\mathbf{V}^{-1}_{\alpha,h}\mathbf{V}_{\alpha,+}(z_{+}-z_{-})\end{pmatrix}\begin{pmatrix}\mathbf{W}^{-1}_{\alpha,h}\mathbf{W}_{\alpha,-}(z_{-}-z_{+})+\mathbf{V}^{-1}_{\alpha,h}\mathbf{V}_{\alpha,-}(z_{-}-z_{+})\\ \mathbf{W}^{-1}_{\alpha,h}\mathbf{W}_{\alpha,-}(0)-\mathbf{V}^{-1}_{\alpha,h}\mathbf{V}_{\alpha,-}(0)\end{pmatrix}^{-1}\begin{bmatrix}\mathbf{0}\\ 2\overleftarrow{\mathbf{U}}\end{bmatrix}. \tag{20b}$$

Then, the layer S-matrix components, $\overleftarrow{\mathbf{R}}$, $\vec{\mathbf{T}}$, $\vec{\mathbf{R}}$, and $\overleftarrow{\mathbf{T}}$, are given by

$$\overleftarrow{\mathbf{R}}=\mathbf{W}^{-1}_{\alpha,h}[\mathbf{W}_{\alpha,+}(0)\mathbf{C}^{+}_{\alpha,a}+\mathbf{W}_{\alpha,-}(z_{-}-z_{+})\mathbf{C}^{-}_{\alpha,a}-\mathbf{W}_{\alpha,h}], \tag{21a}$$

$$\vec{\mathbf{T}}=\mathbf{W}^{-1}_{\alpha,h}[\mathbf{W}_{\alpha,+}(z_{+}-z_{-})\mathbf{C}^{+}_{\alpha,a}+\mathbf{W}_{\alpha,-}(0)\mathbf{C}^{-}_{\alpha,a}], \tag{21b}$$

$$\vec{\mathbf{R}}=\mathbf{W}^{-1}_{\alpha,h}[\mathbf{W}_{\alpha,+}(z_{+}-z_{-})\mathbf{C}^{+}_{\alpha,b}+\mathbf{W}_{\alpha,-}(0)\mathbf{C}^{-}_{\alpha,b}-\mathbf{W}_{\alpha,h}], \tag{21c}$$

$$\overleftarrow{\mathbf{T}}=\mathbf{W}^{-1}_{\alpha,h}[\mathbf{W}_{\alpha,+}(0)\mathbf{C}^{+}_{\alpha,b}+\mathbf{W}_{\alpha,-}(z_{-}-z_{+})\mathbf{C}^{-}_{\alpha,b}]. \tag{21d}$$

The boundary S-matrix [20] components, $\overleftarrow{\mathbf{R}}$, $\vec{\mathbf{T}}$, $\vec{\mathbf{R}}$, and $\overleftarrow{\mathbf{T}}$ of the half-infinite α block with right boundary are given by

$$\begin{aligned}\overleftarrow{\mathbf{R}}=&-[(\mathbf{W}_{\alpha,h})^{-1}\mathbf{W}_{\alpha,-}(z_c)\\&-(\mathbf{V}_{\alpha,h})^{-1}\mathbf{V}_{\alpha,-}(z_c)]^{-1}[(\mathbf{W}_{\alpha,h})^{-1}\mathbf{W}_{\alpha,+}(z_c)\\&-(\mathbf{V}_{\alpha,h})^{-1}\mathbf{V}_{\alpha,+}(z_c)],\end{aligned} \tag{22a}$$

$$\begin{aligned}\vec{\mathbf{T}}=&[(\mathbf{W}_{\alpha,-}(z_c))^{-1}\mathbf{W}_{\alpha,h}\\&-(\mathbf{V}_{\alpha,-}(z_c))^{-1}\mathbf{V}_{\alpha,h}]^{-1}[(\mathbf{W}_{\alpha,-}(z_c))^{-1}\mathbf{W}_{\alpha,+}(z_c)\\&-(\mathbf{V}_{\alpha,-}(z_c))^{-1}\mathbf{V}_{\alpha,+}(z_c)],\end{aligned} \tag{22b}$$

$$\begin{aligned}\vec{\mathbf{R}}=&-[(\mathbf{W}_{\alpha,-}(z_c))^{-1}\mathbf{W}_{\alpha,h}\\&-(\mathbf{V}_{\alpha,-}(z_c))^{-1}\mathbf{V}_{\alpha,h}]^{-1}[(\mathbf{W}_{\alpha,-}(z_c))^{-1}\mathbf{W}_{\alpha,h}\\&+(\mathbf{V}_{\alpha,-}(z_c))^{-1}\mathbf{V}_{\alpha,h}],\end{aligned} \tag{22c}$$

$$\overleftarrow{\mathbf{T}}=2[(\mathbf{W}_{\alpha,h})^{-1}\mathbf{W}_{\alpha,-}(z_c)-(\mathbf{V}_{\alpha,h})^{-1}\mathbf{V}_{\alpha,-}(z_c)]^{-1}. \tag{22d}$$

The boundary S-matrix components, $\overleftarrow{\mathbf{R}}$, $\vec{\mathbf{T}}$, $\vec{\mathbf{R}}$, and $\overleftarrow{\mathbf{T}}$ of the half-infinite α block with left boundary are given by

$$\begin{aligned}\overleftarrow{\mathbf{R}}=&-[(\mathbf{W}_{\alpha,+}(z_c))^{-1}\mathbf{W}_{\alpha,h}+(\mathbf{V}_{\alpha,+}(z_c))^{-1}\mathbf{V}_{\alpha,h}]^{-1}\\&\times[(\mathbf{W}_{\alpha,+}(z_c))^{-1}\mathbf{W}_{\alpha,h}-(\mathbf{V}_{\alpha,+}(z_c))^{-1}\mathbf{V}_{\alpha,h}],\end{aligned} \tag{23a}$$

$$\vec{\mathbf{T}}=2[(\mathbf{W}_{\alpha,h})^{-1}\mathbf{W}_{\alpha,+}(z_c)+(\mathbf{V}_{\alpha,h})^{-1}\mathbf{V}_{\alpha,+}(z_c)]^{-1}, \tag{23b}$$

$$\begin{aligned}\vec{\mathbf{R}}=&-[(\mathbf{W}_{\alpha,h})^{-1}\mathbf{W}_{\alpha,+}(z_c)+(\mathbf{V}_{\alpha,h})^{-1}\mathbf{V}_{\alpha,+}(z_c)]^{-1}\\&\times[(\mathbf{W}_{\alpha,h})^{-1}\mathbf{W}_{\alpha,-}(z_c)+(\mathbf{V}_{\alpha,h})^{-1}\mathbf{V}_{\alpha,-}(z_c)],\end{aligned} \tag{23c}$$

$$\tilde{\mathbf{T}} = [(\mathbf{W}_{\alpha,+}(z_c))^{-1}\mathbf{W}_{\alpha,h} + (\mathbf{V}_{\alpha,+}(z_c))^{-1}\mathbf{V}_{\alpha,h}]^{-1}[(\mathbf{W}_{\alpha,+}(z_c))^{-1}\mathbf{W}_{\alpha,-}(z_c) - (\mathbf{V}_{\alpha,+}(z_c))^{-1}\mathbf{V}_{\alpha,-}(z_c)]. \quad (23d)$$

By a similar manner, we can derive the layer S matrix and the boundary S matrices from the transverse field continuation boundary conditions of the two-port β blocks. The boundary conditions of the down-to-up characterization and the up-to-down characterization of the two-port β blocks read, respectively, as

$$\begin{pmatrix} \mathbf{Y}_{\beta,h} & \mathbf{Y}_{\beta,h} \\ \mathbf{Z}_{\beta,h} & -\mathbf{Z}_{\beta,h} \end{pmatrix}\begin{pmatrix} \mathbf{U}_{\uparrow} \\ \mathbf{R}_{\downarrow} \end{pmatrix} = \begin{pmatrix} \mathbf{Y}_{\beta,+}(0) & \mathbf{Y}_{\beta,-}(x_- - x_+) \\ \mathbf{Z}_{\beta,+}(0) & \mathbf{Z}_{\beta,-}(x_- - x_+) \end{pmatrix} \times \begin{pmatrix} \mathbf{C}^+_{\beta,a} \\ \mathbf{C}^-_{\beta,a} \end{pmatrix} \quad \text{at } x = x_-, \quad (24a)$$

$$\begin{pmatrix} \mathbf{Y}_{\beta,h} & \mathbf{Y}_{\beta,h} \\ \mathbf{Z}_{\beta,h} & -\mathbf{Z}_{\beta,h} \end{pmatrix}\begin{pmatrix} \mathbf{T}_{\uparrow} \\ \mathbf{0} \end{pmatrix} = \begin{pmatrix} \mathbf{Y}_{\beta,+}(x_+ - x_-) & \mathbf{Y}_{\beta,-}(0) \\ \mathbf{Z}_{\beta,+}(x_+ - x_-) & \mathbf{Z}_{\beta,-}(0) \end{pmatrix} \times \begin{pmatrix} \mathbf{C}^+_{\beta,a} \\ \mathbf{C}^-_{\beta,a} \end{pmatrix} \quad \text{at } x = x_+, \quad (24b)$$

$$\begin{pmatrix} \mathbf{Y}_{\beta,h} & \mathbf{Y}_{\beta,h} \\ \mathbf{Z}_{\beta,h} & -\mathbf{Z}_{\beta,h} \end{pmatrix}\begin{pmatrix} \mathbf{0} \\ \mathbf{T}_{\downarrow} \end{pmatrix} = \begin{pmatrix} \mathbf{Y}_{\beta,+}(0) & \mathbf{Y}_{\beta,-}(x_- - x_+) \\ \mathbf{Z}_{\beta,+}(0) & \mathbf{Z}_{\beta,-}(x_- - x_+) \end{pmatrix} \times \begin{pmatrix} \mathbf{C}^+_{\beta,b} \\ \mathbf{C}^-_{\beta,b} \end{pmatrix} \quad \text{at } x = x_-, \quad (24c)$$

$$\begin{pmatrix} \mathbf{Y}_{\beta,h} & \mathbf{Y}_{\beta,h} \\ \mathbf{Z}_{\beta,h} & -\mathbf{Z}_{\beta,h} \end{pmatrix}\begin{pmatrix} \mathbf{R}_{\uparrow} \\ \mathbf{U}_{\downarrow} \end{pmatrix} = \begin{pmatrix} \mathbf{Y}_{\beta,+}(x_+ - x_-) & \mathbf{Y}_{\beta,-}(0) \\ \mathbf{Z}_{\beta,+}(x_+ - x_-) & \mathbf{Z}_{\beta,-}(0) \end{pmatrix} \times \begin{pmatrix} \mathbf{C}^+_{\beta,b} \\ \mathbf{C}^-_{\beta,b} \end{pmatrix} \quad \text{at } x = x_+, \quad (24d)$$

where $\mathbf{Y}_{\beta,h}$ and $\mathbf{Z}_{\beta,h}$ are $[2(2M+1)(2N+1)]\times[2(2M+1)\times(2N+1)]$ matrices given, respectively, by

$$\mathbf{Y}_{\beta,h} = \begin{pmatrix} I & 0 \\ 0 & I \end{pmatrix}, \quad (25a)$$

$$\mathbf{Z}_{\beta,h} = \begin{pmatrix} -\frac{1}{\omega\mu_0}\frac{k_{\beta,z,m}k_{\beta,y,n}}{k_{\beta,x,m,n}} & -\frac{1}{\omega\mu_0}\frac{(k^2_{\beta,x,m,n}+k^2_{\beta,z,m})}{k_{\beta,x,m,n}} \\ \frac{1}{\omega\mu_0}\frac{(k^2_{\beta,y,n}+k^2_{\beta,x,m,n})}{k_{\beta,x,m,n}} & \frac{1}{\omega\mu_0}\frac{k_{\beta,y,n}k_{\beta,z,m}}{k_{\beta,x,m,n}} \end{pmatrix}. \quad (25b)$$

$\mathbf{Y}_{\beta,+}(z)$ and $\mathbf{Z}_{\beta,+}(z)$ are $[2(2M+1)(2N+1)]\times M^+$ matrices indicating the part of the positive modes given, respectively, by

$$\mathbf{Y}_{\beta,+}(x) = \begin{pmatrix} \sum_{m=-M}^{M} \tilde{E}^{(1)+}_{\beta,y,m,n,s} e^{jk^{(1)+}_{x,m}x} & \cdots & \sum_{m=-M}^{M} \tilde{E}^{(M^+)+}_{\beta,y,m,n,s} e^{jk^{(M^+)+}_{x,m}x} \\ \sum_{m=-M}^{M} \tilde{E}^{(1)+}_{\beta,z,m,n,s} e^{jk^{(1)+}_{x,m}x} & \cdots & \sum_{m=-M}^{M} \tilde{E}^{(M^+)+}_{\beta,z,m,n,s} e^{jk^{(M^+)+}_{x,m}x} \end{pmatrix}, \quad (25c)$$

$$\mathbf{Z}_{\beta,+}(x) = \begin{pmatrix} \sum_{m=-M}^{M} \tilde{H}^{(1)+}_{\beta,y,m,n,s} e^{jk^{(1)+}_{x,m}x} & \cdots & \sum_{m=-M}^{M} \tilde{H}^{(M^+)+}_{\beta,y,m,n,s} e^{jk^{(M^+)+}_{x,m}x} \\ \sum_{m=-M}^{M} \tilde{H}^{(1)+}_{\beta,z,m,n,s} e^{jk^{(1)+}_{x,m}x} & \cdots & \sum_{m=-M}^{M} \tilde{H}^{(M^+)+}_{\beta,z,m,n,s} e^{jk^{(M^+)+}_{x,m}x} \end{pmatrix}. \quad (25d)$$

$\mathbf{Y}_{\beta,-}(z)$ and $\mathbf{Z}_{\beta,-}(z)$ are $[2(2M+1)(2N+1)]\times M^-$ matrices indicating the part of the negative modes given respectively, by

$$\mathbf{Y}_{\beta,-}(x) = \begin{pmatrix} \sum_{m=-M}^{M} \tilde{E}^{(1)-}_{\beta,y,m,n,s} e^{jk^{(1)-}_{x,m}x} & \cdots & \sum_{m=-M}^{M} \tilde{E}^{(M^-)-}_{\beta,y,m,n,s} e^{jk^{(M^-)-}_{x,m}x} \\ \sum_{m=-M}^{M} \tilde{E}^{(1)-}_{\beta,z,m,n,s} e^{jk^{(1)-}_{x,m}x} & \cdots & \sum_{m=-M}^{M} \tilde{E}^{(M^-)-}_{\beta,z,m,n,s} e^{jk^{(M^-)-}_{x,m}x} \end{pmatrix}, \quad (25e)$$

$$\mathbf{Z}_{\beta,-}(x) = \begin{pmatrix} \sum_{m=-M}^{M} \tilde{H}^{(1)-}_{\beta,y,m,n,s} e^{jk^{(1)-}_{x,m}x} & \cdots & \sum_{m=-M}^{M} \tilde{H}^{(M^-)-}_{\beta,y,m,n,s} e^{jk^{(M^-)-}_{x,m}x} \\ \sum_{m=-M}^{M} \tilde{H}^{(1)-}_{\beta,z,m,n,s} e^{jk^{(1)-}_{x,m}x} & \cdots & \sum_{m=-M}^{M} \tilde{H}^{(M^-)-}_{\beta,z,m,n,s} e^{jk^{(M^-)-}_{x,m}x} \end{pmatrix}. \quad (25f)$$

The coupling coefficient operators S-matrix components, $\mathbf{C}^+_{\beta,a}$, $\mathbf{C}^-_{\beta,a}$, $\mathbf{C}^+_{\beta,b}$, and $\mathbf{C}^-_{\beta,b}$ are obtained, from Eqs. (24a)–(24d), by

$$\begin{bmatrix} \mathbf{C}^+_{\beta,a} \\ \mathbf{C}^-_{\beta,a} \end{bmatrix} = \begin{pmatrix} (\mathbf{Y}^{-1}_{\beta,h}\mathbf{Y}_{\beta,+}(0) + \mathbf{Z}^{-1}_{\beta,h}\mathbf{Z}_{\beta,+}(0)) & (\mathbf{Y}^{-1}_{\beta,h}\mathbf{Y}_{\beta,-}(x_- - x_+) + \mathbf{Z}^{-1}_{\beta,h}\mathbf{Z}_{\beta,-}(x_- - x_+)) \\ (\mathbf{Y}^{-1}_{\beta,h}\mathbf{Y}_{\beta,+}(x_+ - x_-) - \mathbf{Z}^{-1}_{\beta,h}\mathbf{Z}_{\beta,+}(x_+ - x_-)) & (\mathbf{Y}^{-1}_{\beta,h}\mathbf{Y}_{\beta,-}(0) - \mathbf{Z}^{-1}_{\beta,h}\mathbf{Z}_{\beta,-}(0)) \end{pmatrix}^{-1} \begin{bmatrix} 2\mathbf{U}_{\uparrow} \\ \mathbf{0} \end{bmatrix}, \quad (26a)$$

$$\begin{bmatrix} \mathbf{C}^+_{\beta,b} \\ \mathbf{C}^-_{\beta,b} \end{bmatrix} = \begin{pmatrix} (\mathbf{Y}^{-1}_{\beta,h}\mathbf{Y}_{\beta,+}(0) + \mathbf{Z}^{-1}_{\beta,h}\mathbf{Z}_{\beta,+}(0)) & (\mathbf{Y}^{-1}_{\beta,h}\mathbf{Y}_{\beta,-}(x_- - x_+) + \mathbf{Z}^{-1}_{\beta,h}\mathbf{Z}_{\beta,-}(x_- - x_+)) \\ (\mathbf{Y}^{-1}_{\beta,h}\mathbf{Y}_{\beta,+}(x_+ - x_-) - \mathbf{Z}^{-1}_{\beta,h}\mathbf{Z}_{\beta,+}(x_+ - x_-)) & (\mathbf{Y}^{-1}_{\beta,h}\mathbf{Y}_{\beta,-}(0) - \mathbf{Z}^{-1}_{\beta,h}\mathbf{Z}_{\beta,-}(0)) \end{pmatrix}^{-1} \begin{bmatrix} \mathbf{0} \\ 2\mathbf{U}_{\downarrow} \end{bmatrix}. \quad (26b)$$

The layer S-matrix components, $\mathbf{R}_{\downarrow}$, $\mathbf{T}_{\uparrow}$, $\mathbf{R}_{\uparrow}$, and $\mathbf{T}_{\downarrow}$ of the two-port β block are given by

$$\mathbf{R}_{\downarrow} = \mathbf{Y}_{\beta,h}^{-1}[\mathbf{Y}_{\beta,+}(0)\mathbf{C}_{\beta,a}^{+} + \mathbf{Y}_{\beta,-}(x_- - x_+)\mathbf{C}_{\beta,a}^{-} - \mathbf{Y}_{\beta,h}], \tag{27a}$$

$$\mathbf{T}_{\uparrow} = \mathbf{Y}_{\beta,h}^{-1}[\mathbf{Y}_{\beta,+}(x_+ - x_-)\mathbf{C}_{\beta,a}^{+} + \mathbf{Y}_{\beta,-}(0)\mathbf{C}_{\beta,a}^{-}], \tag{27b}$$

$$\mathbf{R}_{\uparrow} = \mathbf{Y}_{\beta,h}^{-1}[\mathbf{Y}_{\beta,+}(x_+ - x_-)\mathbf{C}_{\beta,b}^{+} + \mathbf{Y}_{\beta,-}(0)\mathbf{C}_{\beta,b}^{-} - \mathbf{Y}_{\beta,h}], \tag{27c}$$

$$\mathbf{T}_{\downarrow} = \mathbf{Y}_{\beta,h}^{-1}[\mathbf{Y}_{\beta,+}(0)\mathbf{C}_{\beta,b}^{+} + \mathbf{Y}_{\beta,-}(x_- - x_+)\mathbf{C}_{\beta,b}^{-}]. \tag{27d}$$

The boundary S-matrix components, $\mathbf{R}_{\downarrow}$, $\mathbf{T}_{\uparrow}$, $\mathbf{R}_{\uparrow}$, and $\mathbf{T}_{\downarrow}$ of the half-infinite β block with upper boundary are given by

$$\mathbf{R}_{\downarrow} = -[(\mathbf{Y}_{\beta,h})^{-1}\mathbf{Y}_{\beta,-}(x_c) - (\mathbf{Z}_{\beta,h})^{-1}\mathbf{Z}_{\beta,-}(x_c)]^{-1}[(\mathbf{Y}_{\beta,h})^{-1}\mathbf{Y}_{\beta,+}(x_c) - (\mathbf{Z}_{\beta,h})^{-1}\mathbf{Z}_{\beta,+}(x_c)], \tag{28a}$$

$$\mathbf{T}_{\uparrow} = [(\mathbf{Y}_{\beta,-}(x_c))^{-1}\mathbf{Y}_{\beta,h} - (\mathbf{Z}_{\beta,-}(x_c))^{-1}\mathbf{Z}_{\beta,h}]^{-1}[(\mathbf{Y}_{\beta,-}(x_c))^{-1}\mathbf{Y}_{\beta,+} - (\mathbf{Z}_{\beta,-}(x_c))^{-1}\mathbf{Z}_{\beta,+}], \tag{28b}$$

$$\mathbf{T}_{\downarrow} = 2[(\mathbf{Y}_{\beta,h})^{-1}\mathbf{Y}_{\beta,-}(x_c) - (\mathbf{Z}_{\beta,h})^{-1}\mathbf{Z}_{\beta,-}(x_c)]^{-1}, \tag{28c}$$

$$\mathbf{R}_{\uparrow} = -[(\mathbf{Y}_{\beta,-}(x_c))^{-1}\mathbf{Y}_{\beta,h} - (\mathbf{Z}_{\beta,-}(x_c))^{-1}\mathbf{Z}_{\beta,h}]^{-1}[(\mathbf{Y}_{\beta,-}(x_c))^{-1}\mathbf{Y}_{\beta,h} + (\mathbf{Z}_{\beta,-}(x_c))^{-1}\mathbf{Z}_{\beta,h}]. \tag{28d}$$

The boundary S-matrix components, $\mathbf{R}_{\downarrow}$, $\mathbf{T}_{\uparrow}$, $\mathbf{R}_{\uparrow}$, and $\mathbf{T}_{\downarrow}$ of the half-infinite β block with lower boundary are given by

$$\mathbf{R}_{\downarrow} = -[(\mathbf{Y}_{\beta,+}(x_c))^{-1}\mathbf{Y}_{\beta,h} + (\mathbf{Z}_{\beta,+}(x_c))^{-1}\mathbf{Z}_{\beta,h}]^{-1}[(\mathbf{Y}_{\beta,+}(x_c))^{-1}\mathbf{Y}_{\beta,h} - (\mathbf{Z}_{\beta,+}(x_c))^{-1}\mathbf{Z}_{\beta,h}], \tag{29a}$$

$$\mathbf{T}_{\uparrow} = 2[(\mathbf{Y}_{\beta,h})^{-1}\mathbf{Y}_{\beta,+}(x_c) + (\mathbf{Z}_{\beta,h})^{-1}\mathbf{Z}_{\beta,+}(x_c)]^{-1}, \tag{29b}$$

$$\mathbf{R}_{\uparrow} = -[(\mathbf{Y}_{\beta,h})^{-1}\mathbf{Y}_{\beta,+}(x_c) + (\mathbf{Z}_{\beta,h})^{-1}\mathbf{Z}_{\beta,+}(x_c)]^{-1}[(\mathbf{Y}_{\beta,h})^{-1}\mathbf{Y}_{\beta,-}(x_c) + (\mathbf{Z}_{\beta,h})^{-1}\mathbf{Z}_{\beta,-}(x_c)], \tag{29c}$$

$$\mathbf{T}_{\downarrow} = \left[(\mathbf{Y}_{\beta,+}(x_c))^{-1}\mathbf{Y}_{\beta,h} + (\mathbf{Z}_{\beta,+}(x_c))^{-1}\mathbf{Z}_{\beta,h}\right]^{-1}\left[(\mathbf{Y}_{\beta,+}(x_c))^{-1}\mathbf{Y}_{\beta,-} - (\mathbf{Z}_{\beta,+}(x_c))^{-1}\mathbf{Z}_{\beta,-}\right]. \tag{29d}$$

4. LOCAL FOURIER MODAL ANALYSIS OF FOUR-PORT INTERSECTION BLOCKS

As stated in Section 3, the eventual objective of this paper is the complete mathematical modeling of four-port crossed nanophotonic structures. As shown in Fig. 2(a), two-dimensional photonic crystal cross-waveguide structure is chosen as an analysis example. This cross-waveguide structure is composed of five subparts; ports 1, 2, 3, and 4 and the intersection cross block. In this section, the LFMA for analyzing the Bloch eigenmodes and S matrix of the four-port intersection block is described. Eventually, the 4×4 S matrices of four-port cross blocks interconnecting two-port α and β blocks will be developed in Section 5 based on the theory described in this section.

Figures 9(a) and 9(b) show the separated intersection block of the photonic crystal cross-waveguide structure and its S-matrix diagram, respectively. In the proposed LFMA, the intersection block is embedded into a larger block with absorbing medium [or perfect matched layer (PML)] block [30] placed within the waveguide branches connected to ports as shown in Fig. 9(a). The internal part indicated by the dashed-line rectangle is the intersection part of the analyzed cross-waveguide structure. The dashed-line rectangle is the boundary of the intersection block defined in Fig. 9. The PML within each waveguide branch is necessary to model nonperiodic structure and prevent the eigenmode profile from being deteriorated by interference induced by periodicity. With the PML, the power flow through each waveguide branch is outward without nonphysical reflection at the interface of the cross block. The basic intuitive assumption of the LFMA is the electromagnetic isolation among individual blocks by the field localization on nanophotonic structures.

The field representation of the Bloch eigenmode within the four-port intersection block should be prepared. The pseudo-Fourier representations of the Bloch modes in the α and β blocks of the four-port intersection block are taken, respectively, as the same forms of Eqs. (12) and (14). The total electromagnetic fields in the four-port cross block can be represented by the superposition of the obtained α and β-Bloch eigenmodes

$$\underline{E}(x,y,z) = \sum_{g=1}^{M^+} C_{\alpha,g}^{+}\underline{E}_{\alpha,(g)}^{+}(x,y,z) + \sum_{g=1}^{M^-} C_{\alpha,g}^{-}\underline{E}_{\alpha,(g)}^{-}(x,y,z) + \sum_{g=1}^{M^+} C_{\beta,g}^{+}\underline{E}_{\beta,(g)}^{+}(x,y,z) + \sum_{g=1}^{M^-} C_{\beta,g}^{-}\underline{E}_{\beta,(g)}^{-}(x,y,z), \tag{30a}$$

$$\underline{H}(x,y,z) = \sum_{g=1}^{M^+} C_{\alpha,g}^{+}\underline{H}_{\alpha,(g)}^{+}(x,y,z) + \sum_{g=1}^{M^-} C_{\alpha,g}^{-}\underline{H}_{\alpha,(g)}^{-}(x,y,z) + \sum_{g=1}^{M^+} C_{\beta,g}^{+}\underline{H}_{\beta,(g)}^{+}(x,y,z) + \sum_{g=1}^{M^-} C_{\beta,g}^{-}\underline{H}_{\beta,(g)}^{-}(x,y,z), \tag{30b}$$

where $C_{\alpha,g}^{+}$ and $C_{\alpha,g}^{-}$ are the coupling coefficients of the positive and the negative α-Bloch eigenmodes, respectively. $C_{\beta,g}^{+}$ and $C_{\beta,g}^{-}$ are the coupling coefficients of the positive and the negative β-Bloch eigenmodes, respectively.

In addition, we take the Fourier series approximations of the exponential functions of the eigenvalues in Eqs. (12a), (12b), (14a), and (14b) as follows:

$$\exp(jk_{\alpha,z,0}^{(g)\pm}z) \approx \sum_{q=-H}^{H} \zeta_{\alpha,q}^{(g)\pm} \exp\left[j\frac{2\pi q}{T_z}z\right], \tag{31a}$$

$$\exp(jk_{\beta,x,0}^{(g)\pm}x) \approx \sum_{q=-H}^{H} \zeta_{\beta,q}^{(g)\pm} \exp\left[j\frac{2\pi q}{T_x}x\right], \tag{31b}$$

where $\zeta_{\alpha,q}^{(g)\pm}$ and $\zeta_{\beta,q}^{(g)\pm}$ are given, respectively, by

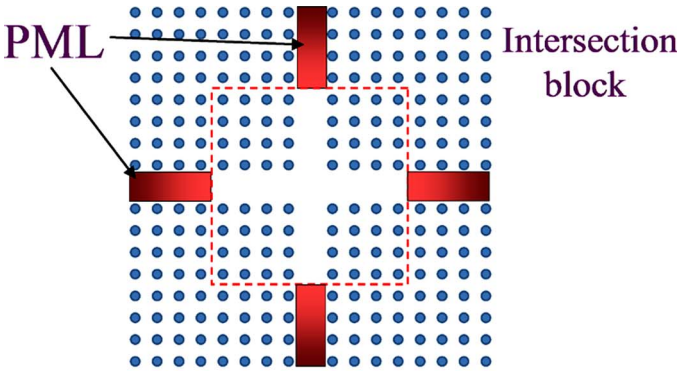

(a)

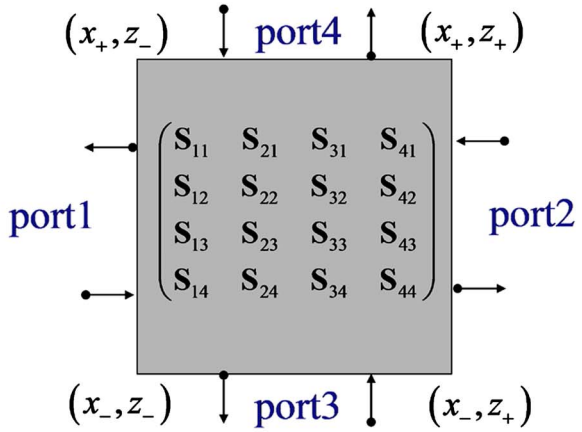

(b)

Fig. 9. (Color online) (a) Intersection block model with PML placed within four waveguide branches, (b) schematic of 4×4 S matrix.

$$\zeta_{\alpha,q}^{(g)\pm} = \mathrm{sinc}\left(\frac{k_{z,0}^{(g)\pm}T_z}{2\pi} - q\right), \tag{32a}$$

$$\zeta_{\beta,q}^{(g)\pm} = \mathrm{sinc}\left(\frac{k_{x,0}^{(g)\pm}T_x}{2\pi} - q\right). \tag{32b}$$

By substituting Eqs. (32a) and (32b) into the pseudo-Fourier representations of the Bloch eigenmodes Eqs. (12a), (12b), (14a), and (14b), we can obtain the Fourier approximation representation of the Bloch eigenmodes. The resultant α-Bloch eigenmode representations read as

$$\underline{E}_{\alpha,(g)}^{\pm}(x,y,z) = \exp(j(k_{x,0}x + k_{y,0}y)) \sum_{m=-M}^{M}\sum_{n=-N}^{N}\sum_{s=-H}^{H} \times(\tilde{E}_{\alpha,x,m,n,s}^{(g)\pm}\underline{x} + \tilde{E}_{\alpha,y,m,n,s}^{(g)\pm}\underline{y} + \tilde{E}_{\alpha,z,m,n,s}^{(g)\pm}\underline{z}) \times\exp(j(G_{x,m}x + G_{y,n}y + G_{z,s}z)), \tag{33a}$$

$$\underline{H}_{\alpha,(g)}^{\pm}(x,y,z) = \exp(j(k_{x,0}x + k_{y,0}y)) \sum_{m=-M}^{M}\sum_{n=-N}^{N}\sum_{s=-H}^{H} \times(\tilde{H}_{\alpha,x,m,n,s}^{(g)\pm}\underline{x} + \tilde{H}_{\alpha,y,m,n,s}^{(g)\pm}\underline{y} + \tilde{H}_{\alpha,z,m,n,s}^{(g)\pm}\underline{z}) \times\exp(j(G_{x,m}x + G_{y,n}y + G_{z,s}z)), \tag{33b}$$

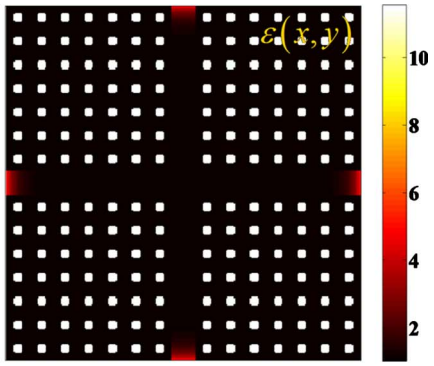

(a)

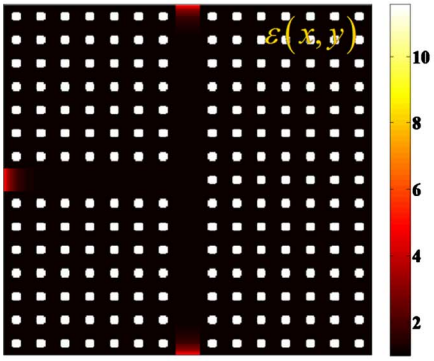

(b)

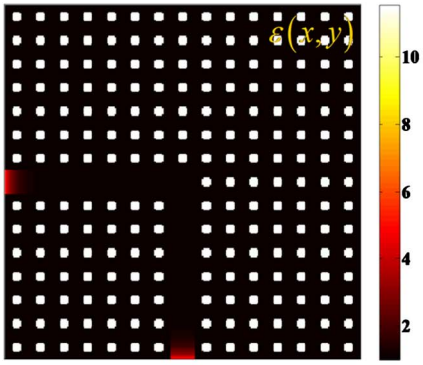

(c)

Fig. 10. (Color online) Permittivity profiles of the intersection blocks of the two-dimensional photonic crystal (a) cross waveguide, (b) T-branch, and (c) 90°-bend structures.

where the Fourier coefficients of the representations are obtained by

$$\tilde{E}_{\alpha,x,m,n,s}^{(g)\pm}\underline{x} + \tilde{E}_{\alpha,y,m,n,s}^{(g)\pm}\underline{y} + \tilde{E}_{\alpha,z,m,n,s}^{(g)\pm}\underline{z} = \sum_{p=-H}^{H}(\zeta_{\alpha,s-p}^{(g)\pm}E_{\alpha,x,m,n,p}^{(g)\pm}\underline{x} + \zeta_{\alpha,s-p}^{(g)\pm}E_{\alpha,y,m,n,p}^{(g)\pm}\underline{y} + \zeta_{\alpha,s-p}^{(g)\pm}E_{\alpha,z,m,n,p}^{(g)\pm}\underline{z})\exp(-jk_{z,p}^{(g)\pm}z_{\mp}), \tag{34a}$$

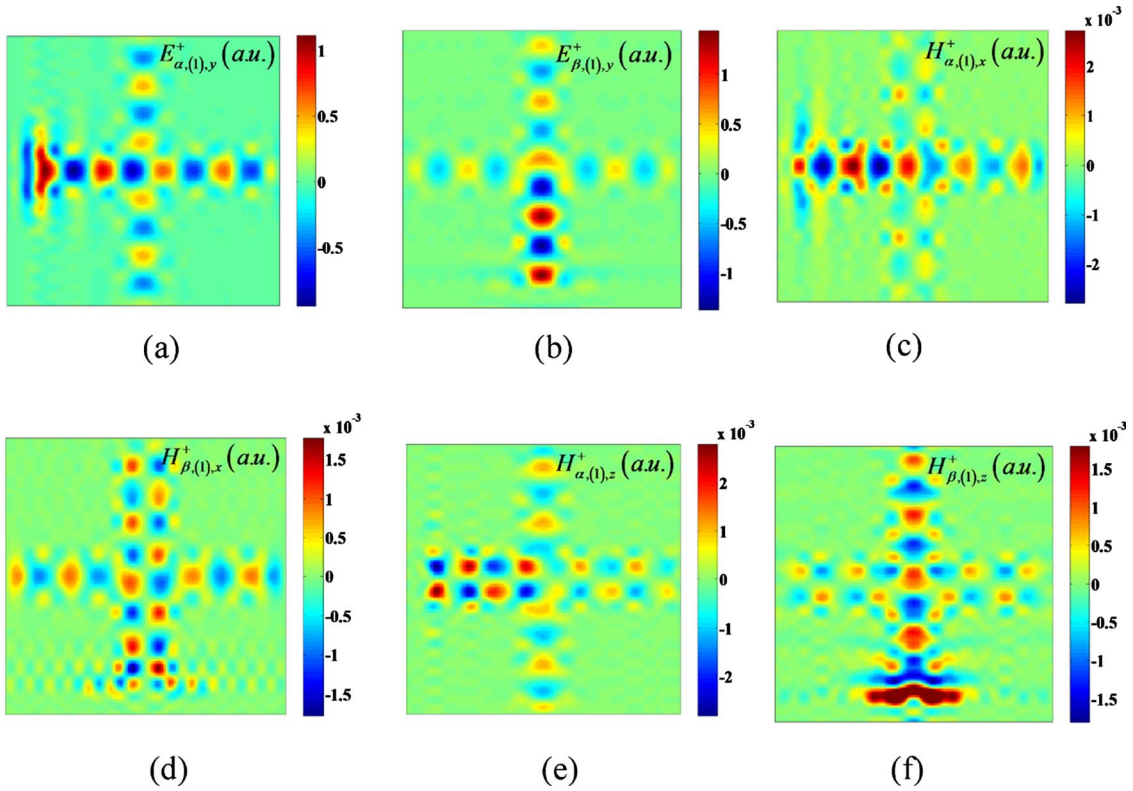

Fig. 11. (Color online) Dominant eigenmode profiles of the intersection block of the cross waveguide structure: (a) $E^{+}_{\alpha,(1),y}$, (b) $E^{+}_{\beta,(1),y}$, (c) $H^{+}_{\alpha,(1),x}$, (d) $H^{+}_{\beta,(1),x}$, (e) $H^{+}_{\alpha,(1),z}$, (f) $H^{+}_{\beta,(1),z}$.

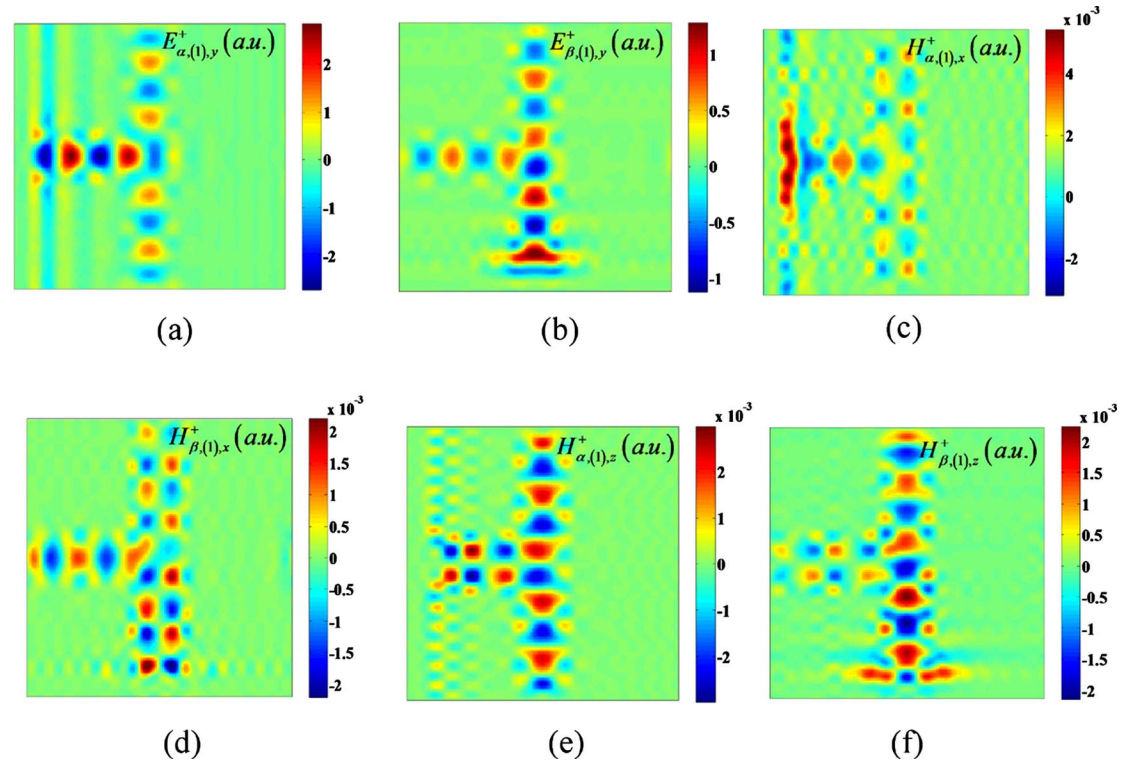

Fig. 12. (Color online) Dominant eigenmode profiles of the intersection block of the photonic crystal T-branch structure: (a) $E^{+}_{\alpha,(1),y}$, (b) $E^{+}_{\beta,(1),y}$, (c) $H^{+}_{\alpha,(1),x}$, (d) $H^{+}_{\beta,(1),x}$, (e) $H^{+}_{\alpha,(1),z}$, (f) $H^{+}_{\beta,(1),z}$.

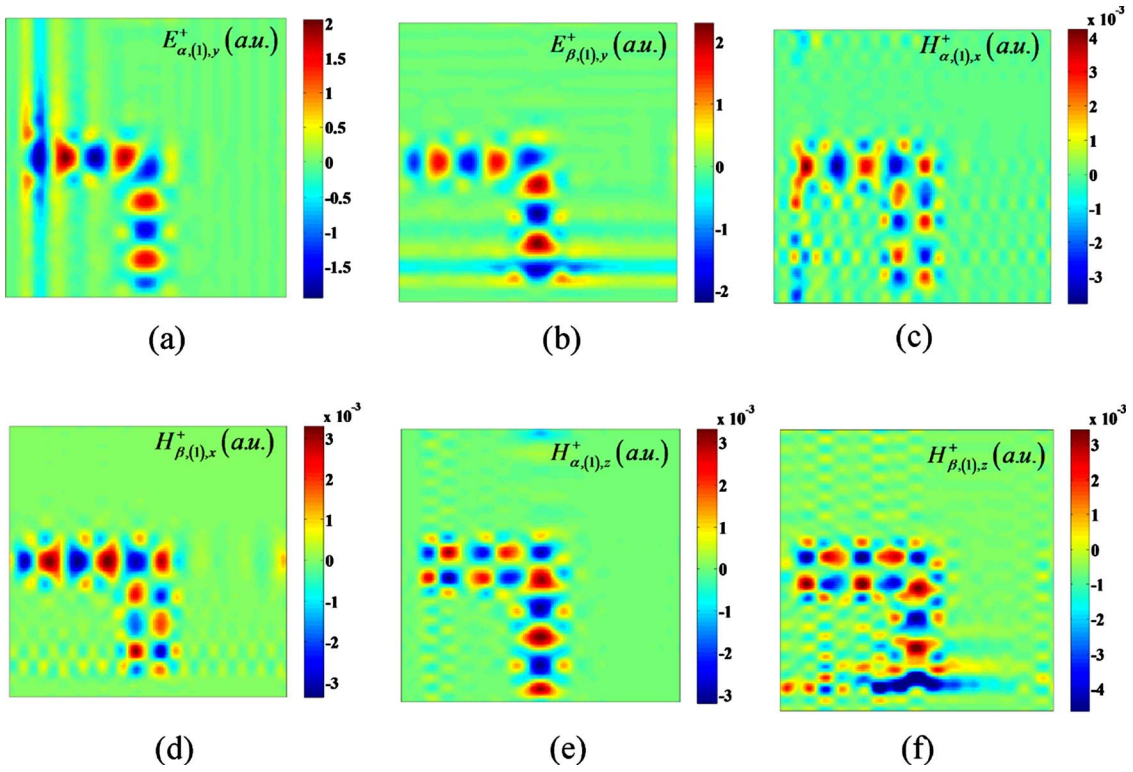

Fig. 13. (Color online) Dominant eigenmode profiles of the intersection block of the photonic crystal 90°-bend structure: (a) $E^{+}_{\alpha,(1),y}$, (b) $E^{+}_{\beta,(1),y}$, (c) $H^{+}_{\alpha,(1),x}$, (d) $H^{+}_{\beta,(1),x}$, (e) $H^{+}_{\alpha,(1),z}$, (f) $H^{+}_{\beta,(1),z}$.

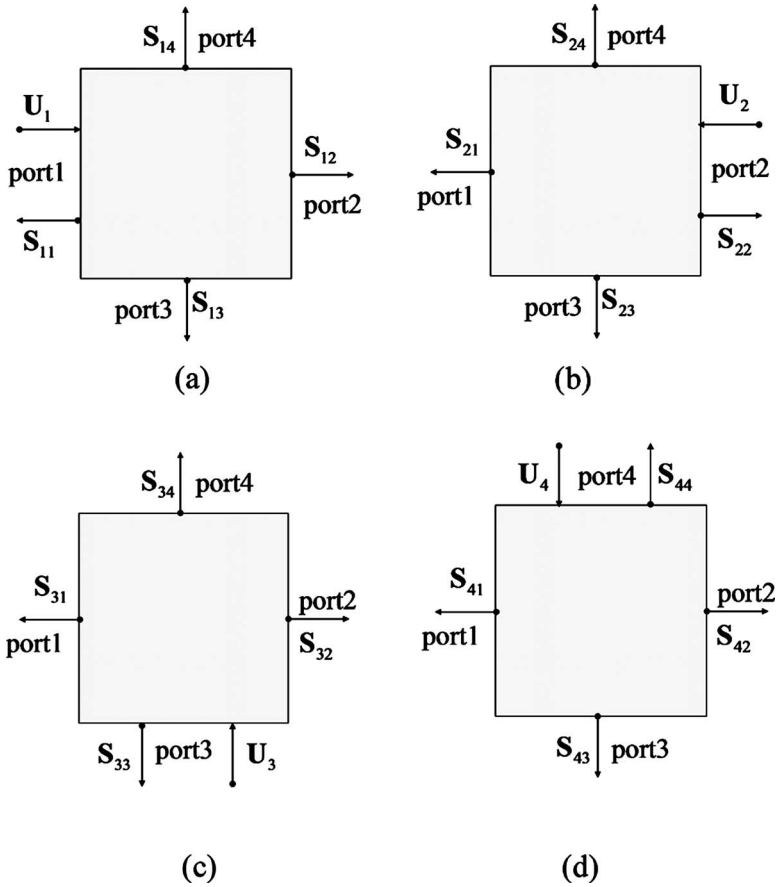

Fig. 14. Excitation of ports (a) 1, (b) 2, (c) 3, and (d) 4.

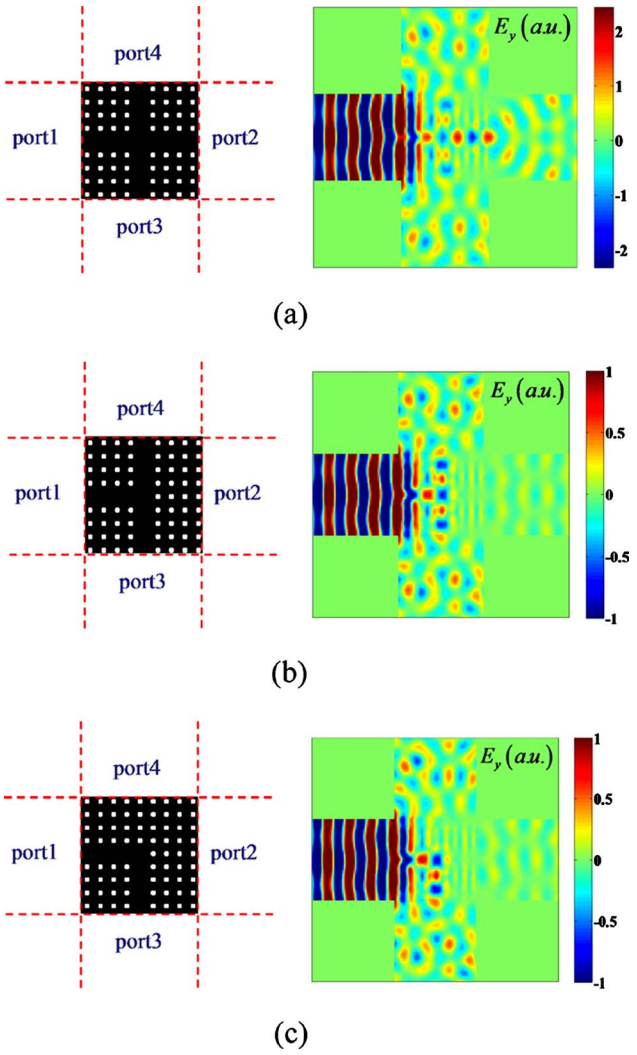

Fig. 15. (Color online) LFMA results of the S-matrix characterization of (a) the intersection block of the photonic crystal cross waveguide structure, (b) the photonic crystal T-branch structure, and (c) the photonic crystal 90°-bend structure.

$$\tilde{H}^{(g)\pm}_{\alpha,x,m,n,s}\underline{x} + \tilde{H}^{(g)\pm}_{\alpha,y,m,n,s}\underline{y} + \tilde{H}^{(g)\pm}_{\alpha,z,m,n,s}\underline{z} = \sum_{p=-H}^{H} \left(\zeta^{(g)\pm}_{\alpha,s-p} H^{(g)\pm}_{\alpha,x,m,n,p}\underline{x} + \zeta^{(g)\pm}_{\alpha,s-p} H^{(g)\pm}_{\alpha,y,m,n,p}\underline{y} + \zeta^{(g)\pm}_{\alpha,s-p} H^{(g)\pm}_{\alpha,z,m,n,p}\underline{z}\right)\exp(-jk^{(g)\pm}_{z,p} z_{\mp}), \quad (34b)$$

The resultant β-Bloch eigenmode representations read as

$$\underline{E}^{\pm}_{\beta,(g)}(x,y,z) = \exp(j(k_{z,0}z + k_{y,0}y)) \sum_{s=-M}^{M}\sum_{n=-N}^{N}\sum_{p=-H}^{H} \times(\tilde{E}^{(g)\pm}_{\beta,s,m,n,p}\underline{x} + \tilde{E}^{(g)\pm}_{\beta,y,s,n,p}\underline{y} + \tilde{E}^{(g)\pm}_{\beta,z,s,n,p}\underline{z}) \times\exp(j(G_{x,s}x + G_{y,n}y + G_{z,p}z)), \quad (35a)$$

$$\underline{H}^{\pm}_{\beta,(g)}(x,y,z) = \exp(j(k_{z,0}z + k_{y,0}y)) \sum_{s=-M}^{M}\sum_{n=-N}^{N}\sum_{s=-H}^{H} \times(\tilde{H}^{(g)\pm}_{\beta,x,s,n,p}\underline{x} + \tilde{H}^{(g)\pm}_{\beta,y,s,n,p}\underline{y} + \tilde{H}^{(g)\pm}_{\beta,z,s,n,p}\underline{z}) \times\exp(j(G_{x,s}x + G_{y,n}y + G_{z,p}z)), \quad (35b)$$

where the Fourier coefficients of the representations are obtained by

$$\tilde{E}^{(g)\pm}_{\beta,x,s,n,p}\underline{x} + \tilde{E}^{(g)\pm}_{\beta,y,s,n,p}\underline{y} + \tilde{E}^{(g)\pm}_{\beta,z,s,n,p}\underline{z} = \sum_{m=-M}^{M} (\zeta^{(g)\pm}_{\beta,s-m} E^{(g)\pm}_{\beta,x,m,n,p}\underline{x} + \zeta^{(g)\pm}_{\beta,s-m} E^{(g)\pm}_{\beta,y,m,n,p}\underline{y} + \zeta^{(g)\pm}_{\beta,s-m} E^{(g)\pm}_{\beta,z,m,n,p}\underline{z})\exp(-jk^{(g)\pm}_{x,m} x_{\mp}), \quad (36a)$$

$$\tilde{H}^{(g)+}_{\beta,x,s,n,p}\underline{x} + \tilde{H}^{(g)+}_{\beta,y,s,n,p}\underline{y} + \tilde{H}^{(g)+}_{\beta,z,s,n,p}\underline{z} = \sum_{m=-M}^{M} (\zeta^{(g)+}_{\beta,s-m} H^{(g)+}_{\beta,x,m,n,p}\underline{x} + \zeta^{(g)+}_{\beta,s-m} H^{(g)+}_{\beta,y,m,n,p}\underline{y} + \zeta^{(g)+}_{\beta,s-m} H^{(g)+}_{\beta,z,m,n,p}\underline{z})\exp(-jk^{(g)\pm}_{x,m} x_{\mp}). \quad (36b)$$

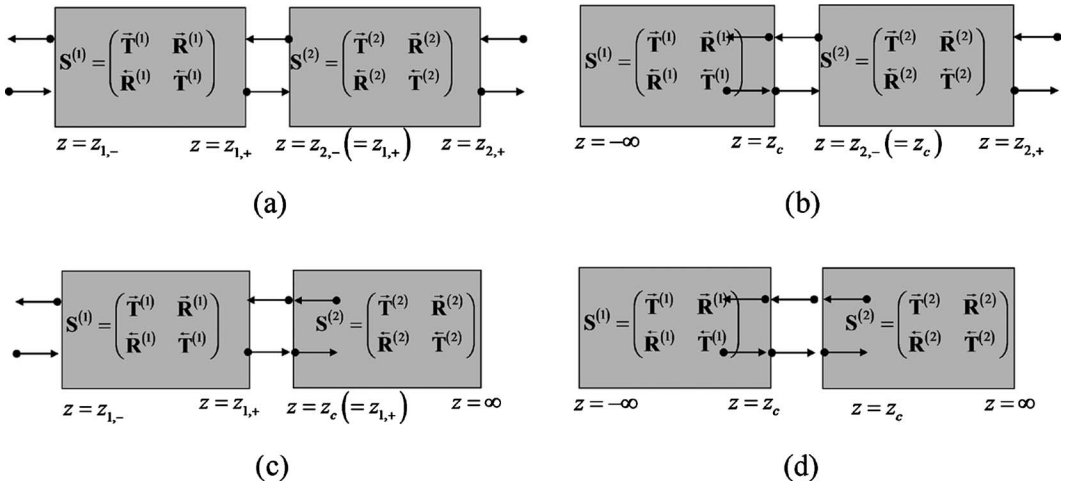

Fig. 16. Two-port α block interconnection: (a) left and right finite size blocks, (b) left half-infinite and right finite size blocks, (c) left finite size and right half-infinite blocks, (d) left and right half-infinite blocks.

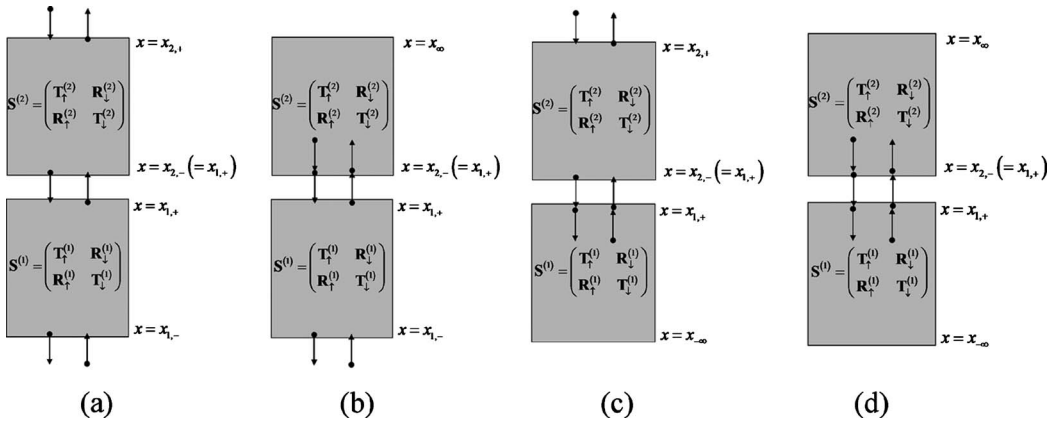

Fig. 17. Two-port β block interconnection: (a) upper and lower finite size blocks, (b) upper half-infinite and lower finite size blocks, (c) upper finite size and lower half-infinite blocks, and (d) upper and lower half-infinite blocks.

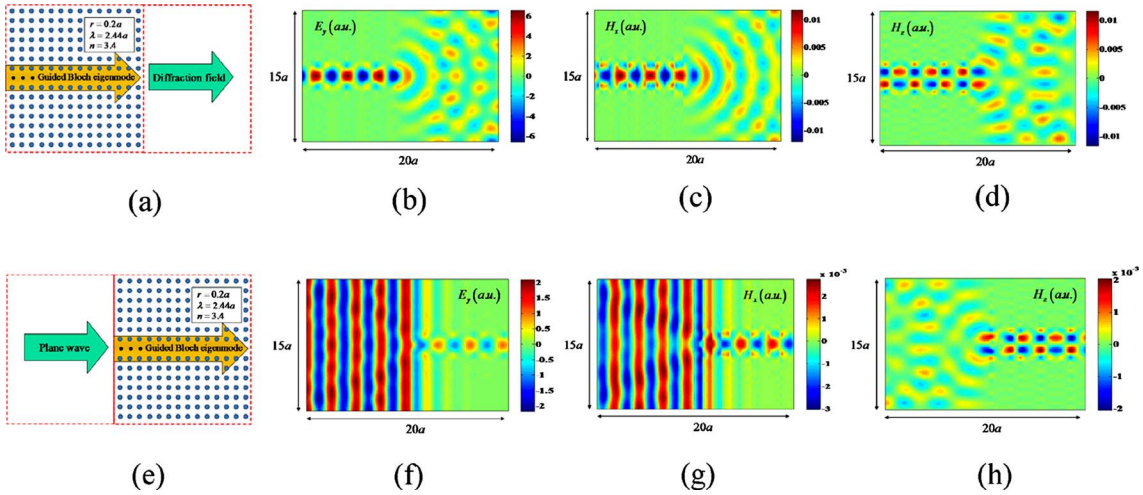

Fig. 18. (Color online) Diffraction of the fundamental guided Bloch eigenmode at the right endface of the two-dimensional half-infinite photonic crystal structure: (a) simulation schematic, (b) y-polarization electric field distribution, (c) x-polarization magnetic field distribution, (d) z-polarization magnetic field distribution. Excitation of the fundamental guided Bloch eigenmode at the left endface of the two-dimensional half-infinite photonic crystal structure: (e) simulation schematic, (f) y-polarization electric field distribution, (g) x-polarization magnetic field distribution, (h) z-polarization magnetic field distribution.

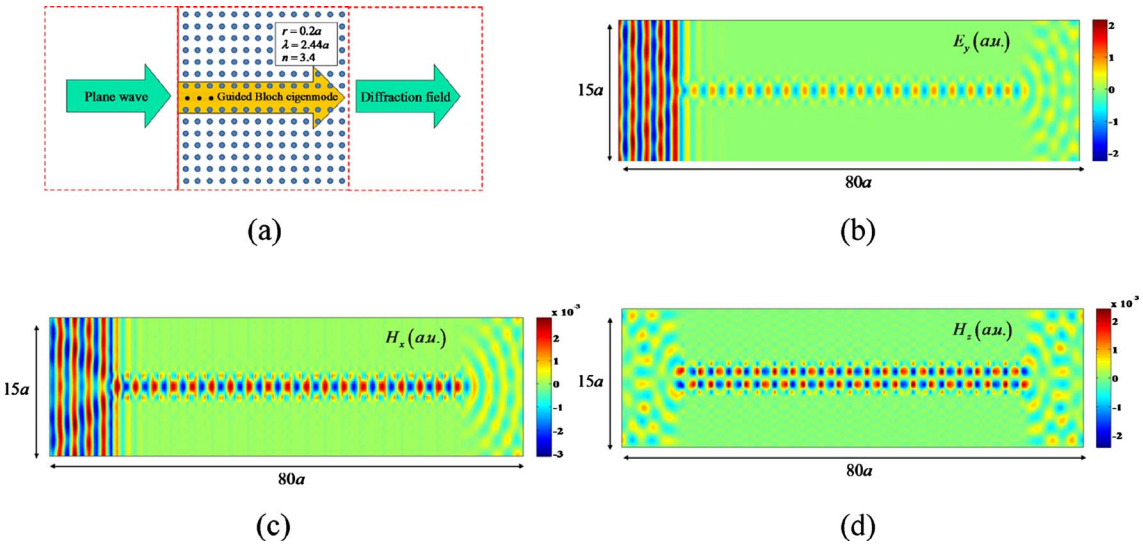

Fig. 19. (Color online) Transmission and reflection of two-dimensional finite sized photonic crystal waveguide by a normally incident plane wave: (a) simulation schematic, (b) y-polarization electric field distribution, (c) x-polarization magnetic field distribution, (d) z-polarization magnetic field distribution.

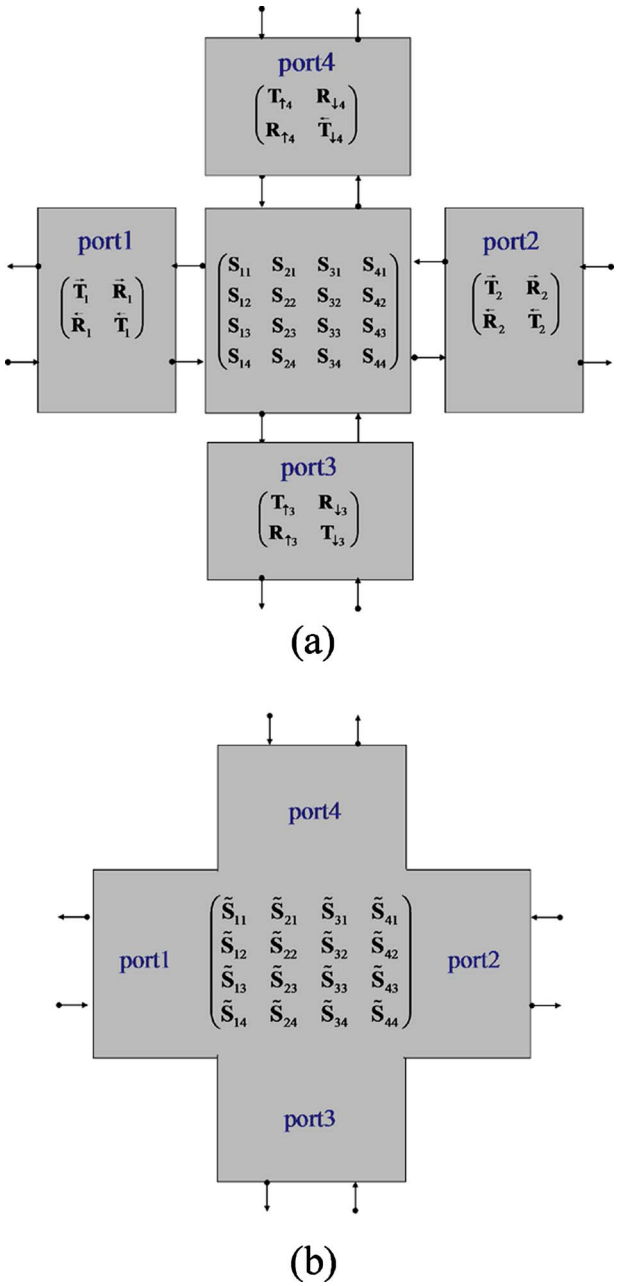

Fig. 20. (Color online) (a) Interconnection of four two-port blocks and a four-port cross block, (b) extended four-port cross block composed of four two-port blocks and a four-port intersection block.

With the Fourier approximation of the pseudo-Fourier Bloch eigenmode representations, we can find the appropriate boundary condition equations to obtain the S matrix of the four-port intersection block.

Let us examine the α- and β-Bloch eigenmodes of three examples: two-dimensional photonic crystal cross-waveguide structure [2], two-dimensional photonic crystal T-branch structure [5], and two-dimensional photonic crystal 90°-bend structure [6], permittivity profiles of which are shown in Fig. 10(a)–10(c), respectively. The PML blocks are placed in the waveguide channels within the dummy region. The mode profiles of the dominant α- and β-Bloch eigenmode transferring electromagnetic power are analyzed by the LFMA with the Fourier truncation order of $M=14$, $N=0$, and $P=14$.

Figures 11–13 show the dominant eigenmode profiles of the intersection blocks of two-dimensional photonic crystal cross-waveguide structure, two-dimensional photonic crystal T-branch structure, and two-dimensional photonic crystal 90°-bend structure, respectively.

The 4×4 S-matrix is derived by solving four boundary conditions at four boundaries of the intersection block. Let us denote four excitation fields at the ports 1–4 as $\underline{U}_1$, $\underline{U}_2$, $\underline{U}_3$, and $\underline{U}_4$ that are represented, respectively, by

$$\underline{U}_1 = \sum_{m=-M}^{M}\sum_{n=-N}^{N}(u_{1,x,m,n}\underline{x} + u_{1,y,m,n}\underline{y} + u_{1,z,m,n}\underline{z}) \times \exp(j(k_{\alpha,x,m}x + k_{\alpha,y,n}y + k_{\alpha,z,m,n}(z - z_-))), \tag{37a}$$

$$\underline{U}_2 = \sum_{m=-M}^{M}\sum_{n=-N}^{N}(u_{2,x,m,n}\underline{x} + u_{2,y,m,n}\underline{y} + u_{2,z,m,n}\underline{z}) \times \exp(j(k_{\alpha,x,m}x + k_{\alpha,y,n}y - k_{\alpha,z,m,n}(z + z_+))), \tag{37b}$$

$$\underline{U}_3 = \sum_{m=-M}^{M}\sum_{n=-N}^{N}(u_{3,x,m,n}\underline{x} + u_{3,y,m,n}\underline{y} + u_{3,z,m,n}\underline{z}) \times \exp(j(k_{\beta,x,m,n}(x - x_-) + k_{\beta,y,n}y + k_{\beta,z,m}z)), \tag{37c}$$

$$\underline{U}_4 = \sum_{m=-M}^{M}\sum_{n=-N}^{N}(u_{4,x,m,n}\underline{x} + u_{4,y,m,n}\underline{y} + u_{4,z,m,n}\underline{z}) \times \exp(j(-k_{\beta,x,m,n}(x - x_+) + k_{\beta,y,n}y + k_{\beta,z,m}z)). \tag{37d}$$

Let us denote the radiation fields (transmission and reflection fields) at ports 1–4 induced by the excitation of port i (for $i=1, 2, 3, 4$) as $\underline{T}_{i1}$, $\underline{T}_{i2}$, $\underline{T}_{i3}$, and $\underline{T}_{i4}$ that are given, respectively, by

$$\underline{T}_{i1} = \sum_{m=-M}^{M}\sum_{n=-N}^{N}(t_{i1,x,m,n}\underline{x} + t_{i1,y,m,n}\underline{y} + t_{i1,z,m,n}\underline{z}) \times \exp(j(k_{\alpha,x,m}x + k_{\alpha,y,n}y - k_{\alpha,z,m,n}(z - z_-))), \tag{38a}$$

$$\underline{T}_{i2} = \sum_{m=-M}^{M}\sum_{n=-N}^{N}(t_{i2,x,m,n}\underline{x} + t_{i2,y,m,n}\underline{y} + t_{i2,z,m,n}\underline{z}) \times \exp(j(k_{\alpha,x,m}x + k_{\alpha,y,n}y + k_{\alpha,z,m,n}(z - z_+))), \tag{38b}$$

$$\underline{T}_{i3} = \sum_{m=-M}^{M}\sum_{n=-N}^{N}(t_{i3,x,m,n}\underline{x} + t_{i3,y,m,n}\underline{y} + t_{i3,z,m,n}\underline{z}) \times \exp(j(-k_{\beta,x,m,n}(x - x_-) + k_{\beta,y,n}y + k_{\beta,z,m}z)), \tag{38c}$$

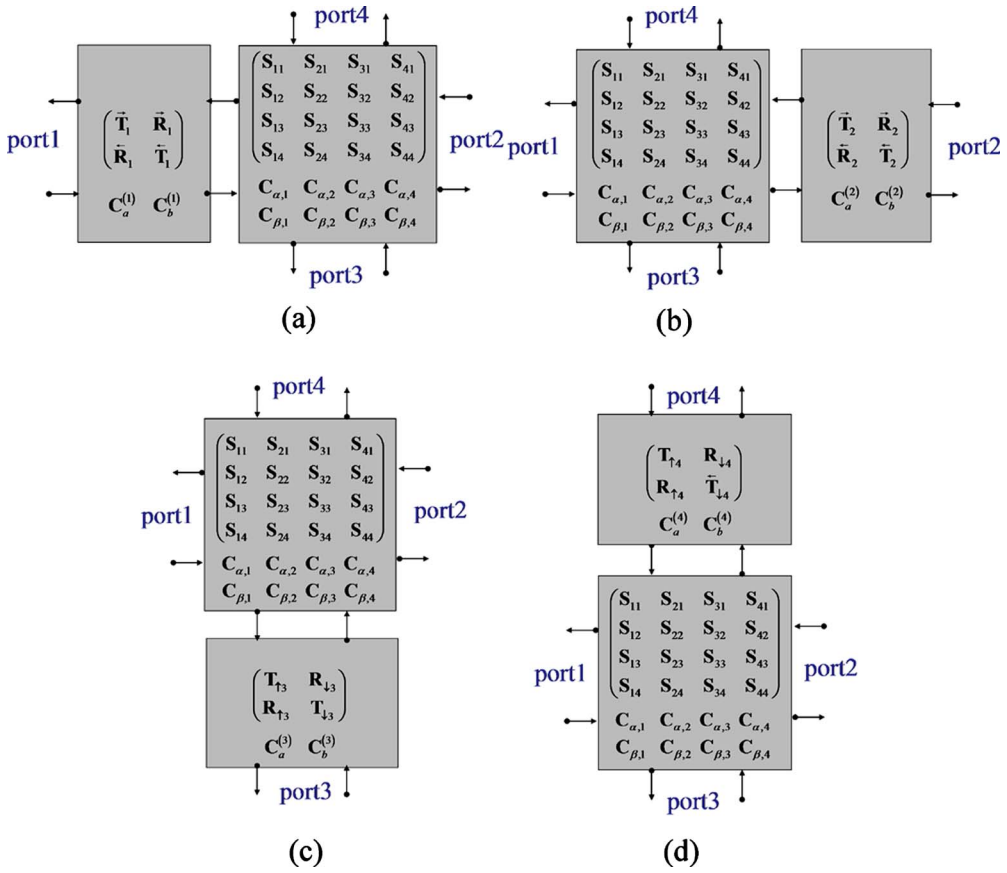

Fig. 21. (Color online) Interconnection through ports (a) 1, (b) 2, (c) 3, and (d) 4.

$$\underline{T}_{i4} = \sum_{m=-M}^{M} \sum_{n=-N}^{N} (t_{i4,x,m,n}\underline{x} + t_{i4,y,m,n}\underline{y} + t_{i4,z,m,n}\underline{z}) \times \exp(j(k_{\beta,x,m,n}(x - x_+) + k_{\beta,y,n}y + k_{\beta,z,m}z)). \tag{38d}$$

The boundary conditions to obtain the scattering matrix and the coupling coefficients operators are described. There are four boundaries as shown in Fig. 9. The boundaries for ports 1–4 are set up at $z_- = -T_z/2 + \Delta T_z$, $z_+ = T_z/2 - \Delta T_z$, $x_- = -T_x/2 + \Delta T_x$, and $x_+ = T_x/2 - \Delta T_x$, respectively. ΔT_x and ΔT_z are the thickness of the x- and z-direction dummy areas, respectively. These are actually the thickness of the PML blocks.

We can obtain the S-matrix components, $\mathbf{S}_{11}$, $\mathbf{S}_{12}$, $\mathbf{S}_{13}$, and $\mathbf{S}_{14}$ by simultaneously matching the boundary condition at four boundaries, when port 1 is excited by the input field operator $\mathbf{U}_1$. Similarly we can obtain $\mathbf{S}_{i1}$, $\mathbf{S}_{i2}$, $\mathbf{S}_{i3}$, and $\mathbf{S}_{i4}$, when the port i is excited by the input field operator $\mathbf{U}_i$. This is illustrated in Fig. 14.

The transverse field continuation boundary conditions at four boundaries can be expressed as the following matrix equations:

$$\begin{pmatrix} \mathbf{W}_{\alpha,h} & \mathbf{W}_{\alpha,h} \\ \mathbf{V}_{\alpha,h} & -\mathbf{V}_{\alpha,h} \end{pmatrix} \begin{pmatrix} \mathbf{U}_1 & \mathbf{0} & \mathbf{0} & \mathbf{0} \\ \mathbf{S}_{11} & \mathbf{S}_{21} & \mathbf{S}_{31} & \mathbf{S}_{41} \end{pmatrix} = \begin{pmatrix} \tilde{\mathbf{W}}_{\alpha,+}(z_-) & \tilde{\mathbf{W}}_{\alpha,-}(z_-) \\ \tilde{\mathbf{V}}_{\alpha,+}(z_-) & \tilde{\mathbf{V}}_{\alpha,-}(z_-) \end{pmatrix} \begin{pmatrix} \mathbf{C}^+_{\alpha,1} & \mathbf{C}^+_{\alpha,2} & \mathbf{C}^+_{\alpha,3} & \mathbf{C}^+_{\alpha,4} \\ \mathbf{C}^-_{\alpha,1} & \mathbf{C}^-_{\alpha,2} & \mathbf{C}^-_{\alpha,3} & \mathbf{C}^-_{\alpha,4} \end{pmatrix} + \begin{pmatrix} \tilde{\mathbf{W}}_{\beta,+}(z_-) & \tilde{\mathbf{W}}_{\beta,-}(z_-) \\ \tilde{\mathbf{V}}_{\beta,+}(z_-) & \tilde{\mathbf{V}}_{\beta,-}(z_-) \end{pmatrix} \begin{pmatrix} \mathbf{C}^+_{\beta,1} & \mathbf{C}^+_{\beta,2} & \mathbf{C}^+_{\beta,3} & \mathbf{C}^+_{\beta,4} \\ \mathbf{C}^-_{\beta,1} & \mathbf{C}^-_{\beta,2} & \mathbf{C}^-_{\beta,3} & \mathbf{C}^-_{\beta,4} \end{pmatrix}, \quad \text{at } z = z_-, \tag{39a}$$

$$\begin{pmatrix} \mathbf{W}_{\alpha,h} & \mathbf{W}_{\alpha,h} \\ \mathbf{V}_{\alpha,h} & -\mathbf{V}_{\alpha,h} \end{pmatrix} \begin{pmatrix} \mathbf{S}_{12} & \mathbf{S}_{22} & \mathbf{S}_{32} & \mathbf{S}_{42} \\ \mathbf{0} & \mathbf{U}_2 & \mathbf{0} & \mathbf{0} \end{pmatrix} = \begin{pmatrix} \tilde{\mathbf{W}}_{\alpha,+}(z_+) & \tilde{\mathbf{W}}_{\alpha,-}(z_+) \\ \tilde{\mathbf{V}}_{\alpha,+}(z_+) & \tilde{\mathbf{V}}_{\alpha,-}(z_+) \end{pmatrix} \begin{pmatrix} \mathbf{C}^+_{\alpha,1} & \mathbf{C}^+_{\alpha,2} & \mathbf{C}^+_{\alpha,3} & \mathbf{C}^+_{\alpha,4} \\ \mathbf{C}^-_{\alpha,1} & \mathbf{C}^-_{\alpha,2} & \mathbf{C}^-_{\alpha,3} & \mathbf{C}^-_{\alpha,4} \end{pmatrix} + \begin{pmatrix} \tilde{\mathbf{W}}_{\beta,+}(z_+) & \tilde{\mathbf{W}}_{\beta,-}(z_+) \\ \tilde{\mathbf{V}}_{\beta,+}(z_+) & \tilde{\mathbf{V}}_{\beta,-}(z_+) \end{pmatrix} \begin{pmatrix} \mathbf{C}^+_{\beta,1} & \mathbf{C}^+_{\beta,2} & \mathbf{C}^+_{\beta,3} & \mathbf{C}^+_{\beta,4} \\ \mathbf{C}^-_{\beta,1} & \mathbf{C}^-_{\beta,2} & \mathbf{C}^-_{\beta,3} & \mathbf{C}^-_{\beta,4} \end{pmatrix} \quad \text{at } z = z_+, \tag{39b}$$

$$\begin{pmatrix}\mathbf{Y}_{\beta,h} & \mathbf{Y}_{\beta,h}\\ \mathbf{Z}_{\beta,h} & -\mathbf{Z}_{\beta,h}\end{pmatrix}\begin{pmatrix}\mathbf{0} & \mathbf{0} & \mathbf{U}_3 & \mathbf{0}\\ \mathbf{S}_{13} & \mathbf{S}_{23} & \mathbf{S}_{33} & \mathbf{S}_{43}\end{pmatrix} = \begin{pmatrix}\tilde{\mathbf{Y}}_{\alpha,+}(x_-) & \tilde{\mathbf{Y}}_{\alpha,-}(x_-)\\ \tilde{\mathbf{Z}}_{\alpha,+}(x_-) & \tilde{\mathbf{Z}}_{\alpha,-}(x_-)\end{pmatrix}\begin{pmatrix}\mathbf{C}^+_{\alpha,1} & \mathbf{C}^+_{\alpha,2} & \mathbf{C}^+_{\alpha,3} & \mathbf{C}^+_{\alpha,4}\\ \mathbf{C}^-_{\alpha,1} & \mathbf{C}^-_{\alpha,2} & \mathbf{C}^-_{\alpha,3} & \mathbf{C}^-_{\alpha,4}\end{pmatrix}$$
$$+\begin{pmatrix}\tilde{\mathbf{Y}}_{\beta,+}(x_-) & \tilde{\mathbf{Y}}_{\beta,-}(x_-)\\ \tilde{\mathbf{Z}}_{\beta,+}(x_-) & \tilde{\mathbf{Z}}_{\beta,-}(x_-)\end{pmatrix}\begin{pmatrix}\mathbf{C}^+_{\beta,1} & \mathbf{C}^+_{\beta,2} & \mathbf{C}^+_{\beta,3} & \mathbf{C}^+_{\beta,4}\\ \mathbf{C}^-_{\beta,1} & \mathbf{C}^-_{\beta,2} & \mathbf{C}^-_{\beta,3} & \mathbf{C}^-_{\beta,4}\end{pmatrix} \quad \text{at } x = x_-, \tag{39c}$$

$$\begin{pmatrix}\mathbf{Y}_{\beta,h} & \mathbf{Y}_{\beta,h}\\ \mathbf{Z}_{\beta,h} & -\mathbf{Z}_{\beta,h}\end{pmatrix}\begin{pmatrix}\mathbf{S}_{14} & \mathbf{S}_{24} & \mathbf{S}_{34} & \mathbf{S}_{44}\\ \mathbf{0} & \mathbf{0} & \mathbf{0} & \mathbf{U}_4\end{pmatrix} = \begin{pmatrix}\tilde{\mathbf{Y}}_{\alpha,+}(x_+) & \tilde{\mathbf{Y}}_{\alpha,-}(x_+)\\ \tilde{\mathbf{Z}}_{\alpha,+}(x_+) & \tilde{\mathbf{Z}}_{\alpha,-}(x_+)\end{pmatrix}\begin{pmatrix}\mathbf{C}^+_{\alpha,1} & \mathbf{C}^+_{\alpha,2} & \mathbf{C}^+_{\alpha,3} & \mathbf{C}^+_{\alpha,4}\\ \mathbf{C}^-_{\alpha,1} & \mathbf{C}^-_{\alpha,2} & \mathbf{C}^-_{\alpha,3} & \mathbf{C}^-_{\alpha,4}\end{pmatrix}$$
$$+\begin{pmatrix}\tilde{\mathbf{Y}}_{\beta,+}(x_+) & \tilde{\mathbf{Y}}_{\beta,-}(x_+)\\ \tilde{\mathbf{Z}}_{\beta,+}(x_+) & \tilde{\mathbf{Z}}_{\beta,-}(x_+)\end{pmatrix}\begin{pmatrix}\mathbf{C}^+_{\beta,1} & \mathbf{C}^+_{\beta,2} & \mathbf{C}^+_{\beta,3} & \mathbf{C}^+_{\beta,4}\\ \mathbf{C}^-_{\beta,1} & \mathbf{C}^-_{\beta,2} & \mathbf{C}^-_{\beta,3} & \mathbf{C}^-_{\beta,4}\end{pmatrix} \quad \text{at } x = x_+, \tag{39d}$$

where $\tilde{\mathbf{W}}_{\alpha,+}(z)$, $\tilde{\mathbf{W}}_{\alpha,-}(z)$, $\tilde{\mathbf{V}}_{\alpha,+}(z)$, $\tilde{\mathbf{V}}_{\alpha,-}(z)$, $\tilde{\mathbf{W}}_{\beta,+}(z)$, $\tilde{\mathbf{W}}_{\beta,-}(z)$, $\tilde{\mathbf{V}}_{\beta,+}(z)$, and $\tilde{\mathbf{V}}_{\beta,-}(z)$ are defined, respectively, by

$$\tilde{\mathbf{W}}_{\alpha,\pm}(z) = \begin{pmatrix}\sum_{s=-H}^{H}\tilde{E}^{(1)\pm}_{\alpha,y,m,n,s}e^{jG_{z,s}z} & \cdots & \sum_{s=-H}^{H}\tilde{E}^{(M^\pm)\pm}_{\alpha,y,m,n,s}e^{jG_{z,s}z}\\ \sum_{s=-H}^{H}\tilde{E}^{(1)\pm}_{\alpha,x,m,n,s}e^{jG_{z,s}z} & \cdots & \sum_{s=-H}^{H}\tilde{E}^{(M^\pm)\pm}_{\alpha,x,m,n,s}e^{jG_{z,s}z}\end{pmatrix}, \tag{40a}$$

$$\tilde{\mathbf{V}}_{\alpha,\pm}(z) = \begin{pmatrix}\sum_{s=-H}^{H}\tilde{H}^{(1)\pm}_{\alpha,y,m,n,s}e^{jG_{z,s}z} & \cdots & \sum_{s=-H}^{H}\tilde{H}^{(M^\pm)\pm}_{\alpha,y,m,n,s}e^{jG_{z,s}z}\\ \sum_{s=-H}^{H}\tilde{H}^{(1)\pm}_{\alpha,x,m,n,s}e^{jG_{z,s}z} & \cdots & \sum_{s=-H}^{H}\tilde{H}^{(M^\pm)\pm}_{\alpha,x,m,n,s}e^{jG_{z,s}z}\end{pmatrix}, \tag{40b}$$

$$\tilde{\mathbf{W}}_{\beta,\pm}(z) = \begin{pmatrix}\sum_{s=-H}^{H}\tilde{E}^{(1)\pm}_{\beta,y,m,n,s}e^{jG_{z,s}z} & \cdots & \sum_{s=-H}^{H}\tilde{E}^{(M^\pm)\pm}_{\beta,y,m,n,s}e^{jG_{z,s}z}\\ \sum_{s=-H}^{H}\tilde{E}^{(1)\pm}_{\beta,x,m,n,s}e^{jG_{z,s}z} & \cdots & \sum_{s=-H}^{H}\tilde{E}^{(M^\pm)\pm}_{\beta,x,m,n,s}e^{jG_{z,s}z}\end{pmatrix}, \tag{40c}$$

$$\tilde{\mathbf{V}}_{\beta,\pm}(z) = \begin{pmatrix}\sum_{s=-H}^{H}\tilde{H}^{(1)\pm}_{\beta,y,m,n,s}e^{jG_{z,s}z} & \cdots & \sum_{s=-H}^{H}\tilde{H}^{(M^\pm)\pm}_{\beta,y,m,n,s}e^{jG_{z,s}z}\\ \sum_{s=-H}^{H}\tilde{H}^{(1)\pm}_{\beta,x,m,n,s}e^{jG_{z,s}z} & \cdots & \sum_{s=-H}^{H}\tilde{H}^{(M^\pm)\pm}_{\beta,x,m,n,s}e^{jG_{z,s}z}\end{pmatrix}, \tag{40d}$$

and $\tilde{\mathbf{Y}}_{\beta,+}(x)$, $\tilde{\mathbf{Y}}_{\beta,-}(x)$, $\tilde{\mathbf{Z}}_{\beta,+}(x)$, $\tilde{\mathbf{Z}}_{\beta,-}(x)$, $\tilde{\mathbf{Y}}_{\alpha,+}(x)$, $\tilde{\mathbf{Y}}_{\alpha,-}(x)$, $\tilde{\mathbf{Z}}_{\alpha,+}(x)$, and $\tilde{\mathbf{Z}}_{\alpha,-}(x)$ are defined, respectively, by

$$\tilde{\mathbf{Y}}_{\beta,\pm}(x) = \begin{pmatrix}\sum_{m=-M}^{M}\tilde{E}^{(1)\pm}_{\beta,y,m,n,s}e^{jG_{x,m}x} & \cdots & \sum_{m=-M}^{M}\tilde{E}^{(M^\pm)\pm}_{\beta,y,m,n,s}e^{jG_{x,m}x}\\ \sum_{m=-M}^{M}\tilde{E}^{(1)\pm}_{\beta,z,m,n,s}e^{jG_{x,m}x} & \cdots & \sum_{m=-M}^{M}\tilde{E}^{(M^\pm)\pm}_{\beta,z,m,n,s}e^{jG_{x,m}x}\end{pmatrix}, \tag{41a}$$

$$\tilde{\mathbf{Z}}_{\beta,+}(x) = \begin{pmatrix}\sum_{m=-M}^{M}\tilde{H}^{(1)+}_{\beta,y,m,n,s}e^{jG_{x,m}x} & \cdots & \sum_{m=-M}^{M}\tilde{H}^{(M^+)+}_{\beta,y,m,n,s}e^{jG_{x,m}x}\\ \sum_{m=-M}^{M}\tilde{H}^{(1)+}_{\beta,z,m,n,s}e^{jG_{x,m}x} & \cdots & \sum_{m=-M}^{M}\tilde{H}^{(M^+)+}_{\beta,z,m,n,s}e^{jG_{x,m}x}\end{pmatrix}, \tag{41b}$$

$$\tilde{\mathbf{Y}}_{\alpha,\pm}(x) = \begin{pmatrix}\sum_{m=-M}^{M}\tilde{E}^{(1)\pm}_{\alpha,y,m,n,s}e^{jG_{x,m}x} & \cdots & \sum_{m=-M}^{M}\tilde{E}^{(M^\pm)\pm}_{\alpha,y,m,n,s}e^{jG_{x,m}x}\\ \sum_{m=-M}^{M}\tilde{E}^{(1)\pm}_{\alpha,z,m,n,s}e^{jG_{x,m}x} & \cdots & \sum_{m=-M}^{M}\tilde{E}^{(M^\pm)\pm}_{\alpha,z,m,n,s}e^{jG_{x,m}x}\end{pmatrix}, \tag{41c}$$

$$\tilde{\mathbf{Z}}_{\alpha,\pm}(x) = \begin{pmatrix}\sum_{m=-M}^{M}\tilde{H}^{(1)\pm}_{\alpha,y,m,n,s}e^{jG_{x,m}x} & \cdots & \sum_{m=-M}^{M}\tilde{H}^{(M^\pm)\pm}_{\alpha,y,m,n,s}e^{jG_{x,m}x}\\ \sum_{m=-M}^{M}\tilde{H}^{(1)\pm}_{\alpha,z,m,n,s}e^{jG_{x,m}x} & \cdots & \sum_{m=-M}^{M}\tilde{H}^{(M^\pm)\pm}_{\alpha,z,m,n,s}e^{jG_{x,m}x}\end{pmatrix}. \tag{41d}$$

From Eqs. (39a)–(39d), the coupling coefficient matrix operators $\mathbf{C}^+_{\alpha,i}$, $\mathbf{C}^-_{\alpha,i}$, $\mathbf{C}^+_{\beta,i}$, and $\mathbf{C}^-_{\beta,i}$ for $i = 1, 2, 3, 4$ are obtained by

$$\begin{bmatrix} \mathbf{C}^{+}_{\alpha,i} \\ \mathbf{C}^{-}_{\alpha,i} \\ \mathbf{C}^{+}_{\beta,i} \\ \mathbf{C}^{-}_{\beta,i} \end{bmatrix} = \begin{pmatrix} (\tilde{\mathbf{W}}^{-1}_{\alpha,h}\tilde{\mathbf{W}}_{\alpha,+}(z_-) + \tilde{\mathbf{V}}^{-1}_{\alpha,h}\tilde{\mathbf{V}}_{\alpha,+}(z_-)) & (\tilde{\mathbf{W}}^{-1}_{\alpha,h}\tilde{\mathbf{W}}_{\alpha,-}(z_-) + \tilde{\mathbf{V}}^{-1}_{\alpha,h}\tilde{\mathbf{V}}_{\alpha,-}(z_-)) & (\tilde{\mathbf{W}}^{-1}_{\alpha,h}\tilde{\mathbf{W}}_{\beta,+}(z_-) + \tilde{\mathbf{V}}^{-1}_{\alpha,h}\tilde{\mathbf{V}}_{\beta,+}(z_-)) & (\tilde{\mathbf{W}}^{-1}_{\alpha,h}\tilde{\mathbf{W}}_{\beta,-}(z_-) + \tilde{\mathbf{V}}^{-1}_{\alpha,h}\tilde{\mathbf{V}}_{\beta,-}(z_-)) \\ (\tilde{\mathbf{W}}^{-1}_{\alpha,h}\tilde{\mathbf{W}}_{\alpha,+}(z_+) - \tilde{\mathbf{V}}^{-1}_{\alpha,h}\tilde{\mathbf{V}}_{\alpha,+}(z_+)) & (\tilde{\mathbf{W}}^{-1}_{\alpha,h}\tilde{\mathbf{W}}_{\alpha,-}(z_+) - \tilde{\mathbf{V}}^{-1}_{\alpha,h}\tilde{\mathbf{V}}_{\alpha,-}(z_+)) & (\tilde{\mathbf{W}}^{-1}_{\alpha,h}\tilde{\mathbf{W}}_{\beta,+}(z_+) - \tilde{\mathbf{V}}^{-1}_{\alpha,h}\tilde{\mathbf{V}}_{\beta,+}(z_+)) & (\tilde{\mathbf{W}}^{-1}_{\alpha,h}\tilde{\mathbf{W}}_{\beta,-}(z_+) - \tilde{\mathbf{V}}^{-1}_{\alpha,h}\tilde{\mathbf{V}}_{\beta,-}(z_+)) \\ (\tilde{\mathbf{Y}}^{-1}_{\beta,h}\tilde{\mathbf{Y}}_{\alpha,+}(x_-) + \tilde{\mathbf{Z}}^{-1}_{\beta,h}\tilde{\mathbf{Z}}_{\alpha,+}(x_-)) & (\tilde{\mathbf{Y}}^{-1}_{\beta,h}\tilde{\mathbf{Y}}_{\alpha,-}(x_-) + \tilde{\mathbf{Z}}^{-1}_{\beta,h}\tilde{\mathbf{Z}}_{\alpha,-}(x_-)) & (\tilde{\mathbf{Y}}^{-1}_{\beta,h}\tilde{\mathbf{Y}}_{\beta,+}(x_-) + \tilde{\mathbf{Z}}^{-1}_{\beta,h}\tilde{\mathbf{Z}}_{\beta,+}(x_-)) & (\tilde{\mathbf{Y}}^{-1}_{\beta,h}\tilde{\mathbf{Y}}_{\beta,-}(x_-) + \tilde{\mathbf{Z}}^{-1}_{\beta,h}\tilde{\mathbf{Z}}_{\beta,-}(x_-)) \\ (\tilde{\mathbf{Y}}^{-1}_{\beta,h}\tilde{\mathbf{Y}}_{\alpha,+}(x_+) - \tilde{\mathbf{Z}}^{-1}_{\beta,h}\tilde{\mathbf{Z}}_{\alpha,+}(x_+)) & (\tilde{\mathbf{Y}}^{-1}_{\beta,h}\tilde{\mathbf{Y}}_{\alpha,-}(x_+) - \tilde{\mathbf{Z}}^{-1}_{\beta,h}\tilde{\mathbf{Z}}_{\alpha,-}(x_+)) & (\tilde{\mathbf{Y}}^{-1}_{\beta,h}\tilde{\mathbf{Y}}_{\beta,+}(x_+) - \tilde{\mathbf{Z}}^{-1}_{\beta,h}\tilde{\mathbf{Z}}_{\beta,+}(x_+)) & (\tilde{\mathbf{Y}}^{-1}_{\beta,h}\tilde{\mathbf{Y}}_{\beta,-}(x_+) - \tilde{\mathbf{Z}}^{-1}_{\beta,h}\tilde{\mathbf{Z}}_{\beta,-}(x_+)) \end{pmatrix}^{-1} \times \begin{bmatrix} 2\mathbf{U}_1\delta_{1i} \\ 2\mathbf{U}_2\delta_{2i} \\ 2\mathbf{U}_3\delta_{3i} \\ 2\mathbf{U}_4\delta_{4i} \end{bmatrix}. \tag{42}$$

The S-matrix components, $\mathbf{S}_{i1}$, $\mathbf{S}_{i2}$, $\mathbf{S}_{i3}$, and $\mathbf{S}_{i4}$ are also obtained, respectively, from Eqs. (39a)–(39d),

$$\mathbf{S}_{i1} = \mathbf{W}^{-1}_{\alpha,h}[\tilde{\mathbf{W}}_{\alpha,+}(z_-)\mathbf{C}^{+}_{\alpha,i} + \tilde{\mathbf{W}}_{\alpha,-}(z_-)\mathbf{C}^{-}_{\alpha,i} + \tilde{\mathbf{W}}_{\beta,+}(z_-)\mathbf{C}^{+}_{\beta,i} + \tilde{\mathbf{W}}_{\beta,-}(z_-)\mathbf{C}^{-}_{\beta,i} - \mathbf{W}_{\alpha,h}\delta_{1i}], \tag{43a}$$

$$\mathbf{S}_{i2} = \mathbf{W}^{-1}_{\alpha,h}[\tilde{\mathbf{W}}_{\alpha,+}(z_+)\mathbf{C}^{+}_{\alpha,i} + \tilde{\mathbf{W}}_{\alpha,-}(z_+)\mathbf{C}^{-}_{\alpha,i} + \tilde{\mathbf{W}}_{\beta,+}(z_+)\mathbf{C}^{+}_{\beta,i} + \tilde{\mathbf{W}}_{\beta,-}(z_+)\mathbf{C}^{-}_{\beta,i} - \mathbf{W}_{\alpha,h}\delta_{2i}], \tag{43b}$$

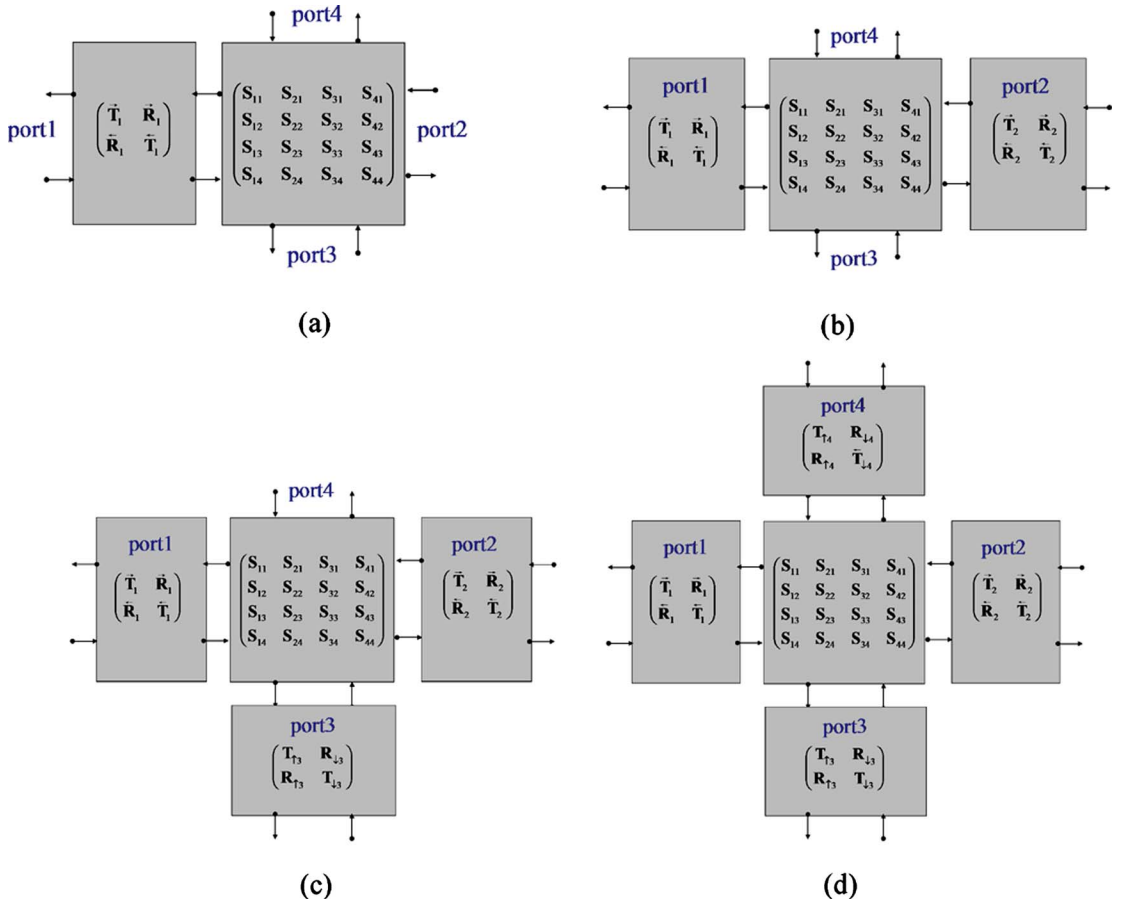

Fig. 22. (Color online) Building the extended four-port cross block: (a) step 1: interconnection of a two-port block to the four-port cross block through port 1, (b) step 2: interconnection of a two-port block to the combined four-port cross block through port 2, (c) step 3: interconnection of a two-port block to the combined four-port cross block through port 3, (d) step 4: building the extended four-port cross block by the interconnection of a two-port block to the combined four-port through port 4.

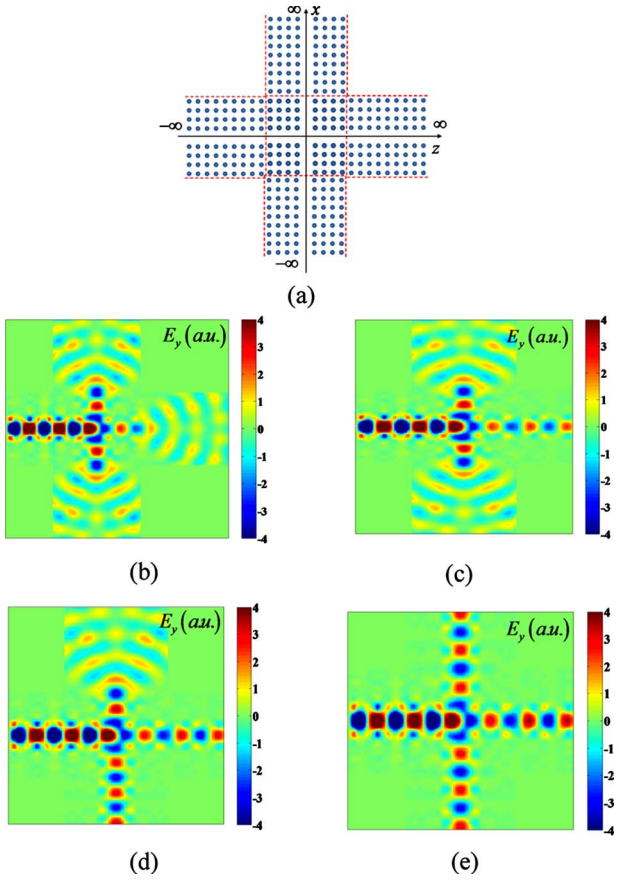

Fig. 23. (Color online) (a) Cross waveguide structure and y-polarization electric field distributions at each step of building the extended four-port cross block by the step-by-step interconnection procedure: steps (b) 1, (c) 2, (d) 3, and (e) 4.

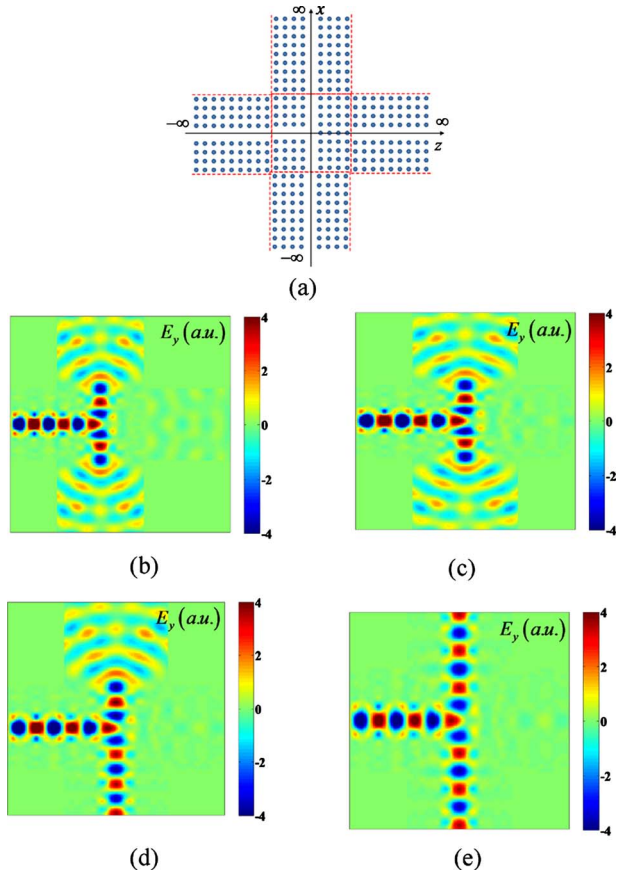

Fig. 24. (Color online) (a) T-branch waveguide structure and y-polarization electric field distributions at each step of building the extended four-port cross block by the step-by-step interconnection procedure: steps (b) 1, (c) 2, (d) 3, and (e) 4.

$$\mathbf{S}_{i3} = \mathbf{Y}_{\beta,h}^{-1}[\tilde{\mathbf{Y}}_{\alpha,+}(x_-)\mathbf{C}_{\alpha,i}^{+} + \tilde{\mathbf{Y}}_{\alpha,-}(x_-)\mathbf{C}_{\alpha,i}^{-} + \tilde{\mathbf{Y}}_{\beta,+}(x_-)\mathbf{C}_{\beta,i}^{+} + \tilde{\mathbf{Y}}_{\beta,-}(x_-)\mathbf{C}_{\beta,i}^{-} - \mathbf{Y}_{\beta,h}\delta_{3i}], \tag{43c}$$

$$\mathbf{S}_{i4} = \mathbf{Y}_{\beta,h}^{-1}[\tilde{\mathbf{Y}}_{\alpha,+}(x_+)\mathbf{C}_{\alpha,i}^{+} + \tilde{\mathbf{Y}}_{\alpha,-}(x_+)\mathbf{C}_{\alpha,i}^{-} + \tilde{\mathbf{Y}}_{\beta,+}(x_+)\mathbf{C}_{\beta,i}^{+} + \tilde{\mathbf{Y}}_{\beta,-}(x_+)\mathbf{C}_{\beta,i}^{-} - \mathbf{Y}_{\beta,h}\delta_{4i}]. \tag{43d}$$

We can easily understand that the S-matrix and coupling coefficients equations of the two-port blocks of Eqs. (20a), (20b), (21a)–(21d), (26a), (26b), (27a), and (27b) are the special cases of the above-stated equations of the four-port cross blocks.

The validity of the derived formulas is examined by the visualization of field distributions when a normally incident plane wave impinges on the port 1 interface of the intersection block. Figures 15(a)–15(c) illustrate the LFMA results of the S-matrix characterization of the intersection block of the photonic crystal cross-waveguide structure, the T-branch structure, and the 90°-bend structure, respectively. Here the regions of ports 1–4 are free space. We can see that the field boundary conditions are well-matched and the field continuity is conserved.

5. GENERALIZED SCATTERING-MATRIX METHOD

The S-matrix characterization of the four-port intersection block provides a basis to construct the GSMM for describing general nanophotonic networks. In this section, the GSMM for the four-port cross nanophotonic structure composed of four two-port blocks and a four-port intersection block is developed. In Subsection 5.A, the interconnection of two-port blocks is described with the 2×2 S-matrix formulation. In Subsection 5.B, the 4×4 GSMM representing the interconnection of a four-port intersection block and four two-port blocks is developed.

A. Interconnection of Two-Port Blocks

The interconnection of two-port blocks can be described by the 2×2 S-matrix model. In Figs. 16 and 17, four kinds of interconnection of two-port α and β blocks are illustrated. The S matrices of the interconnected blocks are established in Section 4.

Let us assume two two-port α blocks with finite size that are characterized by respective S matrix $\mathbf{S}^{(1,1)}$ and $\mathbf{S}^{(2,2)}$. The layer S matrix of the multilayer structure, i.e., the interconnected structure, $\mathbf{S}^{(1,2)}$ and its coupling coefficient matrix operator is obtained by the ESMM [11,20].

The directional characteristics of multilayer can be obtained by properly combining the obtained matrix operators of single layers through the Redheffer's star product relation $\mathbf{S}^{(1,2)}=\mathbf{S}^{(1,1)}*\mathbf{S}^{(2,2)}$ described in [11,20].

The reflection and transmission matrix operators, $\overleftarrow{\mathbf{R}}^{(1,2)}$, $\vec{\mathbf{T}}^{(1,2)}$, $\vec{\mathbf{R}}^{(1,2)}$, and $\overleftarrow{\mathbf{T}}^{(1,2)}$ of $\mathbf{S}^{(1,2)}$ of the multilayer are obtained by the Redheffer's star product relation

$$\overleftarrow{\mathbf{R}}^{(1,2)} = \overleftarrow{\mathbf{R}}^{(1,1)} + \overleftarrow{\mathbf{T}}^{(1,1)}[(\mathbf{I} - \overleftarrow{\mathbf{R}}^{(2,2)}\vec{\mathbf{R}}^{(1,1)})^{-1}]\overleftarrow{\mathbf{R}}^{(2,2)}\vec{\mathbf{T}}^{(1,1)}, \tag{44a}$$

$$\vec{\mathbf{T}}^{(1,2)} = \vec{\mathbf{T}}^{(2,2)}[(\mathbf{I} - \vec{\mathbf{R}}^{(1,1)}\overleftarrow{\mathbf{R}}^{(2,2)})^{-1}]\vec{\mathbf{T}}^{(1,1)}, \tag{44b}$$

$$\vec{\mathbf{R}}^{(1,2)} = \vec{\mathbf{R}}^{(2,2)} + \vec{\mathbf{T}}^{(2,2)}[(\mathbf{I} - \vec{\mathbf{R}}^{(1,1)}\overleftarrow{\mathbf{R}}^{(2,2)})^{-1}]\vec{\mathbf{R}}^{(1,1)}\overleftarrow{\mathbf{T}}^{(2,2)}, \tag{44c}$$

$$\overleftarrow{\mathbf{T}}^{(1,2)} = \overleftarrow{\mathbf{T}}^{(1,1)}[(\mathbf{I} - \overleftarrow{\mathbf{R}}^{(2,2)}\vec{\mathbf{R}}^{(1,1)})^{-1}]\overleftarrow{\mathbf{T}}^{(2,2)}. \tag{44d}$$

Let us denote the internal coupling coefficient matrix operators of the combined multilayer as $\tilde{\mathbf{C}}^{(1,2)}_{\alpha,a,(1,2)}$ and $\tilde{\mathbf{C}}^{(1,2)}_{\alpha,b,(1,2)}$. Here $\tilde{\mathbf{C}}^{(1,2)}_{\alpha,a,(1,2)}$ and $\tilde{\mathbf{C}}^{(1,2)}_{\alpha,b,(1,2)}$ are $[4(2M+1)(2N+1)]\times[8(2M+1)(2N+1)]$ matrices given by

$$\tilde{\mathbf{C}}^{(1,2)}_{\alpha,a,(1,2)} = [\mathbf{C}^{(1,2)}_{\alpha,a,(1)}, \mathbf{C}^{(1,2)}_{\alpha,a,(2)}], \tag{45a}$$

$$\tilde{\mathbf{C}}^{(1,2)}_{\alpha,b,(1,2)} = [\mathbf{C}^{(1,2)}_{\alpha,b,(1)}, \mathbf{C}^{(1,2)}_{\alpha,b,(2)}], \tag{45b}$$

where $(\mathbf{C}^{(1,2)}_{a,1}, \mathbf{C}^{(1,2)}_{b,1})$ and $(\mathbf{C}^{(1,2)}_{a,2}, \mathbf{C}^{(1,2)}_{b,2})$ are the respective coupling coefficient matrix operators corresponding to the first and second layers. Then the formulas of the internal coupling coefficients are derived, by the extended star product of the ESMM, as

$$\begin{pmatrix} \mathbf{C}^{(1,2)}_{a,(1)} \\ \mathbf{C}^{(1,2)}_{b,(1)} \end{pmatrix} = \begin{pmatrix} \mathbf{C}^{(1,1)}_{a,(1)} + \mathbf{C}^{(1,1)}_{b,(1)}(\mathbf{I} - \overleftarrow{\mathbf{R}}^{(2,2)}\vec{\mathbf{R}}^{(1,1)})^{-1}\overleftarrow{\mathbf{R}}^{(2,2)}\vec{\mathbf{T}}^{(1,1)} \\ \mathbf{C}^{(1,1)}_{b,(1)}(\mathbf{I} - \overleftarrow{\mathbf{R}}^{(2,2)}\vec{\mathbf{R}}^{(1,1)})^{-1}\overleftarrow{\mathbf{T}}^{(2,2)} \end{pmatrix}, \tag{46a}$$

$$\begin{pmatrix} \mathbf{C}^{(1,2)}_{a,(2)} \\ \mathbf{C}^{(1,2)}_{b,(2)} \end{pmatrix} = \begin{pmatrix} \mathbf{C}^{(2,2)}_{a,(2)}(\mathbf{I} - \vec{\mathbf{R}}^{(1,1)}\overleftarrow{\mathbf{R}}^{(2,2)})^{-1}\vec{\mathbf{T}}^{(1,1)} \\ \mathbf{C}^{(2,2)}_{b,(2)} + \mathbf{C}^{(2,2)}_{a,(2)}(\mathbf{I} - \vec{\mathbf{R}}^{(1,1)}\overleftarrow{\mathbf{R}}^{(2,2)})^{-1}\vec{\mathbf{R}}^{(1,1)}\overleftarrow{\mathbf{T}}^{(2,2)} \end{pmatrix}. \tag{46b}$$

The layer S matrix and the coupling coefficient matrix of the multilayer $M^{(1,N)}$ can be obtained by

$$\mathbf{S}^{(1,N)} = \mathbf{S}^{(1,1)} * \mathbf{S}^{(2,2)} * \cdots * \mathbf{S}^{(N-1,N-1)} * \mathbf{S}^{(N,N)}, \tag{47a}$$

$$(\tilde{\mathbf{C}}^{(1,N)}_{\alpha,a,(1,N)}, \tilde{\mathbf{C}}^{(1,N)}_{\alpha,b,(1,N)}) = (\tilde{\mathbf{C}}^{(1,1)}_{\alpha,a,(1,1)}, \tilde{\mathbf{C}}^{(1,1)}_{\alpha,b,(1,1)}) * (\tilde{\mathbf{C}}^{(2,2)}_{\alpha,a,(2,2)}, \tilde{\mathbf{C}}^{(2,2)}_{\alpha,b,(2,2)}) * \cdots * (\tilde{\mathbf{C}}^{(N-1,N-1)}_{\alpha,a,(N-1,N-1)}, \tilde{\mathbf{C}}^{(N-1,N-1)}_{\alpha,b,(N-1,N-1)}) * (\tilde{\mathbf{C}}^{(N,N)}_{\alpha,a,(N,N)}, \tilde{\mathbf{C}}^{(N,N)}_{\alpha,b,(N,N)}). \tag{47b}$$

With the above results, we can construct the total S matrix of the whole multilayer $M^{(0,N+1)}$. At the first step, the S matrix $\mathbf{S}^{(0,N)}$ of the multilayer $M^{(0,N)}$ is derived by the Redheffer's star product of $\mathbf{S}^{(0,0)}$ of Eqs. (22a)–(22d) and $\mathbf{S}^{(1,N)}$ of Eq. (47a) as

$$\mathbf{S}^{(0,N)} = \mathbf{S}^{(0,0)} * \mathbf{S}^{(1,N)}. \tag{48a}$$

The coupling coefficient matrices $\mathbf{C}^{(0,N)}_{\alpha,a,(k)}$ and $\mathbf{C}^{(0,N)}_{\alpha,b,(k)}$ $(1 \le k \le N)$ of the layers L_1–L_N in $M^{(0,N)}$ are given as [20]

$$(\mathbf{C}^{(0,N)}_{a,(k)}, \mathbf{C}^{(0,N)}_{b,(k)}) = (\mathbf{C}^{(1,N)}_{a,(k)}(\mathbf{I} - \vec{\mathbf{R}}^{(0,0)}\overleftarrow{\mathbf{R}}^{(1,N)})^{-1}\vec{\mathbf{T}}^{(0,0)}, \mathbf{C}^{(1,N)}_{b,(k)} + \mathbf{C}^{(1,N)}_{a,(k)}(\mathbf{I} - \vec{\mathbf{R}}^{(0,0)}\overleftarrow{\mathbf{R}}^{(1,N)})^{-1}\vec{\mathbf{R}}^{(0,0)}\overleftarrow{\mathbf{T}}^{(1,N)}). \tag{48b}$$

The total S matrix $\mathbf{S}^{(0,N+1)}$ of the multilayer $M^{(0,N+1)}$ is taken as

$$\mathbf{S}^{(0,N+1)} = \mathbf{S}^{(0,N)} * \mathbf{S}^{(N+1,N+1)}. \tag{49a}$$

The final coupling coefficient matrices $\mathbf{C}^{(0,N+1)}_{a,(k)}$ and $\mathbf{C}^{(0,N+1)}_{b,(k)}$ $(1 \le k \le N)$ of the layers L_1–L_N in $M^{(0,N+1)}$ are obtained as

$$(\mathbf{C}^{(0,N+1)}_{a,(k)}, \mathbf{C}^{(0,N+1)}_{b,(k)}) = (\mathbf{C}^{(0,N)}_{a,(k)} + \mathbf{C}^{(0,N)}_{b,(k)}(\mathbf{I} - \overleftarrow{\mathbf{R}}^{(N+1,N+1)}\vec{\mathbf{R}}^{(0,N)})^{-1} \times \overleftarrow{\mathbf{R}}^{(N+1,N+1)}\vec{\mathbf{T}}^{(0,N)}, \mathbf{C}^{(0,N)}_{b,(k)}(\mathbf{I} - \overleftarrow{\mathbf{R}}^{(N+1,N+1)}\vec{\mathbf{R}}^{(0,N)})^{-1}\overleftarrow{\mathbf{T}}^{(N+1,N+1)}). \tag{49b}$$

The S matrix $\mathbf{S}^{(0,N+1)}$ and the coupling coefficient matrices, $\mathbf{C}^{(0,N+1)}_{a,(k)}$ and $\mathbf{C}^{(0,N+1)}_{b,(k)}$, provide the complete characterization of the multilayer $M^{(0,N+1)}$.

Using the boundary S-matrix formulas and the previously analyzed Bloch eigenmodes, we present the reflection and transmission characteristics of the fundamental guided Bloch eigenmode of the half-infinite two-dimensional photonic crystal waveguide structure in Fig. 18. Figure 18(a) illustrates that the fundamental guided Bloch eignmode is incident on the end face of the photonic crystal waveguide. The backward propagating guided Bloch mode is reflected and the diffraction field distribution is generated at the interface of the end face of the photonic crystal waveguide and free space. The y-polarization electric field, x-polarization magnetic electric field, and z-polarization magnetic field distributions are shown in Figs. 18(b)–18(d), respectively. In Fig. 18(e), the excitation of the fundamental guided Bloch eigenmode by a normally incident plane wave from free space region to the interface is presented. The y-polarization electric field, x-polarization magnetic field, and z-polarization magnetic field distributions are shown in Figs. 18(f)–18(h), respectively.

With the layer S-matrix formulas, the reflection and transmission characteristics of the finite sized two-dimensional photonic crystal waveguide structure are analyzed. Figure 19(a) illustrates that a y-polarization plane wave is normally incident from the left free space on the left end face of the photonic crystal waveguide and

a diffraction field distribution is generated in the right free space region. The y-polarization electric field, x-polarization magnetic electric field, and z-polarization magnetic field distributions are shown in Figs. 19(b)–19(d), respectively.

B. Interconnection of Four-Port Block and Two-Port Blocks

In this section, the development of the 4×4 S-matrix model for the four-port block composed of two-port blocks and four-port cross block is elucidated. Figure 20 shows the S-matrix model of the four-port crossed nanophotonic structure that is investigated in this section.

We can take a step-by-step approach to obtain the total S matrix of this four-port cross nanophotonic structure. Before obtaining total S matrix, we need to manifest the interconnections of a two-port block and a four-port cross block. In Fig. 21, the interconnection of a two-port block and a four-port cross block through the port i is illustrated. The S-matrix components of the two-port block are denoted, with the subscript indicating the connected port number, by $\overleftarrow{\mathbf{R}}_i$, $\vec{\mathbf{T}}_i$, $\vec{\mathbf{R}}_i$, $\overleftarrow{\mathbf{T}}_i$ $(i=1,2)$ and $\mathbf{R}_{\uparrow i}$, $\mathbf{T}_{\downarrow i}$, $\mathbf{R}_{\downarrow i}$, $\mathbf{T}_{\uparrow i}$ $(i=3,4)$, respectively. The internal coupling coefficient matrix operators of the two-port block are denoted, with the superscript indicating the connected port number, by $\mathbf{C}_a^{(i)}$ and $\mathbf{C}_b^{(i)}$, respectively.

By the same ray-tracing approach addressed in [20], all components of the total S matrix of the connected structure can be easily derived. The internal infinite multiple reflections through the four-port of the intersection block and a two-port block are intuitively formulated to the recursion equation of the S-matrix components and the coupling coefficient matrix operators.

In the derived formulas, the tilde notation is used in denoting the components of the total S matrix. $\tilde{\mathbf{C}}_{p,1}^{(1)}$, $\tilde{\mathbf{C}}_{p,2}^{(1)}$, $\tilde{\mathbf{C}}_{p,2}^{(1)}$, and $\tilde{\mathbf{C}}_{p,3}^{(1)}$ indicate the coupling coefficient matrix operators of the two-port block induced by the excitations of parts 1–4, respectively. The superscript (1) means the port index through which the two-port block is connected to the four-port cross block. The derived S matrix recursion formulas of the interconnection of the two-port block and the four-port cross block through port 1 are listed as follows:

$$\begin{pmatrix} \tilde{\mathbf{S}}_{11} & \tilde{\mathbf{S}}_{21} & \tilde{\mathbf{S}}_{31} & \tilde{\mathbf{S}}_{41} \\ \tilde{\mathbf{S}}_{12} & \tilde{\mathbf{S}}_{22} & \tilde{\mathbf{S}}_{32} & \tilde{\mathbf{S}}_{42} \\ \tilde{\mathbf{S}}_{13} & \tilde{\mathbf{S}}_{23} & \tilde{\mathbf{S}}_{33} & \tilde{\mathbf{S}}_{43} \\ \tilde{\mathbf{S}}_{14} & \tilde{\mathbf{S}}_{24} & \tilde{\mathbf{S}}_{34} & \tilde{\mathbf{S}}_{44} \end{pmatrix} = \begin{pmatrix} \overleftarrow{\mathbf{R}}_1 + \overleftarrow{\mathbf{T}}_1\mathbf{S}_{11}(\mathbf{I}-\vec{\mathbf{R}}_1\mathbf{S}_{11})^{-1}\vec{\mathbf{T}}_1 & \overleftarrow{\mathbf{T}}_1(\mathbf{I}-\mathbf{S}_{11}\vec{\mathbf{R}}_1)^{-1}\mathbf{S}_{21} & \overleftarrow{\mathbf{T}}_1(\mathbf{I}-\mathbf{S}_{11}\vec{\mathbf{R}}_1)^{-1}\mathbf{S}_{31} & \overleftarrow{\mathbf{T}}_1(\mathbf{I}-\mathbf{S}_{11}\vec{\mathbf{R}}_1)^{-1}\mathbf{S}_{41} \\ \mathbf{S}_{12}(\mathbf{I}-\vec{\mathbf{R}}_1\mathbf{S}_{11})^{-1}\vec{\mathbf{T}}_1 & \mathbf{S}_{22}+\mathbf{S}_{12}\vec{\mathbf{R}}_1(\mathbf{I}-\mathbf{S}_{11}\vec{\mathbf{R}}_1)^{-1}\mathbf{S}_{21} & \mathbf{S}_{32}+\mathbf{S}_{12}\vec{\mathbf{R}}_1(\mathbf{I}-\mathbf{S}_{11}\vec{\mathbf{R}}_1)^{-1}\mathbf{S}_{31} & \mathbf{S}_{42}+\mathbf{S}_{12}\vec{\mathbf{R}}_1(\mathbf{I}-\mathbf{S}_{11}\vec{\mathbf{R}}_1)^{-1}\mathbf{S}_{41} \\ \mathbf{S}_{13}(\mathbf{I}-\vec{\mathbf{R}}_1\mathbf{S}_{11})^{-1}\vec{\mathbf{T}}_1 & \mathbf{S}_{23}+\mathbf{S}_{13}\vec{\mathbf{R}}_1(\mathbf{I}-\mathbf{S}_{11}\vec{\mathbf{R}}_1)^{-1}\mathbf{S}_{21} & \mathbf{S}_{33}+\mathbf{S}_{13}\vec{\mathbf{R}}_1(\mathbf{I}-\mathbf{S}_{11}\vec{\mathbf{R}}_1)^{-1}\mathbf{S}_{31} & \mathbf{S}_{43}+\mathbf{S}_{13}\vec{\mathbf{R}}_1(\mathbf{I}-\mathbf{S}_{11}\vec{\mathbf{R}}_1)^{-1}\mathbf{S}_{41} \\ \mathbf{S}_{14}(\mathbf{I}-\vec{\mathbf{R}}_1\mathbf{S}_{11})^{-1}\vec{\mathbf{T}}_1 & \mathbf{S}_{24}+\mathbf{S}_{14}\vec{\mathbf{R}}_1(\mathbf{I}-\mathbf{S}_{11}\vec{\mathbf{R}}_1)^{-1}\mathbf{S}_{21} & \mathbf{S}_{34}+\mathbf{S}_{14}\vec{\mathbf{R}}_1(\mathbf{I}-\mathbf{S}_{11}\vec{\mathbf{R}}_1)^{-1}\mathbf{S}_{31} & \mathbf{S}_{44}+\mathbf{S}_{14}\vec{\mathbf{R}}_1(\mathbf{I}-\mathbf{S}_{11}\vec{\mathbf{R}}_1)^{-1}\mathbf{S}_{41} \end{pmatrix}, \tag{50a}$$

$$\begin{pmatrix} \tilde{\mathbf{C}}_{p,1}^{(1)} \\ \tilde{\mathbf{C}}_{p,2}^{(1)} \\ \tilde{\mathbf{C}}_{p,3}^{(1)} \\ \tilde{\mathbf{C}}_{p,4}^{(1)} \end{pmatrix} = \begin{pmatrix} \mathbf{C}_a^{(1)} + \mathbf{C}_b^{(1)}\mathbf{S}_{11}(\mathbf{I}-\overleftarrow{\mathbf{R}}_1\mathbf{S}_{11})^{-1}\vec{\mathbf{T}}_1 \\ \mathbf{C}_b^{(1)}(\mathbf{I}-\mathbf{S}_{11}\vec{\mathbf{R}}_1)^{-1}\mathbf{S}_{21} \\ \mathbf{C}_b^{(1)}(\mathbf{I}-\mathbf{S}_{11}\vec{\mathbf{R}}_1)^{-1}\mathbf{S}_{31} \\ \mathbf{C}_b^{(1)}(\mathbf{I}-\mathbf{S}_{11}\vec{\mathbf{R}}_1)^{-1}\mathbf{S}_{41} \end{pmatrix}, \tag{50b}$$

$$\begin{pmatrix} \tilde{\mathbf{C}}_{\alpha,1} & \tilde{\mathbf{C}}_{\alpha,2} & \tilde{\mathbf{C}}_{\alpha,3} & \tilde{\mathbf{C}}_{\alpha,4} \\ \tilde{\mathbf{C}}_{\beta,1} & \tilde{\mathbf{C}}_{\beta,2} & \tilde{\mathbf{C}}_{\beta,3} & \tilde{\mathbf{C}}_{\beta,4} \end{pmatrix} = \begin{pmatrix} \mathbf{C}_{\alpha,1}(\mathbf{I}-\vec{\mathbf{R}}_1\mathbf{S}_{11})^{-1}\vec{\mathbf{T}}_1 & \mathbf{C}_{\alpha,2}+\mathbf{C}_{\alpha,1}\vec{\mathbf{R}}_1(\mathbf{I}-\mathbf{S}_{11}\vec{\mathbf{R}}_1)^{-1}\mathbf{S}_{21} & \mathbf{C}_{\alpha,3}+\mathbf{C}_{\alpha,1}\vec{\mathbf{R}}_1(\mathbf{I}-\mathbf{S}_{11}\vec{\mathbf{R}}_1)^{-1}\mathbf{S}_{31} & \mathbf{C}_{\alpha,4}+\mathbf{C}_{\alpha,1}\vec{\mathbf{R}}_1(\mathbf{I}-\mathbf{S}_{11}\vec{\mathbf{R}}_1)^{-1}\mathbf{S}_{41} \\ \mathbf{C}_{\beta,1}(\mathbf{I}-\vec{\mathbf{R}}_1\mathbf{S}_{11})^{-1}\vec{\mathbf{T}}_1 & \mathbf{C}_{\beta,2}+\mathbf{C}_{\beta,1}\vec{\mathbf{R}}_1(\mathbf{I}-\mathbf{S}_{11}\vec{\mathbf{R}}_1)^{-1}\mathbf{S}_{21} & \mathbf{C}_{\beta,3}+\mathbf{C}_{\beta,1}\vec{\mathbf{R}}_1(\mathbf{I}-\mathbf{S}_{11}\vec{\mathbf{R}}_1)^{-1}\mathbf{S}_{31} & \mathbf{C}_{\beta,4}+\mathbf{C}_{\beta,1}(\mathbf{I}-\mathbf{S}_{11}\vec{\mathbf{R}}_1)^{-1}\mathbf{S}_{41} \end{pmatrix}. \tag{50c}$$

The derived S-matrix recursion formulas of the interconnection of the two-port block and the four-port cross block through port 2 are listed as follows:

$$\begin{pmatrix} \tilde{\mathbf{S}}_{11} & \tilde{\mathbf{S}}_{21} & \tilde{\mathbf{S}}_{31} & \tilde{\mathbf{S}}_{41} \\ \tilde{\mathbf{S}}_{12} & \tilde{\mathbf{S}}_{22} & \tilde{\mathbf{S}}_{32} & \tilde{\mathbf{S}}_{42} \\ \tilde{\mathbf{S}}_{13} & \tilde{\mathbf{S}}_{23} & \tilde{\mathbf{S}}_{33} & \tilde{\mathbf{S}}_{43} \\ \tilde{\mathbf{S}}_{14} & \tilde{\mathbf{S}}_{24} & \tilde{\mathbf{S}}_{34} & \tilde{\mathbf{S}}_{44} \end{pmatrix}$$
$$= \begin{pmatrix} \mathbf{S}_{11} + \mathbf{S}_{21}\bar{\tilde{\mathbf{R}}}_2(\mathbf{I} - \mathbf{S}_{22}\bar{\tilde{\mathbf{R}}}_2)^{-1}\mathbf{S}_{12} & \mathbf{S}_{21}(\mathbf{I} - \bar{\tilde{\mathbf{R}}}_2\mathbf{S}_{22})^{-1}\vec{\tilde{\mathbf{T}}}_2 & \mathbf{S}_{31} + \mathbf{S}_{21}\bar{\tilde{\mathbf{R}}}_2(\mathbf{I} - \mathbf{S}_{22}\bar{\tilde{\mathbf{R}}}_2)^{-1}\mathbf{S}_{32} & \mathbf{S}_{41} + \mathbf{S}_{21}\bar{\tilde{\mathbf{R}}}_2(\mathbf{I} - \mathbf{S}_{22}\bar{\tilde{\mathbf{R}}}_2)^{-1}\mathbf{S}_{42} \\ \vec{\tilde{\mathbf{T}}}_2(\mathbf{I} - \mathbf{S}_{22}\bar{\tilde{\mathbf{R}}}_2)^{-1}\mathbf{S}_{12} & \vec{\tilde{\mathbf{R}}}_2 + \vec{\tilde{\mathbf{T}}}_2\mathbf{S}_{22}(\mathbf{I} - \bar{\tilde{\mathbf{R}}}_2\mathbf{S}_{22})^{-1}\vec{\tilde{\mathbf{T}}}_2 & \vec{\tilde{\mathbf{T}}}_2(\mathbf{I} - \mathbf{S}_{22}\bar{\tilde{\mathbf{R}}}_2)^{-1}\mathbf{S}_{32} & \vec{\tilde{\mathbf{T}}}_2(\mathbf{I} - \mathbf{S}_{22}\bar{\tilde{\mathbf{R}}}_2)^{-1}\mathbf{S}_{42} \\ \mathbf{S}_{13} + \mathbf{S}_{23}\bar{\tilde{\mathbf{R}}}_2(\mathbf{I} - \mathbf{S}_{22}\bar{\tilde{\mathbf{R}}}_2)^{-1}\mathbf{S}_{12} & \mathbf{S}_{23}(\mathbf{I} - \bar{\tilde{\mathbf{R}}}_2\mathbf{S}_{22})^{-1}\vec{\tilde{\mathbf{T}}}_2 & \mathbf{S}_{33} + \mathbf{S}_{23}\bar{\tilde{\mathbf{R}}}_2(\mathbf{I} - \mathbf{S}_{22}\bar{\tilde{\mathbf{R}}}_2)^{-1}\mathbf{S}_{32} & \mathbf{S}_{43} + \mathbf{S}_{23}\bar{\tilde{\mathbf{R}}}_2(\mathbf{I} - \mathbf{S}_{22}\bar{\tilde{\mathbf{R}}}_2)^{-1}\mathbf{S}_{42} \\ \mathbf{S}_{14} + \mathbf{S}_{24}\bar{\tilde{\mathbf{R}}}_2(\mathbf{I} - \mathbf{S}_{22}\bar{\tilde{\mathbf{R}}}_2)^{-1}\mathbf{S}_{12} & \mathbf{S}_{24}(\mathbf{I} - \bar{\tilde{\mathbf{R}}}_2\mathbf{S}_{22})^{-1}\vec{\tilde{\mathbf{T}}}_2 & \mathbf{S}_{34} + \mathbf{S}_{24}\bar{\tilde{\mathbf{R}}}_2(\mathbf{I} - \mathbf{S}_{22}\bar{\tilde{\mathbf{R}}}_2)^{-1}\mathbf{S}_{32} & \mathbf{S}_{44} + \mathbf{S}_{24}\bar{\tilde{\mathbf{R}}}_2(\mathbf{I} - \mathbf{S}_{22}\bar{\tilde{\mathbf{R}}}_2)^{-1}\mathbf{S}_{42} \end{pmatrix}, \tag{51a}$$

$$\begin{pmatrix} \tilde{\mathbf{C}}^{(2)}_{p,1} \\ \tilde{\mathbf{C}}^{(2)}_{p,2} \\ \tilde{\mathbf{C}}^{(2)}_{p,3} \\ \tilde{\mathbf{C}}^{(2)}_{p,4} \end{pmatrix} = \begin{pmatrix} \mathbf{C}^{(2)}_a(\mathbf{I} - \mathbf{S}_{22}\bar{\tilde{\mathbf{R}}}_2)^{-1}\mathbf{S}_{12} \\ \mathbf{C}^{(2)}_b + \mathbf{C}^{(2)}_a\mathbf{S}_{22}(\mathbf{I} - \bar{\tilde{\mathbf{R}}}_2\mathbf{S}_{22})^{-1}\vec{\tilde{\mathbf{T}}}_2 \\ \mathbf{C}^{(2)}_a(\mathbf{I} - \mathbf{S}_{22}\bar{\tilde{\mathbf{R}}}_2)^{-1}\mathbf{S}_{32} \\ \mathbf{C}^{(2)}_a(\mathbf{I} - \mathbf{S}_{22}\bar{\tilde{\mathbf{R}}}_2)^{-1}\mathbf{S}_{42} \end{pmatrix}, \tag{51b}$$

$$\begin{pmatrix} \tilde{\mathbf{C}}_{\alpha,1} & \tilde{\mathbf{C}}_{\alpha,2} & \tilde{\mathbf{C}}_{\alpha,3} & \tilde{\mathbf{C}}_{\alpha,4} \\ \tilde{\mathbf{C}}_{\beta,1} & \tilde{\mathbf{C}}_{\beta,2} & \tilde{\mathbf{C}}_{\beta,3} & \tilde{\mathbf{C}}_{\beta,4} \end{pmatrix}$$
$$= \begin{pmatrix} \mathbf{C}_{\alpha,1} + \mathbf{C}_{\alpha,2}\bar{\tilde{\mathbf{R}}}_2(\mathbf{I} - \mathbf{S}_{22}\bar{\tilde{\mathbf{R}}}_2)^{-1}\mathbf{S}_{12} & \mathbf{C}_{\alpha,2}(\mathbf{I} - \bar{\tilde{\mathbf{R}}}_2\mathbf{S}_{22})^{-1}\vec{\tilde{\mathbf{T}}}_2 & \mathbf{C}_{\alpha,3} + \mathbf{C}_{\alpha,2}\bar{\tilde{\mathbf{R}}}_2(\mathbf{I} - \mathbf{S}_{22}\bar{\tilde{\mathbf{R}}}_2)^{-1}\mathbf{S}_{32} & \mathbf{C}_{\alpha,4} + \mathbf{C}_{\alpha,2}\bar{\tilde{\mathbf{R}}}_2(\mathbf{I} - \mathbf{S}_{22}\bar{\tilde{\mathbf{R}}}_2)^{-1}\mathbf{S}_{42} \\ \mathbf{C}_{\beta,1} + \mathbf{C}_{\beta,2}\bar{\tilde{\mathbf{R}}}_2(\mathbf{I} - \mathbf{S}_{22}\bar{\tilde{\mathbf{R}}}_2)^{-1}\mathbf{S}_{12} & \mathbf{C}_{\beta,2}(\mathbf{I} - \bar{\tilde{\mathbf{R}}}_2\mathbf{S}_{22})^{-1}\vec{\tilde{\mathbf{T}}}_2 & \mathbf{C}_{\beta,3} + \mathbf{C}_{\beta,2}\bar{\tilde{\mathbf{R}}}_2(\mathbf{I} - \mathbf{S}_{22}\bar{\tilde{\mathbf{R}}}_2)^{-1}\mathbf{S}_{32} & \mathbf{C}_{\beta,4} + \mathbf{C}_{\beta,2}\bar{\tilde{\mathbf{R}}}_2(\mathbf{I} - \mathbf{S}_{22}\bar{\tilde{\mathbf{R}}}_2)^{-1}\mathbf{S}_{42} \end{pmatrix}. \tag{51c}$$

The derived S-matrix recursion formulas of the interconnection of the two-port block and the four-port cross block through port 3 are listed as follows:

$$\begin{pmatrix} \tilde{\mathbf{S}}_{11} & \tilde{\mathbf{S}}_{21} & \tilde{\mathbf{S}}_{31} & \tilde{\mathbf{S}}_{41} \\ \tilde{\mathbf{S}}_{12} & \tilde{\mathbf{S}}_{22} & \tilde{\mathbf{S}}_{32} & \tilde{\mathbf{S}}_{42} \\ \tilde{\mathbf{S}}_{13} & \tilde{\mathbf{S}}_{23} & \tilde{\mathbf{S}}_{33} & \tilde{\mathbf{S}}_{43} \\ \tilde{\mathbf{S}}_{14} & \tilde{\mathbf{S}}_{24} & \tilde{\mathbf{S}}_{34} & \tilde{\mathbf{S}}_{44} \end{pmatrix}$$
$$= \begin{pmatrix} \mathbf{S}_{11} + \mathbf{S}_{31}\mathbf{R}_{\uparrow 3}(\mathbf{I} - \mathbf{S}_{33}\mathbf{R}_{\uparrow 3})^{-1}\mathbf{S}_{13} & \mathbf{S}_{21} + \mathbf{S}_{31}\mathbf{R}_{\uparrow 3}(\mathbf{I} - \mathbf{S}_{33}\mathbf{R}_{\uparrow 3})^{-1}\mathbf{S}_{23} & \mathbf{S}_{31}(\mathbf{I} - \mathbf{R}_{\uparrow 3}\mathbf{S}_{33})^{-1}\mathbf{T}_{\uparrow 3} & \mathbf{S}_{41} + \mathbf{S}_{31}\mathbf{R}_{\uparrow 3}(\mathbf{I} - \mathbf{S}_{33}\mathbf{R}_{\uparrow 3})^{-1}\mathbf{S}_{43} \\ \mathbf{S}_{12} + \mathbf{S}_{32}\mathbf{R}_{\uparrow 3}(\mathbf{I} - \mathbf{S}_{33}\mathbf{R}_{\uparrow 3})^{-1}\mathbf{S}_{13} & \mathbf{S}_{22} + \mathbf{S}_{32}\mathbf{R}_{\uparrow 3}(\mathbf{I} - \mathbf{S}_{33}\mathbf{R}_{\uparrow 3})^{-1}\mathbf{S}_{23} & \mathbf{S}_{32}(\mathbf{I} - \mathbf{R}_{\uparrow 3}\mathbf{S}_{33})^{-1}\mathbf{T}_{\uparrow 3} & \mathbf{S}_{42} + \mathbf{S}_{32}\mathbf{R}_{\uparrow 3}(\mathbf{I} - \mathbf{S}_{33}\mathbf{R}_{\uparrow 3})^{-1}\mathbf{S}_{43} \\ \mathbf{T}_{\downarrow 3}(\mathbf{I} - \mathbf{S}_{33}\mathbf{R}_{\uparrow 3})^{-1}\mathbf{S}_{13} & \mathbf{T}_{\downarrow 3}(\mathbf{I} - \mathbf{S}_{33}\mathbf{R}_{\uparrow 3})^{-1}\mathbf{S}_{23} & \mathbf{R}_{\downarrow 3} + \mathbf{T}_{\downarrow 3}\mathbf{S}_{33}(\mathbf{I} - \mathbf{R}_{\uparrow 3}\mathbf{S}_{33})^{-1}\mathbf{T}_{\uparrow 3} & \mathbf{T}_{\downarrow 3}(\mathbf{I} - \mathbf{S}_{33}\mathbf{R}_{\uparrow 3})^{-1}\mathbf{S}_{43} \\ \mathbf{S}_{14} + \mathbf{S}_{34}\mathbf{R}_{\uparrow 3}(\mathbf{I} - \mathbf{S}_{33}\mathbf{R}_{\uparrow 3})^{-1}\mathbf{S}_{13} & \mathbf{S}_{24} + \mathbf{S}_{34}\mathbf{R}_{\uparrow 3}(\mathbf{I} - \mathbf{S}_{33}\mathbf{R}_{\uparrow 3})^{-1}\mathbf{S}_{23} & \mathbf{S}_{34}(\mathbf{I} - \mathbf{R}_{\uparrow 3}\mathbf{S}_{33})^{-1}\mathbf{T}_{\uparrow 3} & \mathbf{S}_{44} + \mathbf{S}_{34}\mathbf{R}_{\uparrow 3}(\mathbf{I} - \mathbf{S}_{33}\mathbf{R}_{\uparrow 3})^{-1}\mathbf{S}_{43} \end{pmatrix}, \tag{52a}$$

$$\begin{pmatrix} \tilde{\mathbf{C}}_{p,1} \\ \tilde{\mathbf{C}}_{p,2} \\ \tilde{\mathbf{C}}_{p,3} \\ \tilde{\mathbf{C}}_{p,4} \end{pmatrix} = \begin{pmatrix} \mathbf{C}^{(3)}_b(\mathbf{I} - \mathbf{S}_{33}\mathbf{R}_{\uparrow 3})^{-1}\mathbf{S}_{13} \\ \mathbf{C}^{(3)}_b(\mathbf{I} - \mathbf{S}_{33}\mathbf{R}_{\uparrow 3})^{-1}\mathbf{S}_{23} \\ \mathbf{C}^{(3)}_a + \mathbf{C}^{(3)}_b\mathbf{S}_{33}(\mathbf{I} - \mathbf{R}_{\uparrow 3}\mathbf{S}_{33})^{-1}\mathbf{T}_{\uparrow 3} \\ \mathbf{C}^{(3)}_b(\mathbf{I} - \mathbf{S}_{33}\mathbf{R}_{\uparrow 3})^{-1}\mathbf{S}_{43} \end{pmatrix}, \tag{52b}$$

$$\begin{pmatrix} \tilde{\mathbf{C}}_{\alpha,1} & \tilde{\mathbf{C}}_{\alpha,2} & \tilde{\mathbf{C}}_{\alpha,3} & \tilde{\mathbf{C}}_{\alpha,4} \\ \tilde{\mathbf{C}}_{\beta,1} & \tilde{\mathbf{C}}_{\beta,2} & \tilde{\mathbf{C}}_{\beta,3} & \tilde{\mathbf{C}}_{\beta,4} \end{pmatrix}$$
$$= \begin{pmatrix} \mathbf{C}_{\alpha,1} + \mathbf{C}_{\alpha,3}\mathbf{R}_{\uparrow 3}(\mathbf{I} - \mathbf{S}_{33}\mathbf{R}_{\uparrow 3})^{-1}\mathbf{S}_{13} & \mathbf{C}_{\alpha,2}\mathbf{C}_{\alpha,3}\mathbf{R}_{\uparrow 3}(\mathbf{I} - \mathbf{S}_{33}\mathbf{R}_{\uparrow 3})^{-1}\mathbf{S}_{23} & \mathbf{C}_{\alpha,3}(\mathbf{I} - \mathbf{R}_{\uparrow 3}\mathbf{S}_{33})^{-1}\mathbf{T}_{\uparrow 3} & \mathbf{C}_{\alpha,4} + \mathbf{C}_{\alpha,3}\mathbf{R}_{\uparrow 3}(\mathbf{I} - \mathbf{S}_{33}\mathbf{R}_{\uparrow 3})^{-1}\mathbf{S}_{43} \\ \mathbf{C}_{\beta,1} + \mathbf{C}_{\beta,3}\mathbf{R}_{\uparrow 3}(\mathbf{I} - \mathbf{S}_{33}\mathbf{R}_{\uparrow 3})^{-1}\mathbf{S}_{13} & \mathbf{C}_{\beta,2} + \mathbf{C}_{\beta,3}\mathbf{R}_{\uparrow 3}(\mathbf{I} - \mathbf{S}_{33}\mathbf{R}_{\uparrow 3})^{-1}\mathbf{S}_{23} & \mathbf{C}_{\beta,3}(\mathbf{I} - \mathbf{R}_{\uparrow 3}\mathbf{S}_{33})^{-1}\mathbf{T}_{\uparrow 3} & \mathbf{C}_{\beta,4} + \mathbf{C}_{\beta,3}\mathbf{R}_{\uparrow 3}(\mathbf{I} - \mathbf{S}_{33}\mathbf{R}_{\uparrow 3})^{-1}\mathbf{S}_{43} \end{pmatrix}. \tag{52c}$$

The derived S-matrix recursion formulas of the interconnection of the two-port block and the four-port cross block through the port 4 are listed as follows:

$$\begin{pmatrix} \tilde{\mathbf{S}}_{11} & \tilde{\mathbf{S}}_{21} & \tilde{\mathbf{S}}_{31} & \tilde{\mathbf{S}}_{41} \\ \tilde{\mathbf{S}}_{12} & \tilde{\mathbf{S}}_{22} & \tilde{\mathbf{S}}_{32} & \tilde{\mathbf{S}}_{42} \\ \tilde{\mathbf{S}}_{13} & \tilde{\mathbf{S}}_{23} & \tilde{\mathbf{S}}_{33} & \tilde{\mathbf{S}}_{43} \\ \tilde{\mathbf{S}}_{14} & \tilde{\mathbf{S}}_{24} & \tilde{\mathbf{S}}_{34} & \tilde{\mathbf{S}}_{44} \end{pmatrix}$$

$$= \begin{pmatrix} \mathbf{S}_{11} + \mathbf{S}_{41}\mathbf{R}_{\downarrow 4}(\mathbf{I} - \mathbf{S}_{44}\mathbf{R}_{\downarrow 4})^{-1}\mathbf{S}_{14} & \mathbf{S}_{21} + \mathbf{S}_{41}\mathbf{R}_{\downarrow 4}(\mathbf{I} - \mathbf{S}_{44}\mathbf{R}_{\downarrow 4})^{-1}\mathbf{S}_{24} & \mathbf{S}_{31} + \mathbf{S}_{41}\mathbf{R}_{\downarrow 4}(\mathbf{I} - \mathbf{S}_{44}\mathbf{R}_{\downarrow 4})^{-1}\mathbf{S}_{34} & \mathbf{S}_{41}(\mathbf{I} - \mathbf{R}_{\downarrow 4}\mathbf{S}_{44})^{-1}\mathbf{T}_{\downarrow 4} \\ \mathbf{S}_{12} + \mathbf{S}_{42}\mathbf{R}_{\downarrow 4}(\mathbf{I} - \mathbf{S}_{44}\mathbf{R}_{\downarrow 4})^{-1}\mathbf{S}_{14} & \mathbf{S}_{22} + \mathbf{S}_{42}\mathbf{R}_{\downarrow 4}(\mathbf{I} - \mathbf{S}_{44}\mathbf{R}_{\downarrow 4})^{-1}\mathbf{S}_{24} & \mathbf{S}_{32} + \mathbf{S}_{42}\mathbf{R}_{\downarrow 4}(\mathbf{I} - \mathbf{S}_{44}\mathbf{R}_{\downarrow 4})^{-1}\mathbf{S}_{34} & \mathbf{S}_{42}(\mathbf{I} - \mathbf{R}_{\downarrow 4}\mathbf{S}_{44})^{-1}\mathbf{T}_{\downarrow 4} \\ \mathbf{S}_{13} + \mathbf{S}_{43}\mathbf{R}_{\downarrow 4}(\mathbf{I} - \mathbf{S}_{44}\mathbf{R}_{\downarrow 4})^{-1}\mathbf{S}_{14} & \mathbf{S}_{23} + \mathbf{S}_{43}\mathbf{R}_{\downarrow 4}(\mathbf{I} - \mathbf{S}_{44}\mathbf{R}_{\downarrow 4})^{-1}\mathbf{S}_{24} & \mathbf{S}_{33} + \mathbf{S}_{43}\mathbf{R}_{\downarrow 4}(\mathbf{I} - \mathbf{S}_{44}\mathbf{R}_{\downarrow 4})^{-1}\mathbf{S}_{34} & \mathbf{S}_{43}(\mathbf{I} - \mathbf{R}_{\downarrow 4}\mathbf{S}_{44})^{-1}\mathbf{T}_{\downarrow 4} \\ \mathbf{T}_{\uparrow 4}(\mathbf{I} - \mathbf{S}_{44}\mathbf{R}_{\downarrow 4})^{-1}\mathbf{S}_{14} & \mathbf{T}_{\uparrow 4}(\mathbf{I} - \mathbf{S}_{44}\mathbf{R}_{\downarrow 4})^{-1}\mathbf{S}_{24} & \mathbf{T}_{\uparrow 4}(\mathbf{I} - \mathbf{S}_{44}\mathbf{R}_{\downarrow 4})^{-1}\mathbf{S}_{34} & \mathbf{R}_{\uparrow 4} + \mathbf{T}_{\uparrow 4}\mathbf{S}_{44}(\mathbf{I} - \mathbf{R}_{\downarrow 4}\mathbf{S}_{44})^{-1}\mathbf{T}_{\downarrow 4} \end{pmatrix} \tag{53a}$$

$$\begin{pmatrix} \tilde{\mathbf{C}}_{p,1} \\ \tilde{\mathbf{C}}_{p,2} \\ \tilde{\mathbf{C}}_{p,3} \\ \tilde{\mathbf{C}}_{p,4} \end{pmatrix} = \begin{pmatrix} \mathbf{C}_a^{(4)}(\mathbf{I} - \mathbf{S}_{44}\mathbf{R}_{\downarrow 4})^{-1}\mathbf{S}_{14} \\ \mathbf{C}_a^{(4)}(\mathbf{I} - \mathbf{S}_{44}\mathbf{R}_{\downarrow 4})^{-1}\mathbf{S}_{24} \\ \mathbf{C}_a^{(4)}(\mathbf{I} - \mathbf{S}_{44}\mathbf{R}_{\downarrow 4})^{-1}\mathbf{S}_{34} \\ \mathbf{C}_b^{(4)} + \mathbf{C}_a^{(4)}\mathbf{S}_{44}(\mathbf{I} - \mathbf{R}_{\downarrow 4}\mathbf{S}_{44})^{-1}\mathbf{T}_{\downarrow 4} \end{pmatrix}, \tag{53b}$$

$$\begin{pmatrix} \tilde{\mathbf{C}}_{\alpha,1} & \tilde{\mathbf{C}}_{\alpha,2} & \tilde{\mathbf{C}}_{\alpha,3} & \tilde{\mathbf{C}}_{\alpha,4} \\ \tilde{\mathbf{C}}_{\beta,1} & \tilde{\mathbf{C}}_{\beta,2} & \tilde{\mathbf{C}}_{\beta,3} & \tilde{\mathbf{C}}_{\beta,4} \end{pmatrix}$$

$$= \begin{pmatrix} \mathbf{C}_{\alpha,1} + \mathbf{C}_{\alpha,4}\mathbf{R}_{\downarrow 4}(\mathbf{I} - \mathbf{S}_{44}\mathbf{R}_{\downarrow 4})^{-1}\mathbf{S}_{14} & \mathbf{C}_{\alpha,2} + \mathbf{C}_{\alpha,4}\mathbf{R}_{\downarrow 4}(\mathbf{I} - \mathbf{S}_{44}\mathbf{R}_{\downarrow 4})^{-1}\mathbf{S}_{24} & \mathbf{C}_{\alpha,3} + \mathbf{C}_{\alpha,4}\mathbf{R}_{\downarrow 4}(\mathbf{I} - \mathbf{S}_{44}\mathbf{R}_{\downarrow 4})^{-1}\mathbf{S}_{34} & \mathbf{C}_{\alpha,4}(\mathbf{I} - \mathbf{R}_{\downarrow 4}\mathbf{S}_{44})^{-1}\mathbf{T}_{\downarrow 4} \\ \mathbf{C}_{\beta,1} + \mathbf{C}_{\beta,4}\mathbf{R}_{\downarrow 4}(\mathbf{I} - \mathbf{S}_{44}\mathbf{R}_{\downarrow 4})^{-1}\mathbf{S}_{14} & \mathbf{C}_{\beta,2} + \mathbf{C}_{\beta,4}\mathbf{R}_{\downarrow 4}(\mathbf{I} - \mathbf{S}_{44}\mathbf{R}_{\downarrow 4})^{-1}\mathbf{S}_{24} & \mathbf{C}_{\beta,3} + \mathbf{C}_{\beta,4}\mathbf{R}_{\downarrow 4}(\mathbf{I} - \mathbf{S}_{44}\mathbf{R}_{\downarrow 4})^{-1}\mathbf{S}_{34} & \mathbf{C}_{\beta,4}(\mathbf{I} - \mathbf{R}_{\downarrow 4}\mathbf{S}_{44})^{-1}\mathbf{T}_{\downarrow 4} \end{pmatrix}. \tag{53c}$$

Next, with the use of the prepared S-matrix recursion formulas, we can construct the total S matrix of the extended four-port cross block through consecutive step-by-step procedure. At the first step, the S matrix of the combined structure of two-port block and four-port cross block through port 1 is analyzed using Eqs. (50a)–(50c). The combined structure can be viewed as a four-port block with its own S matrix and internal coupling coefficients operators. Hence, at the second step, the S-matrix formulas of the interconnection of the two-port block and the four-port cross block through port 2 can be straightforwardly applied to interconnect this combined four-port block structure to a two-port block through port 2 with no modification. By the same way, we can recursively apply the S-matrix formulas to interconnect the combined four-port block and a two-port block to build the extended four-port cross block. This analysis procedure is illustrated in Fig. 22.

For validating the developed GSMM formulas, the electric field distributions at each step of building the extended four-port cross block by the stated step-by-step interconnection procedure are visualized. In Fig. 23, the results of the cross-waveguide structure are shown. In Fig. 23(a), the combined structure is illustrated. In Figs. 23(b)–23(e), the y-polarization electric field distributions at steps 1, 2, 3, and 4 are presented, respectively. The field visualization results are quite well-matched with the results of the previous work done by the finite difference time domain (FDTD) method [2]. For comparison, additional simulation results of the T-branch waveguide structure [5] and the 90°-bend waveguide structure [6] are presented, respectively, in Figs. 24 and 25.

6. CONCLUSION

The proposed scheme is composed of two main subtheories: (i) local Fourier modal analysis method for analyzing internal eigenmodes of four-port cross blocks and (ii) generalized scattering-matrix method for modeling crossed nanophotonic structures by interconnecting four two-port blocks and a four-port block. The established modeling and analysis on crossed nanophotonic structures is a basic element for modeling generalized large scale nanophotonic networks. The general linear system theory of nanophotonic networks will be reported through our successive paper based on this paper.

In the aspects of methodology, the proposed local analysis scheme is efficient since the local field analysis is performed with the reasonable and practical assumption of the field localization in nanophotonic structures. Instead of computing whole structure of network, local regions occupied by functional photonic blocks are characterized by the local Fourier modal analysis. Eventually this local analysis scheme can provide an efficient method of three-dimensional simulation of large scale nanophotonic net-

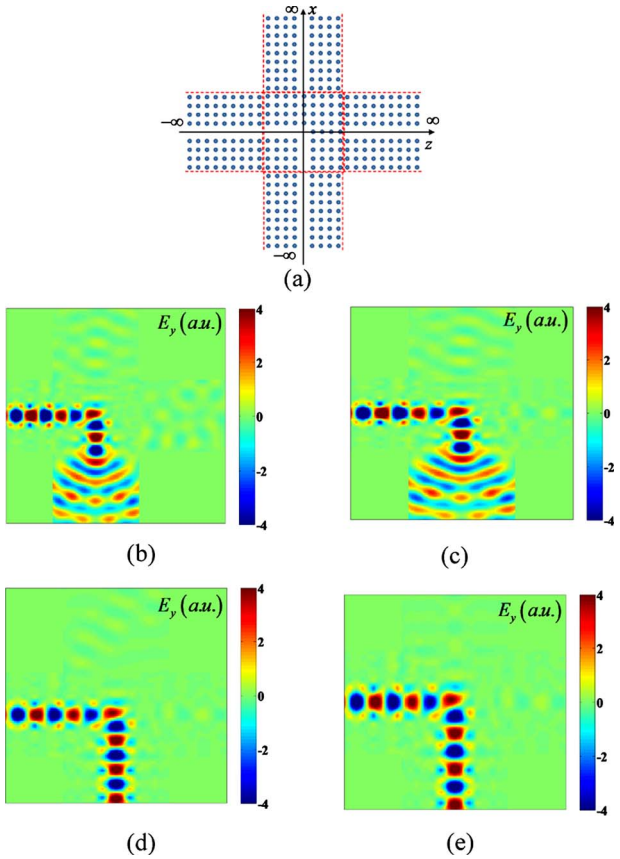

Fig. 25. (Color online) (a) 90°-bend waveguide structure and y-polarization electric field distributions at each step of building the extended four-port cross block by the step-by-step interconnection procedure: steps (b) 1, (c) 2, (d) 3, and (e) 4.

works and systematic methods for the advanced design, analysis, and fabrication of nanophotonic networks.

On the other hand, we have proposed a new theory of the Fourier modal method that overcomes the present theoretical limitation of the conventional Fourier modal method. The proposed local Fourier modal analysis and generalized scattering-matrix method have extended the territory of the conventional Fourier modal method. The conventional Fourier modal method is a Fourier analysis theory for modeling method of multilayer structure composed of layers having transverse periodic structures such as periodic grating structures. At present, many people think that the Fourier modal method has been almost mature and the future issues of the Fourier modal method should be focused on its applications. However, this paper shows that the local Fourier modal method with the generalized scattering-matrix method can have unique advantages in large scale network modeling over other conventional global electromagnetic analysis methods.

ACKNOWLEDGMENT

The authors acknowledge the support by the Ministry of Science and Technology of Korea and Korea Science and Engineering Foundation through the Creative Research Initiative Program (Active Plasmonics Application Systems).

REFERENCES

1. N. Moll, R. Harbers, R. F. Mahrt, and G.-L. Bona, "Integrated all-optical switch in a cross-waveguide geometry," Appl. Phys. Lett. **88**, 171104 (2006).
2. M. F. Yanik, S. Fan, M. Soliacic, and D. Joannopoulos, "All-optical transistor action with bistable switching in a photonic crystal cross-waveguide geometry," Opt. Lett. **28**, 2506–2508 (2003).
3. M. F. Yanik and S. Fan, "Stopping light all-optically," Phys. Rev. Lett. **92**, 083901 (2004).
4. M. F. Yanik, H. A. Altug, J. Vuckovic, and S. Fan, "Submicron all optical digital memory and integration of nanoscale photonic devices without isolators," J. Lightwave Technol. **22**, 2316–2322 (2004).
5. S. Fan, S. G. Johnson, and J. D. Joannopoulos, "Waveguide branches in photonic crystals," J. Opt. Soc. Am. B **18**, 162–165 (2001).
6. A. Mekis, J. C. Chen, I. Kurland, S. Fan, P. R. Villeneuve, and J. D. Joannopoulos, "High transmission through sharp bends in photonic crystal waveguides," Phys. Rev. Lett. **77**, 3787–3790 (1996).
7. M. G. Moharam and T. K. Gaylord, "Rigorous coupled-wave analysis of planar-grating diffraction," J. Opt. Soc. Am. A **71**, 811–818 (1981).
8. P. Lalanne, "Improved formulation of the coupled-wave method for two-dimensional gratings," J. Opt. Soc. Am. A **14**, 1592–1598 (1997).
9. H. Kim, S. Kim, I.-M. Lee, and B. Lee, "Pseudo-Fourier modal analysis on dielectric slabs with arbitrary longitudinal permittivity and permeability profiles," J. Opt. Soc. Am. A **23**, 2177–2191 (2006).
10. W. Jian and R. T. Chen, "Rigorous analysis of diffraction gratings of arbitrary profiles using virtual photonic crystals," J. Opt. Soc. Am. A **23**, 2192–2197 (2006).
11. H. Kim and B. Lee, "Pseudo-Fourier modal analysis of two-dimensional arbitrarily shaped grating structures," J. Opt. Soc. Am. A **25**, 40–54 (2008).
12. M. G. Moharam, E. B. Grann, and D. A. Pommet, "Formulation for stable and efficient implementation of the rigorous coupled-wave analysis of binary gratings," J. Opt. Soc. Am. A **12**, 1068–1076 (1995).
13. L. Li, "Use of Fourier series in the analysis of discontinuous periodic structures," J. Opt. Soc. Am. A **13**, 1870–1876 (1996).
14. L. Li, "Fourier modal method for crossed anisotropic gratings with arbitrary permittivity and permeability tensors," J. Opt. A, Pure Appl. Opt. **5**, 345–355 (2003).
15. L. Li, "Mathematical reflections on the Fourier modal method in grating theory," in *Mathematical Modeling in Optical Science*, G. Bao, ed. (SIAM, Philadelphia, 2001), Chap. 4.
16. E. Popov and M. Neviére, "Differential theory for diffraction gratings: a new formulation for TM polarization with rapid convergence," Opt. Lett. **25**, 598–600 (2000).
17. E. Popov and M. Neviére, "Grating theory: new equations in Fourier space leading to fast converging results for TM polarization," J. Opt. Soc. Am. A **17**, 1773–1784 (2000).
18. J. P. Hugonin and P. Lalanne, "Perfectly matched layers as nonlinear coordinate transforms: a generalized formalization," J. Opt. Soc. Am. A **22**, 1844–1849 (2005).
19. E. Popov, M. Neviére, B. Gralak, and G. Tayeb, "Staircase approximation validity for arbitrary-shaped gratings," J. Opt. Soc. Am. A **19**, 33–42 (2002).
20. H. Kim, I.-M. Lee, and B. Lee, "Extended scattering-matrix method for efficient full parallel implementation of rigorous coupled-wave analysis," J. Opt. Soc. Am. A **24**, 2313–2327 (2007).
21. L. Li, "Formulation and comparison of two recursive matrix algorithms for modeling layered diffraction gratings," J. Opt. Soc. Am. A **13**, 1024–1035 (1996).
22. E. L. Tan, "Note on formulation of the enhanced scattering-(transmittance-) matrix approach," J. Opt. Soc. Am. A **19**, 1157–1161 (2002).
23. L. Li, "Note on the S-matrix propagation algorithm," J. Opt. Soc. Am. A **20**, 655–660 (2003).

24. M. G. Moharam and A. B. Greenwell, "Efficient rigorous calculations of power flow in grating coupled surface-emitting devices," Proc. SPIE **5456**, 57–67 (2004).
25. Q. Cao, P. Lalanne, and J. P. Hugonin, "Stable and efficient Bloch-mode computational method for one-dimensional grating waveguides," J. Opt. Soc. Am. A **19**, 335–338 (2002).
26. J. D. Joannopoulos, R. D. Meade, and J. N. Winn, *Photonic Crystals* (Princeton U. Press, 1995).
27. J.-M. Lourtioz, H. Benisty, V. Berger, J.-M. Gerard, A. Tchelnokov, and P. Fornel, *Photonic Crystals: Towards Nanoscale Photonic Devices* (Springer, 1999).
28. S. G. Johnson and J. D. Joannopoulos, *Photonic Crystals: The Road from Theory to Practice* (Springer, 2002).
29. K. Sakoda, *Optical Properties of Photonic Crystals* (Springer, 2004).
30. S. Kim, H. Kim, Y. Lim, and B. Lee, "Off-axis directional beaming of optical field diffracted by a single subwavelength metal slit with asymmetric dielectric surface gratings," Appl. Phys. Lett. **90**, 051113 (2007).